5-1-2010

Relative contributions of zinc and calcium to acute injury to hippocampal CA1 neurons

Robert Dietz

Robert M. Dietz
Candidate

Neurosciences
Department

This dissertation is approved, and it is acceptable in quality and form for publication on microfilm:

Approved by the Dissertation Committee:

C. Shuttleworth, Chairperson

RELATIVE CONTRIBUTIONS OF ZINC AND CALCIUM TO ACUTE INJURY OF HIPPOCAPMAL CA1 NEURONS

BY

ROBERT M. DIETZ

Bachelor of Science, Biology, University of New Mexico, 2003

M.D., University of New Mexico, 2010

Ph.D., Biomedical Sciences, University of New Mexico, 2010

DISSERTATION

Submitted in Partial Fulfillment of the
Requirements for the Degree of

Doctor of Philosophy
Biomedical Sciences

The University of New Mexico
Albuquerque, New Mexico

May, 2010

Acknowledgements

The greater risk is not that we aim too high and fail – but that we aim too low and succeed...
– Michelangelo

I would like to thank the faculty and staff of the Neurosciences Department for continued support and enthusiasm for my project and for creating an environment that encourages the development of scientific thought and critical thinking from the newest graduate student to the most senior of faculty members.

I am sincerely grateful to my committee members, Dr. Fernando Valenzuela, Dr. Wolf Müller and Dr. Tom Resta, for offering invaluable insight and continued support throughout this project. Thank you for your time and suggestions throughout the course of this study.

I would also like to thank Dr. Fernando Valenzuela for his role as the director of the M.D./Ph.D. program in granting advice outside the scope of this project and for finding ways to keep the M.D./Ph.D. program a critical part of the UNM School of Medicine.

I appreciate the technical assistance of Buz Tyler during my time in the department.

I thank my lab mates, Thom, Jessica, Meg and Angela, for invigorating discussion and thoughtful input along the way.

I would like to convey my deepest gratitude to my family for their never-ending encouragement and continual understanding throughout this process. My mom, dad and sister have been invaluable sources of strength throughout my life. Thank you.

I am genuinely grateful to my mentor and advisor, Dr. Bill Shuttleworth, for uncompromising faith in me and this project. The lessons that have been learned in both science and life will never be forgotten. Thank you for your constant encouragement and continued opportunities for individual enlightenment.

I express my sincerest gratitude to my uncle, Dr. Michael Yeaman for being an unrelenting source of inspiration. From architecting a plan to the exploration and revelation of truth, you have always been there for me. Thank you for the odyssey; then – as now – always.

I am eternally grateful to my wife, Deidre, who has endured all the joys and pains of this research. Thank you for your sacrifices and unyielding support. You have been a constant source of motivation and kindness. Thank you for everything.

RELATIVE CONTRIBUTIONS OF ZINC AND CALCIUM TO ACUTE INJURY OF HIPPOCAMPAL CA1 NEURONS

BY

ROBERT M. DIETZ

ABSTRACT OF DISSERTATION

Submitted in Partial Fulfillment of the
Requirements for the Degree of

Doctor of Philosophy
Biomedical Sciences

The University of New Mexico
Albuquerque, New Mexico

May, 2010

Relative Contributions of Zn^{2+} and Ca^{2+} to Acute Injury of Hippocampal CA1 Neurons

By

Robert M. Dietz

B.S., Biology, University of New Mexico, 2003

M.D., University of New Mexico, 2010

Ph.D., Biomedical Sciences, University of New Mexico, 2010

Abstract

Spreading depression (SD) is a wave of severe depolarization that spreads across brain tissue. For several decades, it has been suggested that (SD) may play a role in the expansion of brain injury following ischemic insults, and may also be involved in non-injurious pathologies such as migraine aura. The major goals of this study were to examine cellular mechanisms that contribute to the initiation of different forms of SD, and in particular the potential roles of the cations Ca^{2+} and Zn^{2+}.

Work in this thesis examined SD in hippocampal slices acutely prepared from adult mice. Initial studies used the Na^{+}/K^{+} ATPase inhibitor ouabain to generate SD, and showed that L-type Ca^{2+} channels are required for initiation of SD, but that Ca^{2+} influx through these channels was not involved. In fact, from NAD(P)H autofluorescence studies, it was

suggested that Ca^{2+} influx may promote mitochondrial function prior to SD, rather than contribute to ionic deregulation. A combination of imaging approaches was then used to demonstrate that Zn^{2+} could enter neurons through L-type Ca^{2+} channels and depolarize the inner mitochondrial membrane prior to SD. Furthermore, chelation of Zn^{2+} completely prevented SD, showing for the first time that Zn^{2+} entry could be critically required for SD. It was then shown that very similar ionic mechanisms appeared to be involved in SD generated by oxygen/glucose deprivation (OGD), an *in vitro* model of ischemia. Zn^{2+}, rather than Ca^{2+} influx appeared to be critically required for the onset of OGD/SD.

SD generated by localized high K^+ applications appeared to involve quite distinct ionic mechanisms. Zn^{2+}-dependent mechanisms were not involved, but Ca^{2+} chelation effectively prevented the propagation of these events. Single-neuron Ca^{2+} imaging studies showed that high K^+/SD resulted in recoverable Ca^{2+} loads throughout neurons, whereas OGD/SD and ouabain/SD lead to irrecoverably high Ca^{2+} levels and rapid neuronal injury.

These results provide the first evidence that Zn^{2+} can selectively contribute to SD in pathological models, and suggest novel approaches to mitigating brain injury following stroke.

Table of Contents

List of Figures

1. Introduction

2. Zn^{2+} Influx via Calcium Channels Can Trigger Spreading Depression in Brain Slices

3. Ca^{2+}-dependent Changes in Mitochondrial Redox Potential Prior to the Onset of Spreading Depression in Hippocampal Slices

4. Contribution of Na^{+}/Ca^{2+} exchange to excessive Ca^{2+} loading in dendrites and somata of CA1 neurons in acute slice

List of Tables

4. Contribution of Na^+/Ca^{2+} exchange to excessive Ca^{2+} loading in dendrites and somata of CA1 neurons in acute slice

1. Introduction

1.1 Ischemic Brain Injury

Stroke is a leading cause of morbidity and mortality in the United States and worldwide. In the United States, it is the third leading cause of death and the leading cause of serious long-term disability. About 750,000 Americans suffer a new or recurrent stroke every year, and the associated mortality exceeds 160,000 (Rosamond et al., 2007). By far the most common cause of stroke is a sudden loss of blood flow to the brain due to a blood clot. This often results in a central core of damage in the tissue that is normally vascularized by the blocked artery and an expansion of injury surrounding the core that can take place over the course of hours and days (Dirnagl et al., 1999; Lee et al., 2000a). For decades, many researchers have investigated the mechanisms that are involved in ischemic cell death and much advancement in the ideas regarding these processes has been made. It has long been hoped that cellular mechanisms that lead to neuronal vulnerability may be identified and blocked, and thereby lead to improved therapy for patients suffering from stroke and related brain injuries.

Some of the tremendous progress that has been made in cellular mechanisms of neuronal injury can be briefly summarized here. A first major step was the discovery that excessive release of the excitatory neurotransmitter glutamate was involved in neuronal injury, in a process termed "excitotoxicity" (Olney, 1978). Since extracellular glutamate levels rise dramatically during experimental stroke, this process is widely held to be important in initiation of stroke injury. The subsequent identification of Ca^{2+} overload as a critical consequence of glutamate receptor activation led to the inclusion of this cation

in most models of excitotoxic injury, including stroke (Lipton, 1999). In the search for targets for therapeutic interventions, mechanisms of excitotoxic Ca^{2+} influx have been examined extensively in isolated neuronal cultures, and have mainly involved studies of events in neuronal somata. From these studies, Ca^{2+} overload appears to involve Ca^{2+}-permeable ion channels as well as Na^{+}/Ca^{2+} exchangers (Choi, 1985; Kiedrowski et al., 1994; Lee et al., 1999). It has been hypothesized that blocking this Ca^{2+} influx may be the key to blocking damage, particularly in the area surrounding the core of ischemic damage (the "ischemic penumbra") where it has been observed that cell death is delayed compared to the cells which are directly damaged by lack of perfusion in the ischemic core. A large number of clinical trials targeting these pathways have been completed, but unfortunately none have been successful.

Another exciting development has been the identification of apoptotic mechanisms as contributors to ischemic injury (Linnik et al., 1993). Markers for apoptosis have been identified in the ischemic penumbra (Heron et al., 1993; MacManus et al., 1993; Okamoto et al., 1993), and since these pathways could be involved in delayed injury (Charriaut-Marlangue et al., 1996), it seemed likely that one or more components of these intricate cell death pathways could be targeted following stroke (Martinou et al., 1994; Linnik et al., 1995; Gottron et al., 1997; Snider et al., 1999). While this still may be achievable in the long term, it is noteworthy that no clinically useful agents have yet emerged from this approach.

Despite the incredible progress that has been made in understanding cellular mechanisms of degeneration, the single pharmacological therapeutic approach in current clinical practice does not target cell death mechanisms. Intravenous delivery of tissue plasminogen activating factor (tPA) is designed to disrupt clots within the cerebral vasculature, and restore the supply of oxygen and glucose to brain tissue. While this approach is in current clinical practice in the United States, it has limited effectiveness and is restricted to a small subpopulation of stroke sufferers (Marler and Goldstein, 2003; Schneck and Biller, 2005). It is therefore of great importance to develop alternative approaches that effectively reduce the progression of neuronal death following acute ischemic injuries. Therefore, an aim of this thesis was to examine a phenomenon which has been hypothesized to contribute substantially to spread of damage following ischemia; the phenomenon of spreading depression. As will be described below, the cellular mechanisms involved in the initiation of spreading depression are not well understood. A motivation for the studies that follow was to identify key mechanisms involved in triggering spreading depression, since this understanding might provide an important new avenue for the treatment of ischemic injuries.

1.2 Spreading Depression

Discovery of Spreading Depression

The phenomenon of spreading depression (SD) was first described in 1944 by the Brazilian investigator, Aristides Leão (1944) who was studying epilepsy mechanisms at Harvard Medical School. Leao‟s experiments involved opening the skull of the rabbit

and arranging a row of recording electrodes on the exposed cortical surface, to record electrocorticogram (EcoG) responses to focal electrical stimulation. While these studies allowed the recording of the expected seizure-like discharges, on occasion, Leão also noted an unexpected silencing of spontaneous EcoG activity. Interestingly, EcoG activity nearest to the stimulation electrode was silenced first, and the depression of activity then spread to subsequent electrodes at a rate of approximately 3 mm/min, eventually covering most of the cortical surface within 3-6 minutes. This phenomenon was reversible, as EcoG activity reappeared several minutes later, following the same progression across the cortical surface as the original depression response (Leao, 1944).

Leao‟s seminal paper was very comprehensive, and described many important features of SD that have subsequently been repeatedly confirmed. Some of these features include 1) the depression of activity lasted several minutes; 2) aside from electrical stimulation, SD could be evoked by mechanical trauma, such as touching the exposed cortex with a blunt rod; 3) the threshold for SD varied among different areas of the cortex, but once triggered, was an all-or-none event spreading in all directions; 4) when a region of tissue was engaged by SD, an evoked potential wave could not be evoked by direct electrical stimulation; 5) in addition to original descriptions in rabbit, SD could be provoked in many other species, including pigeons and cats (Leao, 1944).

When Leão returned to Rio de Janeiro, he described a large negative voltage shift (Leao, 1947) while recording from the extracellular space using direct current (DC)-coupled amplification. This DC shift has since become a well-accepted hallmark of SD in a range

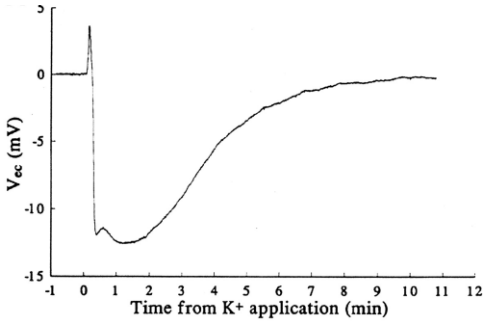

Figure 1.1: Extracellular voltage recording showing the negative shift which is associated with the coordinated depolarization of SD. The slope of the initial drop is very steep, indicating a rapid redistribution of ions followed by a slower recovery toward equilibrium. The stimulus for this SD was a small drop of solution containing high K^+ concentration onto a slice of human hippocampus (Somjen, 2001).

of CNS preparations (**Figure 1.1**). Depending on the recording conditions, the voltage deflection can reach an amplitude of 8-15 mV, the largest extracellular shift observed in living brain tissue (Somjen, 2005). Leão also made the first explicit link between SD and brain injury, when he described a similar negative voltage shift in response to ischemia induced by arterial occlusion in rabbits. He suggested that the mechanisms of the negative voltage shifts of SD and ischemia are likely "of the same nature" (Leao, 1947), and it now appears that this important insight may lead to the development of novel and effective treatment of brain injuries, long after an initial ischemic insult has occurred.

SD and ischemic injury

Despite Leao"s early insights on SD and ischemia, it has taken many years for the idea that SD contributes to stroke injury to become widely accepted. Recurrent spontaneous increases in extracellular K^+ bearing some similarities to SD were described following middle cerebral artery occlusion (MCAO) in the baboon cortex (Branston et al., 1977). Subsequent studies in the penumbra of MCAO lesions in cats showed transient elevations of K^+ (Strong et al., 1983) that were later demonstrated to resemble SD-like

depolarizations emanating from the edge of the infarct (Nedergaard and Astrup, 1986). These SD-like events propagate at approximately 3 mm/min from the edges of infarcted regions (Hasegawa et al., 1995). Because of these observations, the events that originate at the edge of the ischemic core have been termed peri-infarct depolarizations (PIDs) (Hossmann, 1996).

PIDs have been recorded from a range of species, including in human patients following neurosurgery for head trauma or ischemia, as well as non-human primates, cats and rodents (Gill et al., 1992; Iijima et al., 1992; Mies et al., 1993; Back et al., 1996; Mayevsky et al., 1996; Strong et al., 2000; Strong et al., 2002; Strong and Dardis, 2005). Initially, a disparity in PID frequency between different species was taken to suggest that PIDs may be less important contributors to ischemic injury in species with more developed neurocortical structures and by extension may be of only trivial importance in human stroke (Robertson, 2000). However, more recent data shows that the incidence of PIDs may be very dependent on depth of anesthesia during the recording period (Hartings et al., 2003), and that this variable may lead to substantial underestimations of the true frequency of PIDs in many experimental and human clinical settings. An important demonstration of this possibility comes from long-term recordings of cortical electrical activity in awake, freely-moving rats that were monitored for days following a transient ischemic insult (Hartings et al., 2003). In these animals, 70 PIDs

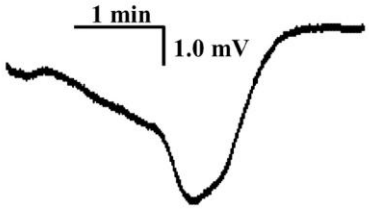

Figure 1.2: Example of a PID event recorded following MCAO in a rat model closely resembles events that take place during SD (Hartings et al, 2003).

were recorded over a 24 hour period, representing an approximate 10-fold increase in PIDs compared to rats that were maintained on anesthetics in previous studies (Hartings et al., 2003). Furthermore, this study revealed that PIDs can be recorded for at least 72 hours after the initial insult (Hartings et al., 2003).

An important question has been whether PIDs are merely correlates of ischemic injury, or alternatively, whether PIDs themselves contribute to the progressive increase in infarct volume during the hours and days following a stroke. A number of lines of evidence have now converged that implicate PIDs as contributors to stroke injury (Nedergaard and Astrup, 1986; Hossmann, 1996; Hartings et al., 2003; Umegaki et al., 2005). Early results found that the occurance of SD-like events in tissue surrounding infarcts was associated with severe neuronal injury (Nedergaard and Astrup, 1986). The relationship revealed a significant correlation between the number of SD events and the size of lesions in *in vivo* rat studies (Mies et al., 1993).

Early studies using the glutamate receptor antagonists MK-801 or NBQX were able to block the depolarizations and decrease the infarct size (Iijima et al., 1992; Mies et al., 1993; Mies et al., 1994; Busch et al., 1996), further supporting a role for PIDs in stroke injury. There are a number of mechanisms by which PIDs could lead to progressive increases in infarct volume. One possible explanation comes from the metabolic consequences of SD. As discussed below, SD events produce very large increases in neuronal Na^+ and Ca^{2+} loads as neurons undergo a period of sustained and almost complete depolarization (Kraig and Nicholson, 1978; Nicholson et al., 1978). In

otherwise healthy brain tissue, it is possible that Na^+ and Ca^{2+} extrusion processes can extrude these cations, albeit at the expense of substantial amounts of ATP consumed by plasma membrane and organellar transport systems. However, in the context of stroke and compromised metabolic substrate availability, it is possible that repetitive and severe cation loads produced by PIDs can not be effectively resolved, and lead to complete exhaustion of cellular ATP levels, and catastrophic deregulation of ionic homeostasis and permanent cell swelling (Busch et al., 1996; Kempski et al., 2000). It has also been suggested that substantial decreases in PO_2 (Back et al., 1994) and transient or permanent reduction in blood flow (Strong et al., 2002) are associated with PIDs.

Due to the increasing evidence that PIDs are likely contributors to the size of ischemic lesions, an important goal is to find approaches to prevent the induction of PIDs in the hours and days following the onset of a stroke. Unfortunately, agents such as MK-801 or NBQX have not been successful in clinical stroke, possibly because of important physiological actions of glutamate receptors are blocked (Lee et al., 1999). Thus, an important goal is to find approaches which block PIDs without disrupting normal synaptic function.

SD in migraine

Shortly before Leão published his initial findings on SD in rabbit cortex, an American psychologist by the name of Karl Lashley described the visual aura that he experienced during his own ophthalmic migraine syndrome (Lashley, 1941). He carefully mapped the

trajectory of the aura across his visual field and predicted a velocity of approximately 3 mm/min. Lashley suggested that a propagating physiological mechanism must be responsible, and it was later noted by Milner that the velocity described by Lashley was very similar to Leao‟s spreading depression (Milner, 1958). Subsequent studies have confirmed that SD is likely a key mechanism that is involved in the spread of aura experienced with migraine (Welch, 1993; Flippen and Welch, 1997; Bowyer, 1999; Cao et al., 1999; Bramanti et al., 2005). Indeed, a recent functional MRI imaging study provided evidence for a spreading event reminiscent of SD, that propagated across the occipital cortex contralateral to the visual aura (Hadjikhani et al., 2001). The origin of the event was found in visual area V3A, and would often spread to visual area V1 and V2, but would not cross into the parietal cortex (Hadjikhani et al., 2001). These findings led to the recent suggestion that migraine aura is due to the abnormal firing of neurons characteristic with SD, in combination with vascular changes that accompany such an event (Buzzi and Moskowitz, 2005). Interestingly, recent links between SD and the pain associated with migraine have been made with the discovery that SD activates trigeminal neurons (Bolay et al., 2002) and matrix metalloproteinase (MMP)-9 (Gursoy-Ozdemir et al., 2004). The combination of these events could lead to the extravasation of pro-inflammatory peptides, resulting in inflammation of the meninges, which in turn may lead to pain that persists after SD events subside (Dalkara et al., 2006).

Is all SD the same?

The discussion above suggests that SD is critically involved in the enlargement of ischemic or traumatic injuries. However, strictly degenerative action of SD is difficult to reconcile with observations from migraine, since repetitive migraine does not lead to neuronal death or persistent neurological deficits. Indeed, some have even suggested that SD may be a protective mechanism which has been phylogenetically conserved as a way to silence neuronal activity and protect brain areas following some types of insult (Bures et al., 1984). This discrepancy raises a number of important questions about the mechanisms and consequences of SD, and whether different types of SD exist. Most researchers consider that, once initiated, all types of SD are generally the same, regardless of stimulus (Somjen, 2001). However, this view has been disputed (Tegtmeier, 1993), and it is possible that ionic shifts in non-detrimental SD are significantly different from SD involved in degeneration. Another question is whether mechanisms involved in the initiation of SD may be quite different with varying types of stimuli, and whether different conditions may underlie differential vulnerability of neurons following the triggering of identical SD events. Because of these important issues, there has been extensive prior work on the mechanisms of SD, in a variety of *in vivo* and *in vitro* preparations.

Models to study SD mechanisms

Early studies of SD used tetanic stimulation of exposed rabbit cortex (Leao, 1944; Leao and Morrison, 1945; Ochs et al., 1961; Bures et al., 1984), but this strong electrical stimulation often led to convulsive activity, which greatly complicates studies of SD mechanisms. Other methods that have been used include controlled mechanical stimuli, such as stroking the cortical surface, and dropping a weight or applying pressure or puncture to the tissue (Leao, 1944; Zachar and Zacharova, 1963; Kaube and Goadsby, 1994; Lambert et al., 1999). While all these procedures can generate SD, probably the most widely used stimulus for experimental SD has become localized applications of high K^+ concentrations (Nedergaard and Hansen, 1988; Kraig et al., 1991; Herreras et al., 1994; Busch et al., 1995; Busch et al., 1996; Osuga et al., 1997; Sonn and Mayevsky, 2000; Takano et al., 2007). Typical recent studies of *in vivo* SD utilize a cranial window or burr holes to apply drops of KCl solution directly onto the cortical surface. Because SD triggered by high K^+ has been shown to have no long lasting physiological changes (Buresova and Bures, 1969), it is possible that this procedure is a good model for SD involved in migraine, or other non-degenerative neurological conditions.

SD evoked by high K^+ has also been studied in brain slices and other tissues, most notably in a comprehensive series of studies utilizing isolated retinal preparations (Van Harreveld and Fifkova, 1970; Bures et al., 1984; Nedergaard and Hansen, 1988; Jing et al., 1993; Bahar et al., 2000; Martins-Ferreira et al., 2000; Smith et al., 2000; Richter et al., 2002; Takano et al., 2007). In all these cases, SD propagated with very similar

characteristics as SD generated *in vivo*, and these models have been important for studying SD mechanisms.

Recently, the Na^+/K^+ ATPase inhibitor ouabain has been introduced as a reliable trigger of SD. The effectiveness of this compound is probably related to its ability to increase extracellular K^+ concentrations (see below), and has the advantage that it is easy to control its application and reproducibility between preparations. The use of ouabain has been particularly important in hippocampal slices, where SD is robustly generated without complications of trauma or metabolic compromise (LaManna and Rosenthal, 1975; Haglund and Schwartzkroin, 1990; Basarsky et al., 1998; Obeidat and Andrew, 1998; Balestrino et al., 1999).

Because of the interest in PIDs in stroke injury, many studies of SD mechanisms have been undertaken using *in vitro* ischemia models. Either severe hypoxia, or deprivation of both oxygen and glucose (OGD) readily produces SD in brain slices (Jing et al., 1993; Tanaka et al., 1997; Obeidat and Andrew, 1998; Bahar et al., 2000; Obeidat et al., 2000). Removal of oxygen in hippocampal slices leads to SD over a period of minutes and, if oxygen is not very rapidly restored, leads to severe injury in these preparations (Tanaka et al., 1997; Obeidat and Andrew, 1998; Jarvis et al., 2001). To acknowledge the possibility that SD generated by ischemia is different from other forms of SD, the term "hypoxic SD" (HSD) has been used by some authors to describe events triggered in these ischemia models (Somjen, 2001).

Hypotheses regarding propagation of SD

Relatively soon after the first descriptions of SD, an influential hypothesis concerning the propagation of SD was formulated by Bernice Grafstein (Grafstein, 1956). This hypothesis rests on the observation that K^+ is released during intense action potential firing and accumulates in the extracellular space. It was proposed that excess K^+ then goes on to further depolarize the neurons that released the K^+, as well as cause neighboring neurons to depolarize, fire, and release more K^+. In this way, the K^+ leads to a feed-forward mechanism for SD propagation (Grafstein, 1956). While this hypothesis is still important for the field (Strong, 2005), there are some limitations with the idea that K^+ alone can be responsible for SD propagation. First, it was found that application of tetrodotoxin (TTX) did not prevent SD, despite its ability to block action potential firing (Sugaya et al., 1975). Second, in otherwise normal brain tissue, it does not appear that there is a significant change in $[K^+]$ ahead of the spreading front when SD is generated by localized K^+ applications, as would be expected if K^+ was a key to the propagation, rather than simply a consequence of the spreading event (Herreras and Somjen, 1993). Interestingly though, extracellular K^+ increases do appear to precede SD triggered by hypoxia (Hansen, 1985), suggesting that the mechanisms of initiation may be significantly different with different SD triggers.

A second hypothesis for SD propagation was proposed by Anthonie van Harreveld, in an effort to explain some of the shortcomings of the original K^+ hypothesis (VanHarreveld, 1959; Van Harreveld and Fifkova, 1970). Van Harreveld's hypothesis centered on the

release of the excitatory neurotransmitter glutamate, and was initially based on observations that substantial amounts of glutamate are released during SD, and that glutamate can induce SD when applied to the surface of the brain (Van Harreveld and Fifkova, 1970). Supporting the hypothesis is more recent evidence that glutamate levels increase in the extracellular space during SD, being released from both neurons and glia (Van Harreveld and Fifkova, 1970; Kimelberg et al., 1990; Szatkowski et al., 1990; Szerb, 1991; Iijima et al., 1992; Fabricius et al., 1993; Davies et al., 1995; Tanaka et al., 1999). Unlike the concern about the lack of effect of TTX on SD in Grafstein"s K^+ hypothesis (see above), TTX has no effect on the excitatory activity of glutamate, nor does it completely antagonize its release. However, evidence also exists that glutamate does not play nearly as prominent a role as predicted by Van Harreveld's glutamate hypothesis, as some studies have found that application of glutamate does not always reliably induce SD (do Carmo and Leao, 1972; Obrenovitch and Zilkha, 1995; Obrenovitch et al., 1996).

To take into account possible roles of both K^+ and glutamate, van Harreveld developed a revised hypothesis for SD propagation in 1978 (Van Harreveld, 1978) which basically allows for two distinct types of SD, one in which K^+ is responsible for propagation and another in which glutamate is a key mediator. This dual hypothesis has received much favor in the SD field, and has also been supported from computer modeling studies (Kager et al., 2000).

While K^+ and glutamate may be critically important for propagation of SD, these two mediators may not be reasonable candidates for therapeutic interventions to prevent SD. K^+ homeostasis is essential for normal neurophysiological function, and inhibition of normal glutamate mediated transmission is likely to have widespread deleterious effects on brain function. The possibility that only excessive K^+ accumulation, or only inappropriately strong AMPA- or NMDA-type receptor stimulation can be mitigated, without disrupting normal neurophysiological function is a theoretical possibility, that could have application to SD in the future. However, in the absence of such approaches, most efforts to identify blockers of SD have concentrated on identifying ion channels or other intracellular targets that may be involved in these events.

Ionic consequences of SD

Approaches to limit damage caused by SD, have concentrated on understanding the ionic consequences of SD propagation. A major redistribution of ions between the intracellular and extracellular spaces has been described as a consequence of an SD event. Upon arrival of SD, extracellular [K^+] rises rapidly (**Figure 1.3**), leading to neuronal depolarization (Vyskocil et al., 1972; Kraig and Nicholson, 1978; Nicholson et al., 1978; Paulson and Newman, 1987; Iadecola and Kraig, 1991; Canals et al., 2005). At the same time,

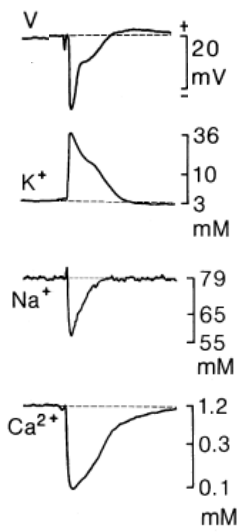

Figure 1.3: Examples of extracellular DC trace (V) and extracellular ionic changes (K^+, Na^+, Ca^{2+}) during SD induced by a train of local electronic stimuli in rat cerebellum. (Adapted from Martins-Ferreira et al., 2000.)

extracellular [Na^+], [Cl^-] and [Ca^{2+}] fall, implying very large fluxes of these ions into cells (Kraig and Nicholson, 1978; Nicholson et al., 1978).

Metabolic consequences of SD

Restoration of ionic homeostasis requires energy, and is expected to create substantial ATP demands following SD. Na^+ and K^+ levels must be restored by the activity of Na^+/K^+ ATPase, while Ca^{2+}ATPases are required for sequestration and extrusion of high Ca^{2+} levels. Consistent with these demands, dramatically increased oxidative and non-oxidative metabolic activity has been observed following SD. For example, it has been reported that SD is associated with increased mitochondrial oxidation (Rosenthal and Somjen, 1973; Lothman et al., 1975) and also increased lactate production in cerebral cortex (Cruz et al., 1999). Furthermore, O_2 consumption in the neocortex also increases dramatically (Mayevsky and Weiss, 1991) as do glucose uptake rates in rat cortical tissues (Shinohara et al., 1979) following SD.

Because of these metabolic demands, SD can be readily assessed by monitoring mitochondrial redox potential (Mayevsky et al., 1996; Rex et al., 1999; Hashimoto et al., 2000; Shuttleworth et al., 2003; Takano et al., 2007). A major electron donor for mitochondrial electron transport is NADH, which is fluorescent under UV excitation. Since the oxidized form (NAD^+) is non-fluorescent, mitochondrial metabolism can be monitored throughout brain regions during the spread of SD. This approach has been applied to the study of PIDs following ischemia *in vivo* (Strong et al., 2000) and also

using high K^+ applications to the exposed cortex of gerbils or mice (Hashimoto et al., 2000; Takano et al., 2007) or ouabain on acute hippocampal slices (Shuttleworth et al., 2003). In all these cases, the NAD(P)H signal results in a rapid, transient decrease associated with the DC deflection of SD, followed by more sustained increases, although it is unclear whether these post-SD changes reflect NAD(P)H changes due to decreased respiration or are an artifact of neuronal swelling, or both (Shuttleworth et al., 2003; Takano et al., 2007).

While the hypoxic SD event itself appears similar to the normoxic SD events described above (i.e. sharp drop in extracellular potential, propagation rate, etc.), some of the metabolic mechanisms leading to the event and the outcome of the depolarization appear to be quite different. For example, in hippocampal slice preparations mitochondrial inner membrane potential remained unchanged prior to SD elicited by high K^+ (Bahar et al., 2000). On the other hand, in response to hypoxia, it was shown that mitochondria slowly depolarize prior to SD (Bahar et al., 2000) and the inhibition of mitochondrial function which accompanies hypoxia likely contributes to SD (Gerich et al., 2006). It is clear that the energy substrates that are produced by oxidative phosphorylation are required to restore the dramatic ionic changes associated with SD and the inability to restore these gradients becomes detrimental to the tissue (Somjen, 2001). The damage that is caused by this event has been termed terminal (Tanaka et al., 1997), likely because of the difficulty to restore energy metabolism to a brain slice in an adequate amount of time (Somjen, 2001).

Studies have revealed that Ca^{2+} may be the critical ion in the irreversible damage during these events. In a study in which Ca^{2+} concentrations were reduced to 25% of normal, recovery of orthodromic population spikes following anoxic SD occurred in over 90% of slices (Roberts and Sick, 1988). Additionally, it appears that if Ca^{2+} levels can be reduced within 1.5 minutes of SD, complete recovery of function can be regained during OGD in hippocampal CA1 neurons of acute rat brain slices (Tanaka et al., 1999). Similar studies showing the critical nature of Ca^{2+} during OGD-induced SD have been described in rat hippocampal slices (Rader and Lanthorn, 1989; Yamamoto et al., 1997). High levels of Ca^{2+} can have dramatic effects on mitochondrial energy production as it has been shown that both the TCA cycle and ATP production from the electron transport chain can be inhibited by Ca^{2+} (Takeuchi et al., 1991).

Role of Ca^{2+} Channels in Spreading Depression

Interest in degenerative mechanisms have concentrated on Ca^{2+} influx, in part because of the establishment of the central role of Ca^{2+} overload in excitotoxic injury, and also because of the evidence that Ca^{2+} accumulation during extended hypoxic exposures clearly contributes to neuronal injury following SD (see above). It is clear that large amounts of Ca^{2+} leave the extracellular space during SD (Nicholson et al., 1978) and PIDs (Ohta et al., 2001), but there have been surprisingly few imaging studies that have examined the characteristics of neuronal and/or glial Ca^{2+} accumulation following SD. Basarsky and colleagues used bulk loading of the membrane permeable Ca^{2+} indicator Fura-2AM and found that a slow Ca^{2+} wave preceded SD, and concluded that this wave

was largely due to changes in astrocytic Ca^{2+} levels, but preventing this Ca^{2+} wave by removing extracellular Ca^{2+} did not affect the occurrence of SD (see below) (Basarsky et al., 1998). In addition to this pre-SD wave, there was a large Ca^{2+} increase that occurred concomitantly with SD induced by ouabain (Basarsky et al., 1998). While these bulk-loading studies give important information about the general accumulation of intracellular Ca^{2+}, this approach is generally unable to distinguish Ca^{2+} elevations in neuronal dendrites or other structures. Resolution of signals in such structures is increased by single-cell loading with Ca^{2+} indicators, and there appears to be only a single study in which this has been done to examine consequences of SD. In that study, single CA3 neurons in slice culture were filled with Fura-2 and SD was elicited by synaptic stimulation in sodium-acetate (NaAc) Ringer"s solution (Kunkler and Kraig, 2004). Upon arrival of SD, a transient Ca^{2+} increase occurred, with the highest Ca^{2+} levels being observed in the apical dendrites (Kunkler and Kraig, 2004), before Ca^{2+} levels throughout the neuron recovered to pre-stimulus levels. It is not known whether similar Ca^{2+} elevations are observed in other forms of SD, including those that may be detrimental to neuronal survival.

While the evidence above clearly supports a substantial translocation of Ca^{2+} from the extracellular space after the establishment of SD to intracellular compartments, there is considerable controversy about whether intracellular Ca^{2+} accumulation is actually required for the initiation and/or propagation of spreading depression. In the absence of detailed Ca^{2+} imaging studies of events prior to SD, information on the topic has been derived from a range of pharmacological and ion replacement studies.

The effects of Ca^{2+} removal on the spread of SD appears to depend on the preparation. For example, SD can be completely prevented by Ca^{2+} removal in retina (Martins-Ferreira et al., 1974; Nedergaard et al., 1995) and in young mouse neocortical slices (Peters et al., 2003). All of these studies used K^+ or mechanical stimulation as the trigger for SD (both of which have been shown to elicit reversible forms of SD). In contrast, removal of extracellular Ca^{2+} did not prevent the initiation of ouabain- or hypoxia-induced SD, measured electrically or optically (Basarsky et al., 1998; Balestrino et al., 1999; Bahar et al., 2000), however the kinetics of the optical events were significantly modified by Ca^{2+} removal; optical responses were faster to rise, and faster to fall without Ca^{2+} (Basarsky et al., 1998).

Perhaps because it has been shown that SD can still be produced in Ca^{2+}-free media (and the emphasis of this point in some recent influential reviews (e.g. Somjen, 2001)) there have been relatively few studies on the effects of Ca^{2+} channel blockers on SD. In a prior study using acutely-prepared hippocampal slices, Ni^{2+} and Co^{2+} were used to probe involvement of voltage-gated Ca^{2+} channels (VGCCs) and prevented or significantly delayed SD induced by hypoxia and prevented the propagation of high K^+-induced SD (Jing et al., 1993). *In vivo* studies showed that these same nonselective channel blockers were unable to prevent SD (Herreras et al., 1994). On the other hand, it was shown that application of specific blockers of different VGCCs (ω-agatoxin GIVA, ω-conotoxin IVA or nimodipine) resulted in a decrease of repetitive spreading depression in anesthetized rats following KCl administration (Richter et al., 2002). Moreover, a case

for P/Q type channel involvement has been made, showing that in mice with mutations in this channel, the threshold for SD was increased, in some cases by more than 10-fold (Ayata et al., 2000). Also, the use of P/Q antagonists blocked SD in hippocampal slice culture that was triggered by synaptic stimulation to area CA3 in NaAc Ringer"s solution (Kunkler and Kraig, 2004). These findings are interesting given the revelation that the P/Q type channel is mutated in some cases of familial hemiplegic migraine (Ophoff et al., 1996). Other Ca^{2+} channels are also likely involved, as the T- and L-type calcium channel blocker KB-2796 was reported to prolong the latency to SD following hypoxia in rat hippocampal slices (Akaike et al., 1993; Takagi et al., 1998).

Clearly, there are inconsistencies in the literature regarding the roles of Ca^{2+} and Ca^{2+} channels in SD and leaves the following question: How might Ca^{2+} channel blockers prevent SD in a way that is not mimicked by removal of extracellular Ca^{2+}? One possibility favored by Somjen (2001), is that some Ca^{2+} channel blockers may have non-specific effects, and block SD by mechanisms unrelated to Ca^{2+} influx. An alternative possibility, addressed in this thesis, is that influx of a different cation (Zn^{2+}) through Ca^{2+} channels could be critically involved in SD. The basis for this suggestion is addressed below.

1.3 Zinc and neuronal injury

Physiological roles for Zn^{2+}

The brain may have the highest Zn^{2+} content of all organs, having an overall concentration of ~150μM (Weiss et al., 2000). The importance of Zn^{2+} for maintenance of protein structure and function has been appreciated for almost 70 years, beginning with the discovery that Zn^{2+} is critically involved with the enzyme carbonic anhydrase (Keilin and Mann, 1940). This finding opened the door for the descriptions of over 300 such Zn^{2+}-dependent proteins which have been termed metalloenzymes. In most of these proteins, Zn^{2+} serves a catalytic role, involved in such reactions ranging from the formation of hydroxide ions at neutral pH to Lewis Acid catalysis (Choi and Koh, 1998). In addition to catalyzing reactions, Zn^{2+} often serves a structural role as well, particularly in stabilizing active peptide conformations.

Zn^{2+} has also been shown to bind to proteins other than metalloenzymes. In particular, it plays a crucial role in proteins involved with gene regulation (O'Halloran, 1993). The discovery of these proteins with structural Zn^{2+} binding domains (termed "Zn^{2+} fingers"), led to the delineation of similar domains in many transcription factors including Zn^{2+} twists in steroid receptors and Zn^{2+} clusters in the glucose metabolism activator GAL4 (Vallee et al., 1991).

In the central nervous system, the role for Zn^{2+} goes beyond protein interaction. The distribution of Zn^{2+} in the brain is not homogenous as there appear to be higher

concentrations in gray matter compared to white matter. Furthermore, the highest concentrations have been reported in the hippocampus, amygdala and neocortex (Frederickson et al., 1989). An overwhelming majority of Zn^{2+} in the brain is normally bound to proteins called metallothioneins, which serve a crucial buffering role within the cytosol of neurons (Aschner et al., 1997). Because of this, free Zn^{2+} is usually maintained at extremely low levels in the CNS. Free Zn^{2+} can be visualized using histochemical stains such as Timm‟s or by use of Zn^{2+}-sensitive fluorescent dyes and has been referred to as "histochemically reactive" or "chelatable" Zn^{2+} (Frederickson et al., 1989; Kay, 2003).

In 1984, it was discovered that Zn^{2+} can be synaptically released from excitatory neurons (Assaf and Chung, 1984; Howell et al., 1984). It was later found that a family of Zn^{2+} transporters is present in the presynaptic glutamatergic vesicles of these neurons (Palmiter et al., 1996; Wenzel et al., 1997). It has been estimated that these vesicles contain millimolar amounts of Zn^{2+} and strong activation of nerve terminals can result in transient local Zn^{2+} concentrations in the hundreds of micromolar range (Assaf and Chung, 1984; Howell et al., 1984; Qian and Noebels, 2005).

Zn^{2+} and pathogenesis

The first description that Zn^{2+} can have deleterious effects on neurons came in 1978 when Gaskin and colleagues showed that exposing organotypic cultures of dorsal root ganglion cells to 1mM Zn^{2+} disrupted microtubular assemblies and caused "degenerative changes"

to some neurons (Gaskin et al., 1978). The first suggestion that endogenous Zn^{2+} may contribute to neurodegenerative diseases came a few years later when it was calculated that enough Zn^{2+} may be released from hippocampal synapses to cause cell death (Assaf and Chung, 1984). Experimental evidence supporting this idea came from studies where perforant path stimulation led to the loss of interneurons and CA3 pyramidal cells (Sloviter, 1985). Zn^{2+} is normally present in high amounts in mossy fiber terminals projecting to these cells and is revealed by robust Timm‟s staining. Following strong repetitive stimulation, Timm‟s staining increases relatively in degenerating neurons, leading to the suggestion that release of synaptic Zn^{2+} was responsible for neuronal injury (Sloviter, 1985). Several studies followed to evaluate Zn^{2+} toxicity in cortical and hippocampal cell culture (Yokoyama et al., 1986; Choi et al., 1988; Koh et al., 1990; Weiss et al., 1993; Koh and Choi, 1994; Lobner et al., 2000) and it was considered that Zn^{2+} toxicity may share many aspects with the well established phenomenon of Ca^{2+}-dependent excitotoxicity (see Section 1.1).

In 1996, it was revealed that Zn^{2+} contributes to neuronal death in a transient global ischemia model (Koh et al., 1996). In this seminal paper it was first shown that chelation of extracellular Zn^{2+} by the cell-impermeant Zn^{2+} chelator CaEDTA blocked cell death when present in the bathing medium of cultured cortical neurons exposed to Zn^{2+} (Koh et al., 1996). When expanded to *in vivo* experiments, it was revealed that following a 10 minute forebrain ischemia, Zn^{2+} accumulation occured in hippocampal neurons prior to neuronal degeneration (assessed by acid fuchsin staining). Furthermore, injection of CaEDTA into lateral ventricles prior to the transient ischemia procedure significantly

reduced neurodegeneration (Koh et al., 1996), providing the first clear demonstration that release of endogenous Zn^{2+} in the brain could be a critical contributor to stroke injury. This idea was expanded upon recently when it was shown that application of CaEDTA hours after MCAO continued to be effective at limiting injury (Calderone et al., 2004).

The mechanisms through which Zn^{2+} may be toxic have been examined extensively. The idea that Zn^{2+} moves from pre- to postsynaptic neurons has been termed "Zn^{2+} translocation" (Frederickson et al., 1989). The mechanism of the extracellular Zn^{2+} accumulation is unknown, but is likely to be made up at least in part by presynaptic release (Assaf and Chung, 1984; Howell et al., 1984; Thompson et al., 2000; Qian and Noebels, 2005). It is also possible that other non-synaptic extracellular sources of Zn^{2+} contribute (Lee et al., 2000b; Kay, 2003). Nonetheless, there is clear evidence that Zn^{2+} enters neurons from extracellular sources as described below.

Zn^{2+} enters neurons through Ca^{2+} pathways

Once Zn^{2+} is in the extracellular space, it appears that it can enter neurons via a number of routes (**Figure 1.4**). Studies using cultured neurons indicated that Zn^{2+} can enter through a subpopulation of AMPA glutamate receptors which are Ca^{2+} permeable (Weiss et al., 1993; Yin and Weiss, 1995; Weiss and Sensi, 2000). Zn^{2+} inhibits NMDA glutamate receptors (Mayer and Westbrook, 1987; Peters et al., 1987; Christine and Choi, 1990; Legendre and Westbrook, 1990) but it also appears that Zn^{2+} can also enter neurons through these channels (Koh and Choi, 1994). These routes may be particularly relevant

given that Zn^{2+} is apparently co-released with glutamate (Assaf and Chung, 1984; Howell et al., 1984; Vogt et al., 2000). Zn^{2+} has also been suggested to enter neurons via Na^{+}/Ca^{2+} exchangers (Sensi et al., 1997).

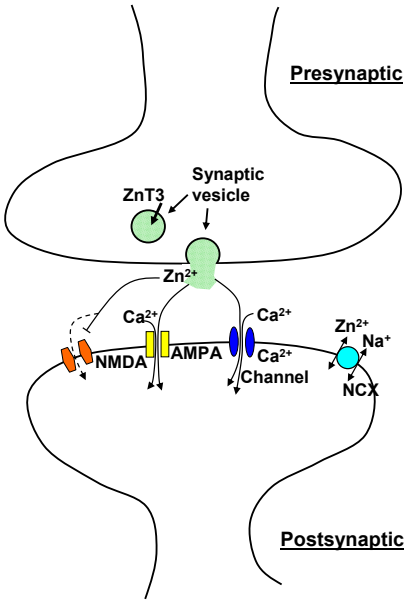

Figure 1.4: Schematic representation of Zn^{2+} influx pathways which include Ca^{2+}-permeable AMPA receptors, L- and N-type Ca^{2+} channels and the Na^{+}/Ca^{2+} exchanger (NCX) and possibly NMDA receptors. (Adapted from Weiss et al., 2000.)

Another route for Zn^{2+} is voltage-gated Ca^{2+} channels. An important initial study showed an increase in intracellular Zn^{2+} indicator fluorescence following depolarization of cultured cortical neurons. Fluorescence was attenuated by the application of La^{3+} or diltiazem (Weiss et al., 1993) suggesting influx via L-type channels. Support for the specific involvement of L-type and, to a lesser extent, N-type channels soon followed as Zn^{2+} toxicity in cultured cortical neurons was reduced by nimodipine (L-type blocker) and ω-conotoxin GVIA (N-type blocker) (Freund and Reddig, 1994; Kerchner et al., 2000). More recently, L-type channels have been suggested to be a prominent route of Zn^{2+} influx following K^{+}-induced depolarization of cultured cortical neurons (Sheline et al., 2002).

Intracellular sources for pathogenic Zn^{2+}

In addition to extracellular sources of injurious Zn^{2+}, an emerging role for intracellular Zn^{2+} release has also been described (Sensi and Jeng, 2004). The first evidence for this

came from observations that mice lacking the vesicular Zn^{2+} transporter (ZnT-3 knock-out mice) experienced Zn^{2+} accumulation and degeneration in CA1 and CA3 neurons in response to kainate induced seizures (Lee et al., 2000b). While this report could not specifically comment on the origins of the Zn^{2+} (intracellular vs. extracellular), other data suggests that Zn^{2+} can be released from metallothioneins (MT) in response to ischemic injury. In a similar study as above in which mice were subjected to kainate-induced seizures, knocking out both ZnT-3 and the most prominent MT isoform in neurons (MT-3) provided substantial protection in CA1 neurons (Cole et al., 2000). Furthermore, under conditions that favor Zn^{2+} release from MTs, apoptotic death was reported in cortical cultures (Aizenman et al., 2000). This injury was attenuated by the Zn^{2+}-specific chelator N,N,N‘,N‘-tetrakis-(2-pyridylmethyl)ethylenediamine (TPEN) and other strategies to reduce Zn^{2+} accumulation (Aizenman et al., 2000). Additional evidence supports the idea that MTs are able to release Zn^{2+} under conditions of oxidative stress, as seen during ischemia (Sensi and Jeng, 2004).

1.4 Consequences of intracellular Zn^{2+} increases

The study of the mechanisms through which Zn^{2+} is toxic to neurons is still relatively new, and it is not yet clear which mechanism(s) are most important in ischemic injury. It has been described that Zn^{2+} may impair the important glycolytic enzymes glyceraldahyde-3-phosphate dehydrogenase (GAPDH) (Ikeda et al., 1980) and phosphofructokinase (Krotkiewska and Banas, 1992). Particular attention has been placed on GAPDH recently because elevated Zn^{2+} levels were shown to increase metabolites upstream of GAPDH and deplete downstream intermediates in cultured

cortical neurons (Sheline et al., 2000). Furthermore, cell death was attenuated by the addition of downstream substrates such as pyruvate. While these results clearly show a role for Zn^{2+} inhibition of glycolysis, some have questioned whether this would translate to an *in vivo* setting where energy in the brain comes mostly from mitochondrial oxidative phosphorylation, whereas cultured neurons may rely heavily on glycolysis (Dineley et al., 2003).

In light of this, it is important to note that Zn^{2+} can also alter mitochondrial energy production. In studies of isolated liver mitochondria, it was found that Zn^{2+} inhibits the α-ketoglutarate dehydrogenase complex of the TCA cycle (Brown et al., 2000). Furthermore, it has been known for decades that Zn^{2+} inhibits the electron transport chain, with the most sensitive site thought to be the cytochrome bc_1 complex (Skulachev et al., 1967; Nicholls and Malviya, 1968; Kleiner, 1974; Lorusso et al., 1991; Link and von Jagow, 1995). While most of this early work was performed in isolated heart mitochondria, similar results have been reported recently from isolated rat brain mitochondria (Dineley et al., 2005). Furthermore, several studies have reported that the inner mitochondrial membrane potential dissipates in response to Zn^{2+} influx in cultured neurons (Sensi et al., 1999; Sensi et al., 2003; Dineley et al., 2005). This depolarization of mitochondrial membrane is thought to be in response to Zn^{2+} entering neurons and inhibiting the electron transport chain.

In addition to inhibiting energy production, there is evidence that Zn^{2+} induces accumulation of reactive oxygen species (ROS) (Kim et al., 1999; Noh et al., 1999; Sensi

et al., 1999; Sensi et al., 2003). ROS production is likely due to the inhibition of the same mitochondrial enzymes mentioned above (Dineley et al., 2003), but other sources of ROS, such as the superoxide generating enzyme NADPH oxidase, have been suggested to be activated by Zn^{2+} from studies of cultured neurons and astrocytes (Noh and Koh, 2000).

In light of the growing evidence which suggests that mitochondrial dysfunction may contribute to the induction of SD (Bahar et al., 2000; Gerich et al., 2006), one has to wonder if the ability of Zn^{2+} to enter neurons and disrupt energy metabolism plays a role in SD.

1.5 Interaction of Ca^{2+} and Zn^{2+} in Mitochondria

For nearly two decades, the idea that Ca^{2+} is continuously cycled across the mitochondrial membrane has been well studied (Crompton et al., 1978; Crompton and Heid, 1978; Nicholls and Chalmers, 2004). It is apparent that mitochondria have a complex system through which to buffer large amounts of Ca^{2+}, and this contributes critically to the regulation of appropriate cytoplasmic Ca^{2+} levels (Rossi and Lehninger, 1964; Nicholls, 1978).

Once Ca^{2+} enters mitochondria, it has been shown that its accumulation can significantly stimulate dehydrogenases of the TCA cycle, including pyruvate dehydrogenase, 2-oxoglutarate dehydrogenase, and isocitrate dehydrogenase (Denton and McCormack, 1990; McCormack et al., 1990). The activation of each of these dehydrogenases directly

leads to the generation of NADH and such activation has been proposed to link neuronal activation with increased mitochondrial metabolism. This process is likely beneficial to neurons when intramitochondrial Ca^{2+} is relatively low (Nicholls and Budd, 2000; Nicholls and Chalmers, 2004). However, when cytoplasmic free Ca^{2+} overwhelms active transport of the ion out of the cell, mitochondria will act as a „sink" and take up large amounts of Ca^{2+} (Nicholls, 1985). When this occurs, this large Ca^{2+} sequestration can interfere with the TCA cycle and uncouple electron transport (Takeuchi et al., 1991) leading the demise of the cell (Nicholls and Budd, 2000).

There are increasing indications that both Ca^{2+} and Zn^{2+} are capable of entering mitochondria and causing mitochondrial depolarization (Sensi et al., 2003; Nicholls and Chalmers, 2004). Both of these ions likely enter the mitochondria via the uniporter, though it has been suggested that Zn^{2+} can enter mitochondria through non-uniporter routes as well (Malaiyandi et al., 2005). While mitochondrial uptake of Ca^{2+} and it positive and negative effects on metabolism have been studied much more extensively than that of Zn^{2+}, the interplay between these ions presents an intriguing question.

Recent work has suggested that Zn^{2+} is much more toxic to neuronal mitochondria than Ca^{2+} in studies carried out in cultured cortical neurons (Sensi et al., 2003). As discussed above, Zn^{2+} can be taken up by mitochondria and negatively effect TCA cycle activity as well as the efficiency of the electron transport chain (Dineley et al., 2003). Indeed, it was found that the same inhibitory effects on mitochondria were elicited by far smaller amounts of Zn^{2+} (40pmol/mg) than Ca^{2+} (50nmol/mg) (Sensi et al., 2003). Thus, it

appears that small accumulations of Zn^{2+} within mitochondria may strongly negatively influence mitochondrial metabolism.

No studies have been carried out that investigate the effects of Ca^{2+} and Zn^{2+} on mitochondrial function in the same preparation. One could hypothesize that small fluxes of both of these ions into neuronal mitochondria would have opposing effects on energy production. It would be interesting to test if the actions of one ion would overpower the other, especially in the setting of SD where alterations in mitochondrial function may play a role (Bahar et al., 2000; Hashimoto et al., 2000; Gerich et al., 2006).

1.6 Prevention of SD and neuroprotection

Despite the tremendous advances made in the last two decades in understanding mechanisms of neuronal death, there remains a critical lack of neuroprotective compounds available for post-stroke therapy (Lee et al., 1999). At the same time, growing evidence indicates that the occurrence of SD-like events (PIDs) in the penumbra contribute to cell death following stroke (Strong et al., 2002; Hartings et al., 2003), and since these events contribute to damage in the hours and days following ischemia, they appear to be very good targets for therapeutic intervention. In fact, over a decade ago, it was suggested that reducing infarction of the penumbra would increase a patient‟s potential for recovery (Furlan et al., 1996) and the importance of the search for drug therapy to prevent SD (and hence PIDs) has been emphasized recently, as powerful tools in the fight against stroke damage (Jarvis et al., 2001; Anderson and Andrew, 2002; Anderson et al., 2005). While there are some treatments that can decrease the occurrence

of SD (TTX, NMDA antagonists), these drugs are not good candidates for clinical use, because of their own deleterious effects on CNS function. Anderson and colleagues described the use of sigma-1 receptor agonists at concentrations that effectively block or delay SD in response to OGD or ouabain without significantly altering neuronal function (Anderson et al., 2005). In this study using neocortical and hippocampal slices, it was reported that the normal cell damage that is associated with SD was prevented. This is an exciting development, but the mechanism of action for sigma-1 receptor agonists is not yet known, and the agents were only tested with quite brief stimuli (Bahar et al., 2000; Obeidat et al., 2000; Jarvis et al., 2001; Anderson and Andrew, 2002; Anderson et al., 2005). It remains unclear whether these approaches would be useful with more extended challenges. Nonetheless, this idea that blocking SD is potentially beneficial in a clinical setting is particularly stimulating and should be explored further as a neuroprotective strategy.

1.7 Goals of this Study

This study is designed to assess the relative roles of Ca^{2+} and Zn^{2+} in a model of acute neuronal injury. Specifically, the model of spreading depression is used, as it may be particularly relevant in the expansion of neuronal damage following stroke. Experiments for the study test the overall hypothesis that: *Accumulation of endogenous Zn^{2+} can initiate Ca^{2+}-dependent neuronal injury.*

These studies focus on hippocampal CA1 neurons in acute slices, as it has been suggested that these neurons are particularly susceptible to SD (Somjen, 2001). This is likely due to

the architecture of the neurons in this brain region, and also the relatively small extracellular space that allows for depolarizing agents such as K^+ to attain high local concentrations rapidly (Perez-Pinzon et al., 1995; Somjen, 2001). The first sets of studies address mechanisms of SD using the inhibitor of Na^+/K^+ ATPase, ouabain. This inhibitor provides a robust and reliable SD, without the additional complications of metabolic compromise, and is routinely used for hippocampal slice preparations (Basarsky et al., 1998; Obeidat and Andrew, 1998; Balestrino et al., 1999; Anderson et al., 2005).

The studies in Chapter 2 examine the role of Ca^{2+} channels during SD, which is currently a controversial subject in the SD literature. Given that removal of Ca^{2+} from extracellular media often has little or no effect on SD, these studies test the hypothesis that *Zn^{2+} influx contributes to the initiation and/or propagation of SD.* This hypothesis is assessed using imaging of Ca^{2+}, Zn^{2+} and mitochondrial potential, as well as pharmacological manipulation of Ca^{2+} channels and chelation of these two cations.

Experiments in Chapter 3 consider the interaction that Zn^{2+} could have with Ca^{2+}. Mitochondrial dysfunction appears to play a role in the initiation of SD, and therefore these studies examine the hypothesis that *Ca^{2+} and Zn^{2+} have detrimental effects on mitochondrial function prior to SD*. Imaging of mitochondrial autofluorescence and single cell Ca^{2+} imaging were used to test this hypothesis.

An exciting possibility has emerged that blocking SD may be a key to preventing neuronal injury following stroke, however it is not yet known whether block of SD is

always sufficient to prevent acute cell death. Therefore, studies in Chapter 4 are designed to test the hypothesis that *blocking SD will always prevent neuronal damage.* To test this hypothesis, a reliable method of blocking SD is required, then single cell Ca^{2+} imaging will be used to assess the ultimate fate of neurons following extended ouabain exposures.

Finally, Chapter 5 seeks to expand on the mechanistic information from the previous chapters, to address the question of whether Zn^{2+}-dependent mechanisms contribute to models of SD involved in CNS pathologies. A comparison is made between SD evoked by localized application of high K^+ solution and exposing brain slices to oxygen-glucose deprivation (OGD). While these two stimuli produce SD-like events that resemble each other, there is clearly a difference in the metabolic state of the neurons leading up to such events. Of particular interest is the idea that Zn^{2+} may play a role in SD. If it is found that Zn^{2+} does contribute to SD elicited by ouabain, a final set of studies examine the hypothesis that *Zn^{2+} contributes to all forms of SD.* Similar methods are used as above to examine whether different stimuli produce relatively similar SD events or whether the mechanisms involved in the initiation or propagation of such events are fundamentally different.

Taken together, this group of studies should build on previous work in the SD literature, and help resolve some current controversies concerning the mechanisms of SD initiation and propagation, as well as the ultimate fate of neurons regarding SD. If Zn^{2+} is found to play a role in SD, this could potentially be of considerable value for development of

interventions for stroke damage and could also unite the emerging fields of peri-infarct depolarization injury and Zn^{2+} toxicity.

2. Zn^{2+} Influx via Calcium Channels Can Trigger Spreading Depression in Brain Slices.

R.M. Dietz[1], J. H. Weiss[2] & C.W. Shuttleworth[1]

[1]Department of Neurosciences

University of New Mexico School of Medicine

Albuquerque NM 87131

[2]Departments of Neurology & Anatomy and Neurobiology

University of California Irvine,

Irvine, CA 92697

(In review; "Journal of Neuroscience")

2.1 Abstract

Spreading depression (SD) is wave of profound depolarization that propagates throughout brain tissue and can contribute to the spread of injury following stroke or traumatic insults. Massive Ca^{2+} influx occurs after SD has swept through a region, and contributes to neuronal cell death. However, the role of Ca^{2+} in the initiation and/or propagation of SD is not well understood. We used the Na^{+}/K^{+} ATPase inhibitor ouabain to generate SD in murine hippocampal slices. Under conditions where adenosine A1 receptors were activated, SD was always prevented by L-type Ca^{2+} channel blockers. A slow mitochondrial depolarization observed prior to SD was also abolished by L-type channel block, however Ca^{2+} influx was not responsible for these L-type effects. Cytosolic Ca^{2+} increases were not detectable in CA1 neurons prior to SD, and removal of extracellular Ca^{2+} did not prevent mitochondrial depolarization, nor did it prevent SD. In contrast, cytosolic Zn^{2+} increases were observed in CA1 neurons prior to SD, and L-type channel block prevented the intracellular Zn^{2+} rises. Zn^{2+} accumulation also contributed substantially to initial mitochondrial depolarizations. Selective chelation of Zn^{2+} abolished SD, implying that Zn^{2+} entry can play a critical contributory role to the generation of SD. These results imply that flux of endogenous Zn^{2+} can explain the effects of Ca^{2+} channel blockade on SD, and also identify Zn^{2+} as a new target for the block of spreading depolarizations following brain injury.

2.2 Introduction

Spreading depression (SD) is characterized as a wave of severe depolarization that spreads throughout CNS tissues at a rate of several millimeters per second (Somjen, 2001; Smith et al., 2006). SD can be triggered by brief exposures to elevated extracellular K^+, strong synaptic stimulation, inhibitors of Na^+/K^+ ATPase activity or by hypoxia (Somjen, 2001). SD-like events are thought to be involved in the spread of injury following ischemic and traumatic brain injuries, and also contribute to migraine aura (Hossmann, 1996; Hadjikhani et al., 2001; Somjen, 2001; Hartings et al., 2003; Church and Andrew, 2005; Umegaki et al., 2005).

In injury models, it is clear that large Ca^{2+} increases that persist following SD contribute to neuronal death (Somjen, 2001). In contrast, most studies have concluded that Ca^{2+} accumulation is not required for initiation or progression of the SD event itself, since removal of extracellular Ca^{2+} generally does not prevent SD (Ramos, 1975; Young and Somjen, 1992; Basarsky et al., 1998; Somjen, 2001). Despite these observations, the non-specific Ca^{2+} channel blockers Ni^{2+} and Co^{2+} delayed or prevented SD propagation in hippocampal slices (Jing et al., 1993), and P/Q-type channel blockers prevented SD in slice cultures (Kunkler and Kraig, 2004). We thus wondered how Ca^{2+} channel blockers might prevent SD in a way that is not mimicked by removal of extracellular Ca^{2+}, and considered the possibility that flux of Zn^{2+} (rather than Ca^{2+}) through voltage gated Ca^{2+} channels might be a critical trigger of SD.

Zn^{2+} is an abundant ion in the brain and in many regions Zn^{2+} is present in presynaptic vesicles where it appears to be released with glutamate in response to synaptic activation (Assaf and Chung, 1984; Howell et al., 1984; Thompson et al., 2000; Qian and Noebels, 2005). Zn^{2+} can enter cells through several routes, including Ca^{2+} channels, and induce neuronal injury (Koh et al., 1996; Choi and Koh, 1998; Weiss et al., 2000; Calderone et al., 2004). Zn^{2+} can accumulate in mitochondria (Sensi et al., 1999; Jiang et al., 2001; Malaiyandi et al., 2005), and mitochondrial dysfunction has in turn been suggested to contribute to the induction of SD (Bahar et al., 2000; Hashimoto et al., 2000; Gerich et al., 2006). Bahar and colleagues (Bahar et al., 2000) demonstrated a large and rapid mitochondrial depolarization coincident with SD, but also noted that there was a slow progressive mitochondrial depolarization prior to the onset of SD. Since these effects were not prevented by the removal of extracellular Ca^{2+} (Bahar et al., 2000), we also examined the possibility that mitochondrial depolarization prior to SD, could instead be a consequence of Zn^{2+} increases.

Here we report conditions under which L-type Ca^{2+} channel activation is essential for ouabain-induced SD, and also for the mitochondrial depolarization that precedes SD. Further observations that Zn^{2+} entry through L-type channels contributes to the mitochondrial depolarization and that chelation of Zn^{2+} (but not Ca^{2+}) prevents SD provide compelling new evidence that influx of Zn^{2+} rather than Ca^{2+} can be critically responsible for the onset of SD.

2.3 Materials and Methods

Slice preparation

Male FVB/N mice were obtained from Harlan (Bar Harbor, ME) and were housed in standard conditions (12hr/12hr light/dark cycle) before sacrifice at 4-6 weeks of age. All procedures were carried out in accordance with the National Institute of Health guidelines for the humane treatment of laboratory animals, and the protocol for these procedures was reviewed annually by the Institutional Animal Care and Use Committee at the University of New Mexico School of Medicine. Acute slices were prepared as previously described (Shuttleworth and Connor, 2001). After cutting and holding for 1 hour at 35^{o}C, artificial cerebrospinal fluid (ACSF) was changed, and slices were held at room temperature until used for recording. Individual slices were transferred to the recording chamber, and were superfused with oxygenated ACSF at 2 ml/min.

Recording

Extracellular measurements of DC potentials were made using borosilicate glass microelectrodes, filled with ACSF (~5MΩ) and placed in stratum radiatum approximately 50 μm below the surface of the slice. Ca^{2+} and Zn^{2+} measurements were made from individual CA1 pyramidal neurons. Neurons were impaled with glass microelectrodes, and were microinjected with a fluorescent indicators for Ca^{2+} (Fura-2 or Fura-6F) and/or Zn^{2+} indicator (FluoZin-3). The procedures for recording/indicator injection were as described previously (Shuttleworth and Connor, 2001), with some

modifications. Impalements were made using the step function of a Sutter manipulator (225, Sutter Instruments), and neurons were visualized and imaged using a water immersion objective (40X, NA 0.8, Olympus). In all experiments, the recording/filling electrode was carefully withdrawn, and the cell allowed to recover for 20 min before ouabain exposure. Fura-2 and Fura-6F, were excited at 350/380 nm, and emission detected at 510/50 nm using a monochromator-based imaging system (Till Photonics). FluoZin-3 was excited at 495 nm, and emission detected at 535/50nm. When near-simultaneous Fura-6F/FluoZin-3 measurements were made, co-loaded neurons were excited sequentially at 350/380/495nm and emission of both indicators was detected at 535/50nm. Estimation of Ca^{2+} concentration, and preparation of figures was as previously described (Shuttleworth and Connor, 2001).

Changes in mitochondrial potential were made using slices bulk-loaded with Rh123. Slices were exposed to 26 μM Rh123 for 30 minutes at room temperature in a holding chamber prior to transfer to recording platform where the slices were washed with ACSF for 30 minutes prior to experimentation. Under these conditions, Rh123 is in the "quenched" mode, where fluorescence increases are interpreted as mitochondrial depolarizations. Because of its relatively slow kinetics, mitochondrial Rh123 signals are not significantly complicated by plasma membrane effects under these conditions (Duchen et al., 2003).

Reagents and solutions

Slice cutting solution contained (in mM): 2 KCl, 1.25 NaH_2PO_4, 6 $MgSO_4$, 26 $NaHCO_3$, 0.2 $CaCl_2$, 10 glucose, 220 sucrose and 0.43 ketamine). ACSF contained in mM: 126 NaCl, 2 KCl, 1.25 NaH_2PO_4, 1 $MgSO_4$, 26 $NaHCO_3$, 2 $CaCl_2$, and 10 glucose and was equilibrated with 95%O_2 / 5%CO_2). Cutting and recording solutions were both 315-320 mOsm. Fluorescent indicators and N,N,N′,N′-tetrakis(2-pyridylmethyl)ethylenediamine (TPEN) were obtained from Invitrogen (Carlsbad, CA), and all other reagents were obtained from Sigma (St. Louis, MO). Ouabain was prepared as a 15 mM stock in H_2O for 30 μM experiments. Nimodipine and nicardipine were prepared as 10 mM stock in ethanol. DPCPX was prepared as a 100 μM stock in EtOH. All other chemicals were diluted in ACSF. Zero-Ca^{2+} experiments used ACSF with the $CaCl_2$ replaced by $MgSO_4$, and 0.5 mM EGTA or 1 mM BAPTA was added. In all experiments using nimodipine and ion chelators, slices were incubated in solution containing the molecule for 30 min prior to ouabain application and solutions were warmed slowly during this time to 30°C or 35°C where appropriate.

Statistical Analysis

Significant differences between group data was evaluated using paired or unpaired Student‟s t-tests. Bonferroni's multiple comparison test was used for post-hoc analysis where the effects of multiple drug treatments were compared against each other.

Dunnett's multiple comparison test was used for post-hoc comparisons of multiple time points of single drug treatment, when compared with responses immediately prior to drug treatment. $p<0.05$ was considered significant in all cases.

2.4 Results

L-type channels can contribute to SD.

A low concentration of ouabain (30 μM) reliably produced SD in acutely-prepared hippocampal slices maintained at 35°C (7.9±0.9 min latency, n=13). **Figure 2.1A** shows an example of the rapid negative voltage deflection recorded with an extracellular electrode. This event is characteristic of SD, and was confirmed in all experiments by visualization a spreading wave of tissue autofluorescence decrease that was coincident with the voltage deflection (see Hashimoto et al., 2000; Shuttleworth et al., 2003). Figure 2.1B shows that an L-type Ca^{2+} channel blocker (nimodipine, 10 μM) prevented SD in most preparations tested at 35°C. The effectiveness of nimodipine was dependent on concomitant adenosine A1 receptor activation. When slices were pre-treated with an A1 receptor agonist (N^6-cyclopentyladenosine, CPA, 300 nM), nimodipine always blocked SD. Conversely, when slices were pre-treated with an A1 receptor antagonist (DPCPX; 8-cyclopentyl-1,3-dipropylxanthine; 100 nM), nimodipine never prevented SD and the latency to SD (8.8±0.8 min; n=6) was similar to controls (see above, p=0.50). A dependence on endogenous adenosine receptor activation was supported by experiments at a lower recording temperature (30°C), under which conditions extracellular adenosine accumulation is reported to be reduced (Masino and Dunwiddie, 1999). At 30°C, SD was

little affected by nimodipine, unless the exogenous A1 receptor agonist was co-applied. In six slices, nimodipine blocked SD one time in ouabain alone, but blocked SD in 6/6 slices when pre-treated with CPA. Control experiments showed that CPA or DPCPX alone did not influence the propagation rate or time to SD onset (n=6 each).

These effects of nimodipine were mimicked by an alternative L-type Ca^{2+} channel blocker (nicardipine, 10 μM). Thus in the presence of CPA at 35°C, nicardipine prevented SD in 6/6 slices, and was without effect on SD when A1 receptors were blocked (DPCPX, 6/6 slices).

The following studies investigated mechanisms that link L-type Ca^{2+} function to SD initiation. Except where noted, recording conditions were chosen that emphasized a contribution of L-type channels; i.e. experiments were done at 35°C, and CPA was included to "clamp" slices at a high level of adenosine A1 receptor activation, and thereby minimize the impact of slice-slice variation in endogenous adenosine levels.

L-type flux causes mitochondrial depolarization prior to SD

Changes in mitochondrial inner membrane potential (Ψm) after ouabain exposure were assessed in slices loaded with Rh123. Rh123 was used in the quenched mode, where fluorescence increases represent Ψm depolarization (see Methods). **Figure 2.2** shows results from stratum pyramidale, where a large and rapid ΔΨm depolarization was observed coincident with the onset of SD, but in addition, a significant progressive

depolarization was observed for approximately 5 min before SD (Figure 2.2A). Figure 2.2B shows that nimodipine prevented both phases of ΔΨm changes during ouabain exposures. The slow initial ΔΨm depolarization was abolished, and since SD was blocked, the large ΔΨm depolarization associated with SD was prevented.

Comparison of neuronal Ca^{2+} and Zn^{2+} dynamics

We next examined whether intracellular Ca^{2+} and/or Zn^{2+} increases were likely responsible for the events described above. **Figure 2.3A** shows an example of simultaneous measurements of intracellular Zn^{2+} and Ca^{2+} increases in the soma of a CA1 neuron co-loaded with the high affinity Zn^{2+} indicator FluoZin-3 and the low affinity Ca^{2+} indicator Fura-6F. Prior to the onset of SD, there was no detectable increase in cytosolic Ca^{2+} levels in individual CA1 neurons. In contrast, there was a significant increase in neuronal Zn^{2+} levels, that was seen for approximately 5 min before SD propagated through the region. Coincident with the onset of SD, large increases in both Ca^{2+} and Zn^{2+} were detected. Since Fura-6F might miss small Ca^{2+} elevations prior to SD, experiments were repeated in neurons loaded with only the high-affinity indicator Fura-2. Figure 2.3B shows there was no detectable cytosolic Ca^{2+} elevation prior to SD measured in these Fura-2-loaded neurons, in contrast to FluoZin-3 fluorescence increases.

Figure 2.4 shows that the Zn^{2+}-selective chelator TPEN (50 μM) abolished ouabain-induced FluoZin-3 increases prior to SD and prevented SD in all preparations tested. These results suggest that Zn^{2+}, rather than Ca^{2+} increases are required for SD initiation.

Consistent with this suggestion, superfusion of slices with nominally Ca^{2+}-free ACSF did not prevent SD in 6/6 slices tested.

Sources of Zn^{2+} and strong correlation of early Zn^{2+} rises with subsequent SD induction

TPEN is membrane permeable, and thus can not distinguish between intracellular and extracellular sources of Zn^{2+} that might contribute to SD. When both Ca^{2+} and Zn^{2+} were removed from the extracellular space (superfusion with Ca^{2+}-free ACSF supplemented with EGTA, 0.5mM; $K_{D,Ca}=10^{-8}M$, $K_{D,Zn}=10^{-12}M$), there was still a significant initial FluoZin-3 increase and SD was not prevented (Fig. 4). Selective extracellular Zn^{2+} chelation with Ca^{2+}-EDTA (1 mM, $K_{D,Zn}=10^{-16}M$) was also ineffective at preventing either Zn^{2+} rises or SD (6/6 preparations). Despite the lack of effect of these extracellular Zn^{2+} chelators, increases in FluoZin-3 fluorescence prior to SD were completely prevented by pre-exposure with nimodipine. This was demonstrated in experiments with nimodipine in Ca^{2+}-free media containing EGTA, and under these same conditions SD was always prevented (**Figure 2.4**). Taken together, these results suggested that Zn^{2+} increases prior to SD were mediated by L-type Ca^{2+} channels, but that the Zn^{2+} flux was not accessible to chelation by EGTA or Ca^{2+}-EDTA.

EGTA and Ca^{2+}-EDTA both have relatively slow on-rates for divalent cation binding (Smith et al., 1984; Vogt et al., 2000). We therefore tested the effects of BAPTA, which chelates both Ca^{2+} and Zn^{2+} ($K_{D,Ca}=10^{-7}M$, $K_{D,Zn}=10^{-9}M$) but with significantly faster binding kinetics (Adler et al., 1991). BAPTA blocked SD in 6/10 cases and significantly

decreased FluoZin-3 increases prior to SD (Figure 2.4). These observations suggest that Zn^{2+} may accumulate outside neurons and enter through L-type channels before it can be bound by the slower extracellular chelators.

The occurrence of transmembrane Zn^{2+} flux was further supported by measurements of extracellular FluoZin-3 fluorescence (**Figure 2.5**). FluoZin-3 was included in ACSF, together with 1mM Ca^{2+}-EDTA to reduce background fluorescence (**Appendix figure A.1,** see Qian and Noebels, 2005). Under these conditions, fluorescence was stable at baseline but was noted to decrease prior to SD, with a time course that corresponded well with the intracellular FluZin-3 increases signals shown above (Figure 2.3). Furthermore, nimodipine pre-exposures that prevented SD also abolished this FluoZin-3 fluorescence decrease, consistent with the hypothesis that extracellular Zn^{2+} decreases were due to flux through activated L-type channels. In slices where SD was not blocked, a large extracellular FluoZin3 increase propagated across the slice following the onset of the SD response. Control studies showed that slice autofluorescence changes did not contaminate extracellular FluoZin-3 measurements (Appendix figure A1).

Zn^{2+} and Ca^{2+} can both contribute to the depolarization of mitochondrial inner membrane potential prior to SD

The findings illustrated in Figure 2.4 above provide evidence that Zn^{2+} entry through L-type Ca^{2+} channels plays a crucial role in the induction of SD, but do not indicate the ionic contributions to the slow $\Delta\Psi m$ preceding SD. Indeed, as shown in **Figure 2.6**, a

slow ΔΨm still occurs in the presence of TPEN, which is presumably Ca^{2+} dependent, since the addition of Ca^{2+}-free EGTA in addition to TPEN abolished the ΔΨm completely. To separate Zn^{2+} from Ca^{2+} dependent components to the slow ΔΨm, we compared effects of selective Zn^{2+} removal (by TPEN) with Ca^{2+}-free/EGTA ACSF. Figure 2.6B shows that with Ca^{2+}-free/EGTA, the slow ΔΨm occurred early, whereas with selective Zn^{2+} removal it was more delayed, indicating that Zn^{2+} is the primary contributor to the earliest phase of the ΔΨm. Indeed, suggesting that Zn^{2+} from the same extracellular source accounts for the measured Zn^{2+} rises that correlates with SD in Figure 2.4 and the early ΔΨm, both are blocked by TPEN and the fast extracellular chelator, BAPTA (data not shown for ΔΨm), but are not blocked by the slow extracellular chelator, Ca^{2+}-free EGTA. Thus, although ouabain can cause a slow Ca^{2+} dependent ΔΨm, it is not sufficient to cause SD, which seems to be selectively associated with intracellular Zn^{2+} entry through L-type channels.

2.5 Discussion

Zn^{2+} influx via L-type Ca^{2+} channels can contribute to SD

We find that L-type channel blockers prevent SD induced by ouabain under conditions in which adenosine A1 receptors are activated. Surprisingly however, Ca^{2+} influx is not responsible for these effects. The effects of the L-type blockers were not mimicked by removal of Ca^{2+} from the bathing medium, and there was no demonstrable cytosolic Ca^{2+} increase prior to the onset of SD. In contrast, cytosolic Zn^{2+} increases were detected prior to SD, within the same time frame as the initial mitochondrial depolarization.

These Zn^{2+} increases were blocked by L-type channel blockers and selective chelation of Zn^{2+} completely prevented SD under these conditions. As far as we are aware, this is the first description of a critical contribution of endogenous Zn^{2+} to the phenomenon of SD, and shows that under some circumstances, SD can be abolished by selective chelation of Zn^{2+}, a treatment that does not inhibit synaptic transmission or itself lead to acute injury (Choi and Koh, 1998; Weiss et al., 2000).

Detection and Sources of Zn^{2+}

Although some Ca^{2+} indicators do have significant sensitivity to Zn^{2+}, neuronal intracellular Ca^{2+} and Zn^{2+} transients can be distinguished by using combinations of fluorescent indicators (Cheng and Reynolds, 1998; Devinney et al., 2005). For example, in cultured cortical neurons co-loaded with Fura-2FF and the Zn^{2+} indicator FluoZin-3, these indicators responded robustly to Ca^{2+} and Zn^{2+}, respectively following intense glutamate exposures (Devinney et al., 2005). We report here a similar discrimination in CA1 neurons co-loaded with FluoZin-3 and Fura-6F. We have concentrated here on events that occur prior to the onset of SD, when the Zn^{2+} rises are relatively low, and it remains possible that there may be cross-talk between indicator signals during the large ionic shifts that occur following the establishment of SD.

The present data provide clues to the source of these Zn^{2+} rises that were strongly correlated with a progressive $\Delta\Psi m$ and the induction of SD. Specifically, they were blocked by L-type channel blockers and were substantially attenuated by the fast

extracellular Ca^{2+} and Zn^{2+} chelator, BAPTA (Adler et al., 1991), but were not affected by extracellular chelators with slow kinetics (EGTA, Ca-EDTA). Thus, they appear to result from Zn^{2+} accumulation in the extracellular space and rapid entry through L-type channels before being bound by the slower chelators. Fluorescence measurements of extracellular Zn^{2+} also support an extracellular source of Zn^{2+} for the initiation of SD, rather than liberation from intracellular binding sites. The mechanism of the extracellular Zn^{2+} accumulation is unknown, but is likely to be made up in part at least by presynaptic release (Assaf and Chung, 1984; Howell et al., 1984; Thompson et al., 2000; Qian and Noebels, 2005). It is also possible that other non-synaptic extracellular sources of Zn^{2+} contribute (Kay, 2003), and the relative contribution of different potential sources remains to be determined.

Mechanisms of SD induction

For this study of Ca^{2+} and Zn^{2+}-dependent mechanisms, ouabain was used to stimulate SD, since it reliably produces a robust SD in hippocampal slices (Basarsky et al., 1998; Obeidat and Andrew, 1998; Balestrino et al., 1999), and under some conditions SD could be completely prevented by Ca^{2+} channel blockers. At the submaximal ouabain concentrations used here (30 μM), it is likely that a partial block of the Na^+/K^+ ATPase will result in a depolarization of the plasma membrane and increased neuronal excitability prior to SD (Haglund and Schwartzkroin, 1990; Vaillend et al., 2002). As discussed above, the present findings suggest that under these conditions (and with high adenosine tone), Zn^{2+} accumulates in the extracellular space where its entry through L-

type channels of depolarizing neurons contributes to the induction of SD. Reasons for such a prominent role of L-type channels are unknown, but might include their preferential localization in the mitochondria-rich somatic regions of CA1 neurons , their relatively slow inactivation kinetics, as well as their substantial permeability to Zn^{2+} .

The conditions of A1 receptor activation studied here are likely to be particularly relevant for *in vivo* injury conditions like ischemia, where substantial increases in extracellular adenosine are observed (Rudolphi et al., 1992) and L-type flux may be enhanced by tissue acidosis (Kerchner et al., 2000). We note that L-type activity was not required for SD when adenosine tone was low (with A1 receptors blocked, Figure 2.1). However, TPEN still blocked SD under these conditions (data not shown), indicating that Zn^{2+} still played a crucial role in SD induction and that Zn^{2+} entry routes other than L-type channels may be sufficient to exceed the threshold for SD initiation.

Our results suggest that mitochondrial accumulation is a possible mechanism by which Zn^{2+} contributes to the induction of SD. Zn^{2+} uptake can induce depolarization of isolated mitochondria (Jiang et al., 2001) and mitochondria within cultured cortical neurons (Sensi et al., 1999). Notably, the studies on isolated mitochondria indicate that Zn^{2+} induces this effect with far greater potency than Ca^{2+} (10 nM for Zn^{2+} vs ~100 μM for Ca^{2+}; (Jiang et al., 2001)), consistent with present indications of Zn^{2+}-dependent mitochondrial depolarization. Besides effects on mitochondrial potential, previously described consequences of mitochondrial Zn^{2+} uptake also include ROS production (Sensi et al., 1999), increased mitochondrial membrane permeability (Bonanni et al.,

2006) and possibly compromised ATP production (Dineley et al., 2003), although Gerich and co-authors concluded that ATP depletion is not the cause of hypoxic SD (Gerich et al., 2006). In any event, whereas most prior studies of Zn^{2+} effects on mitochondria have examined effects of adding exogenous Zn^{2+}, the present data provide new documentation of significant mitochondrial depolarization resulting from mobilization of endogenous Zn^{2+}.

Relationship to other forms of SD

SD-like events can be generated by diverse stimuli, including localized K^+ exposures, hypoxia, ouabain and strong synaptic stimulation (Somjen, 2001; Smith et al., 2006). While these events are clearly similar in many aspects, there are also differences in the mechanisms and consequences of different forms of SD, as SD associated with migraine aura may not lead to neuronal injury, in contrast to post-ischemic events. In a recent study N and P/Q (but not L-type) channel blockers were effective at preventing SD that was triggered by synaptic stimulation to area CA3 (Kunkler and Kraig, 2004). However, the effects of Ca^{2+} removal were not tested in that work, so it is not yet known whether Zn^{2+} influx is a candidate for Ca^{2+} channel effects in that model.

Observations that the extracellular Zn^{2+} chelator, Ca-EDTA, decreases both intracellular Zn^{2+} accumulation and infarct size following in vivo ischemia (Koh et al., 1996; Calderone et al., 2004), provide a strong indication that neuronal Zn^{2+} accumulation contributes to ischemic neurodegeneration. It is tempting to consider the possibility that

one of the ways that Zn^{2+} contributes to post-ischemic injury is by facilitating the induction of SD. SD-like events, termed peri-infarct depolarizations, have been described following in vivo ischemia and propagate from the edges of infarcted regions to contribute to the spread of ischemic injury in the hours following an insult (Strong et al., 1983; Nedergaard and Astrup, 1986; Hossmann, 1996; Hartings et al., 2003; Umegaki et al., 2005).

Previous work has suggested that mitochondrial dysfunction contributes to SD generated by hypoxia (Gerich et al., 2006) and, much as found here, Bahar and colleagues (Bahar et al., 2000) showed a progressive mitochondrial depolarization that preceded SD-like events in hypoxia. Ca^{2+} influx is well-established to produce depolarization of the mitochondrial inner membrane but despite this, mitochondrial depolarization associated with hypoxic SD was not prevented by Ca^{2+} removal (Bahar et al., 2000). These findings are strikingly similar to present observations of ouabain-induced SD, since Ca^{2+} removal from the ACSF did not prevent the mitochondrial depolarization or SD induction. In contrast to ouabain and OGD, no significant mitochondrial depolarization was observed preceding SD initiated by high K^+ (Bahar et al., 2000). In preliminary observations we have found that TPEN effectively prevented SD produced by oxygen and glucose deprivation, but not SD produced by local K^+ ejection (Dietz et al., submitted). Thus it is possible that progressive accumulation of Zn^{2+} in neurons could be an important contributor to SD where initial membrane depolarizations are slow and progressive, but not necessarily in other SD models where the time course of initial depolarization is very rapid.

The present work provides the first evidence that endogenous Zn^{2+} can contribute to SD, and could provide a key to distinguishing between different types of SD, in different pathophysiological settings. Further understanding of mechanisms involved in the induction of SD and its role in propagation of injury in conditions including ischemia and trauma should help in the development of new neuroprotective strategies in these conditions.

2.6 Figure Legends

Figure 2.1: Nimodipine can block SD. A: Example of SD triggered by ouabain (30 μM, 35°C). The sharp voltage deflection (asterisk) characteristic of SD was recorded with an extracellular electrode placed in stratum radiatum. **B:** Effectiveness of nimodipine depended on A1 receptor activation. Block of A1 receptors with DPCPX (100 nM) prevented nimodipine block of SD. Conversely, pre-exposure to the A1 agonist CPA (300 nM) improved the effectiveness of nimodipine block.

Figure 2.2: Mitochondrial depolarization prior to SD blocked by nimodipine. A: Representative records showing electrically measured SD (top trace, asterisk), with Rh123 fluorescence signals monitored simultaneously from the same slice (bottom trace). Rh123 is in the quenched mode under these loading conditions, and a slow initial Rh123 fluorescence increase was observed prior to the sharp fluorescence increase which accompanied SD. **B:** Mean Rh123 fluorescence increases recorded before the onset of SD. Because the time to SD onset varied between slices, measurements from 7 slices

have been aligned with respect to SD onset time (0 min). A slow increase in Rh123 fluorescence, interpreted as a mitochondrial depolarization, was observed prior to SD under control conditions (filled circles), but was not observed in slices pre-exposed to nimodipine (open circles, n=6).

Figure 2.3: Neuronal Zn^{2+}, but not Ca^{2+} increases prior to SD. A: Representative records showing electrically measured SD (top trace, asterisk) with plot of a single CA1 neuron co-loaded with the Zn^{2+} indicator FluoZin-3 (bottom trace, filled squares) and the ratiometric Ca^{2+} indicator Fura-6F (open circles). Prior to SD, the Zn^{2+} signal increased while the Ca^{2+} signal stays near basal levels. Following SD, large increases in both Ca^{2+} and Zn^{2+} signals were observed. **B:** Mean FluoZin-3 increases recorded before the onset of SD from 6 slices (filled squares) and mean Ca^{2+} levels measured using Fura-2 from 6 different slices (open circles). The measurements have been aligned with respect to SD onset time (time 0) due to variance in the time to SD.

Figure 2.4: Sources of Zn^{2+} responsible for increases prior to SD. A: Mean data from single neuron FluoZin-3 measurements. Slices were pre-exposed to TPEN (50 μM) in regular ACSF. EGTA (0.5 mM), nimodipine (10 μM) or BAPTA (1 mM) were all added in Ca^{2+}-free ACSF. TPEN and nimodipine virtually abolished pre-SD FluoZin-3 increases. EGTA did not prevent FluoZin-3 increases, but a significant decrease was observed with BAPTA. *$p<0.05$, **$p<0.01$, ANOVA with Bonferroni‟s post-hoc tests. **B:** Effects of the same treatments (as described for panel A) on the incidence of SD. TPEN and nimodipine both prevented SD. EGTA did not prevent SD, while BAPTA

reduced the susceptibility to SD to less than 50%. Open bars: incidence of SD; black bars: time to SD.

Figure 2.5: Extracellular Zn^{2+} decreases prior to SD. A: Representative records showing electrically measured SD (top trace, asterisk) with plot of extracellular FluoZin-3 fluorescence (bottom trace). Prior to SD, the FluoZin-3 signal decreased. Following SD, transient increases in the Zn^{2+} signals were observed. **B:** Mean extracellular FluoZin-3 changes recorded before the onset of SD from 5 slices following ouabain (filled circles) and 5 slices exposed to nimodipine (10μM) prior to ouabain (open circles). Nimodipine abolished the initial decrease in extracellular FlouZin-3 fluorescence and blocked SD in every case.

Figure 2.6: Zn^{2+} contributes to mitochondrial depolarization prior to SD. A: Representative records showing the ability of TPEN (50 μM) to block SD (top trace) with corresponding preparation loaded with Rh123 (bottom trace, black line). TPEN delayed, but did not prevent slow Rh123 fluorescent increases Combined exposure to TPEN and Ca^{2+}-free/EGTA solutions virtually abolished Rh123 increases. (bottom trace, grey line). **B:** Mean Rh123 increases following that Ca^{2+}-free/EGTA solutions did not prevent an early mitochondrial depolarization prior to SD (black circles, n=6). TPEN application delayed mitochondrial depolarization and prevented SD (grey circles, n=6). Chelation of both Ca^{2+} and Zn^{2+} abolished all mitochondrial depolarization (white circles, n=6).

Figure 2.1

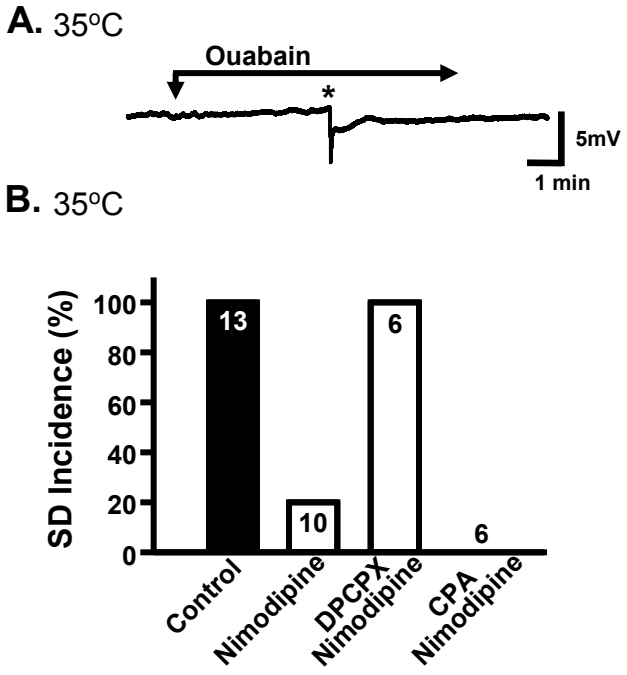

Figure 2.2

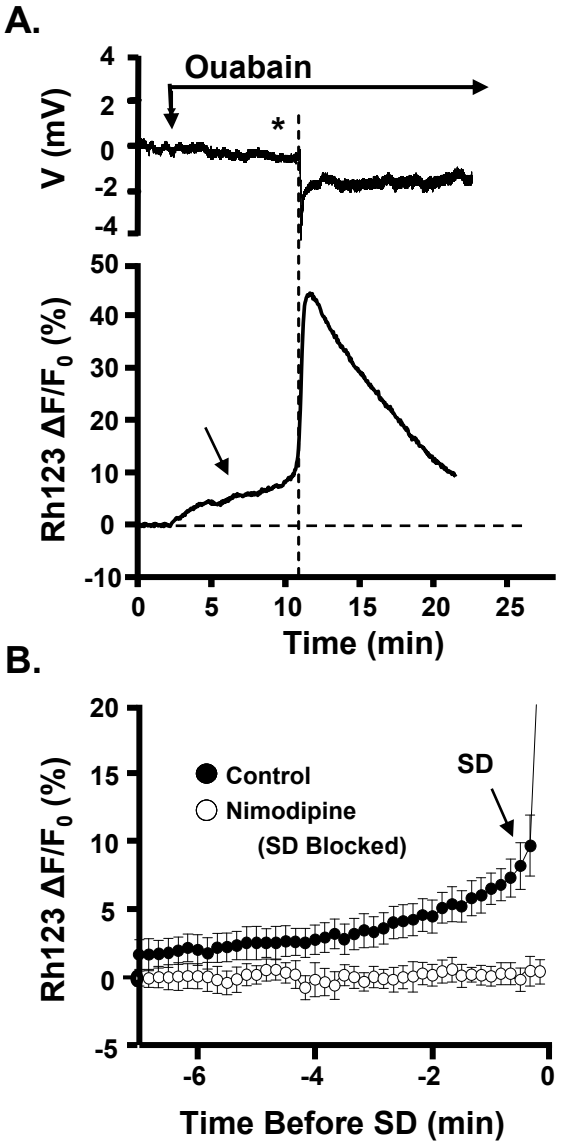

Figure 2.3

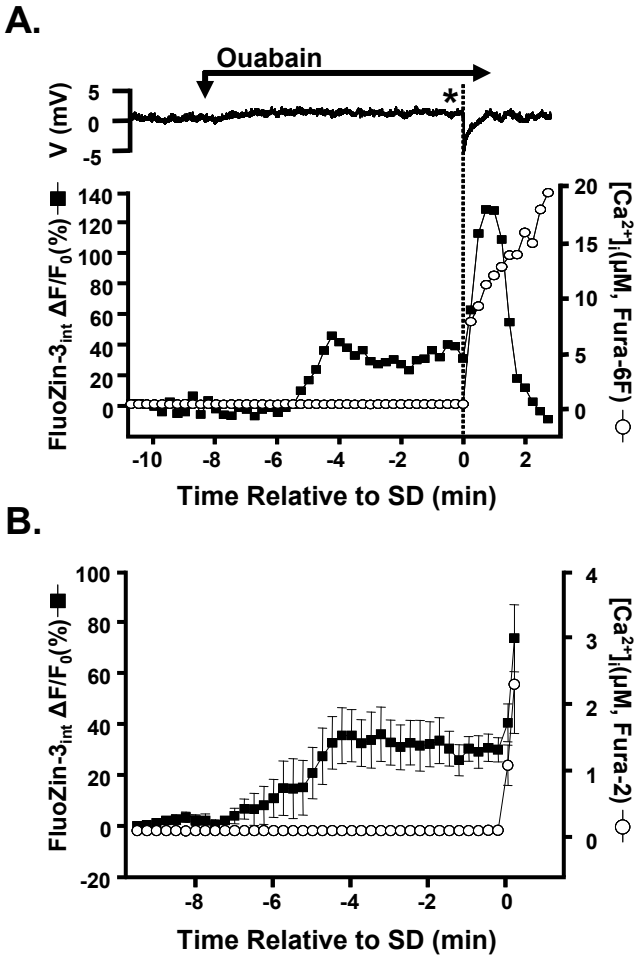

Figure 2.4

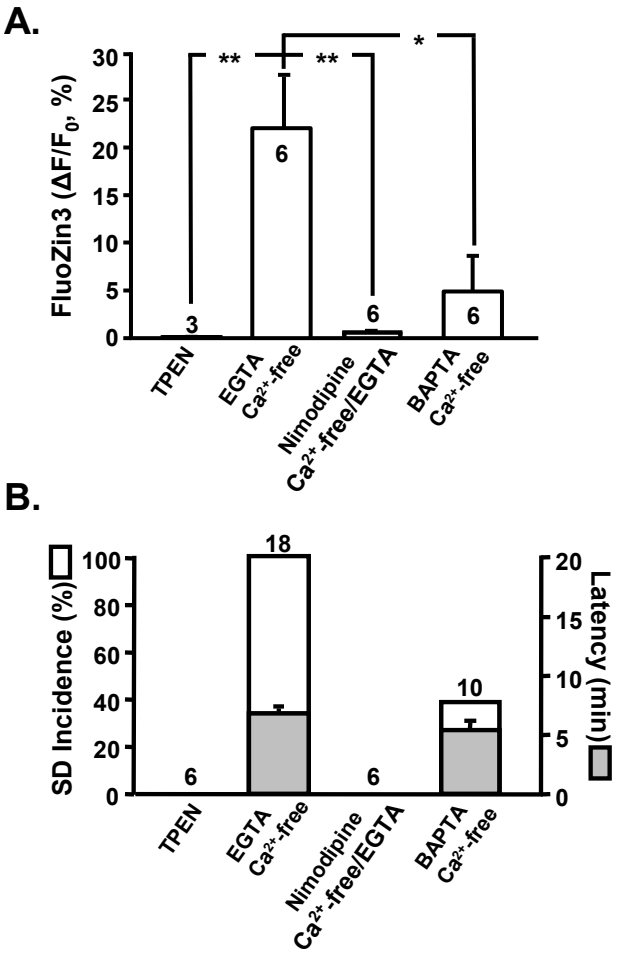

Figure 2.5

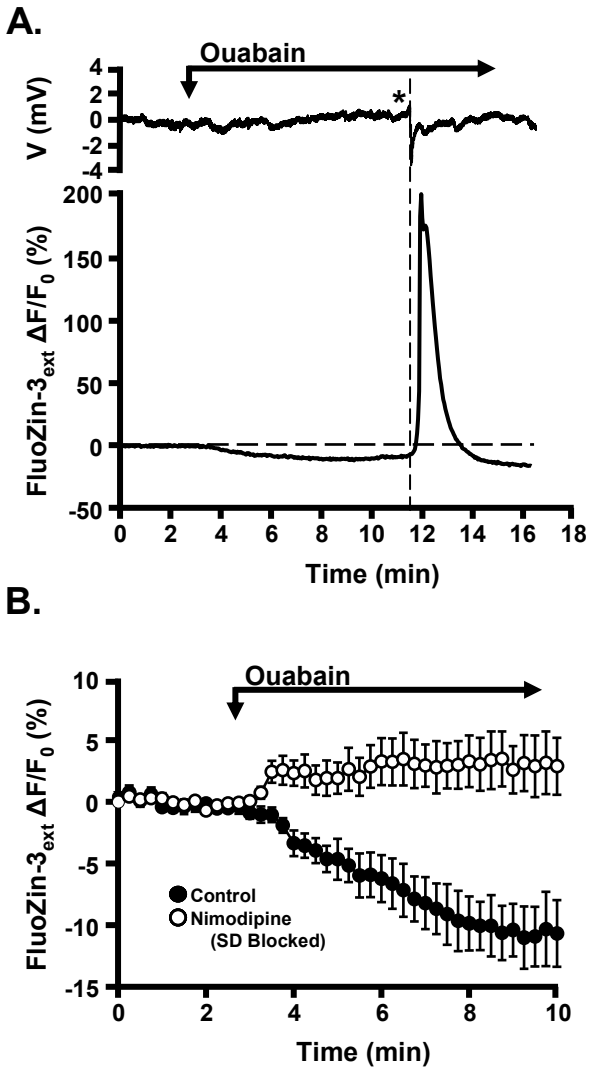

Figure 2.6

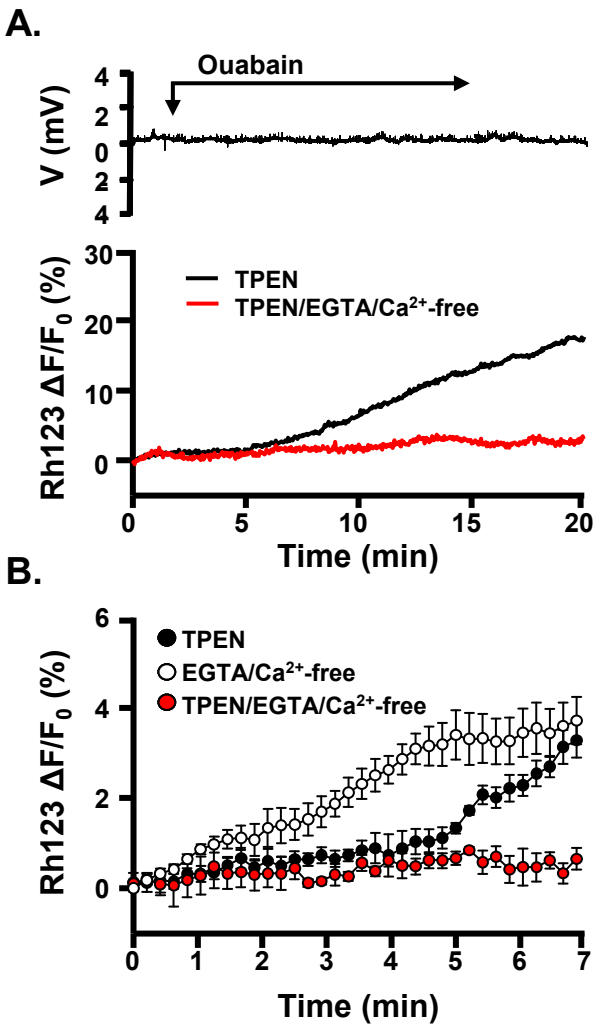

3. Ca^{2+}-dependent Changes in Mitochondrial Redox Potential Prior to the Onset of Spreading Depression in Hippocampal Slices

R.M. Dietz[1], J.A. Connor[1], J. H. Weiss[2] & C.W. Shuttleworth[1]

[1]Department of Neurosciences

University of New Mexico School of Medicine

Albuquerque NM 87131

[2]Departments of Neurology & Anatomy and Neurobiology

University of California Irvine,

Irvine, CA 92697

3.1 Abstract

Spreading depression (SD) is readily evoked in murine hippocampal slices by exposure to the Na^+/K^+ ATPase inhibitor ouabain. Ouabain-induced SD is preceded by a slow mitochondrial depolarization. We recently showed that influx of both Ca^{2+} and Zn^{2+} contribute to mitochondrial depolarization, but that Zn^{2+} influx was selectively involved in the initiation and/or propagation of SD across hippocampal slices. Since mitochondrial dysfunction may contribute to SD, the present study determined the effects of mitochondrial Ca^{2+} and Zn^{2+} loading on mitochondrial redox potential, under these same conditions. Prior to the onset of SD, there was a significant increase (~5-10%) in NAD(P)H autofluorescence, and the kinetics of this response were matched by flavoprotein autofluorescence decreases. After the onset of SD, both autofluorescence signals were greatly reduced, presumably due to tissue swelling, rather than due to mitochondrial redox changes. The initial NAD(P)H increase was also abolished by removal of extracellular Ca^{2+} from the superfusate, or by L-type channel block, but was not significantly affected by Zn^{2+} chelation with TPEN. Ca^{2+}-dependent mitochondrial effects were not associated with significant increase in cytosolic Ca^{2+} accumulation, but when mitochondria were partially uncoupled with FCCP, a significant cytosolic Ca^{2+} increase was observed prior to SD. These findings suggest that while both Zn^{2+} and Ca^{2+} increase following ouabain, Ca^{2+} uptake is rapid enough to prevent detection with cytosolic Ca^{2+} indicators, and likely leads to stimulation of mitochondrial dehydrogenases. Zn^{2+} accumulation has no demonstrable effect on mitochondrial redox potential, suggesting that detrimental effects of this cation are elsewhere, and possible

inhibitory effects of Zn^{2+} on mitochondrial respiration are overshadowed by the strong Ca^{2+}-dependent stimulation.

3.2 Introduction

Spreading depression (SD) has been characterized as a profound depolarization of neurons and glia which propagates across brain tissue at 2-5 mm/min (Somjen, 2001; Smith et al., 2006). Originally described as an abrupt silencing of spontaneous electrical activity that progressed across the cortical surface (Leao, 1944), SD has subsequently been shown to be involved in migraine aura and may contribute to the spread of injury following ischemia and trauma (Hadjikhani et al., 2001; Somjen, 2001; Hartings et al., 2003; Church and Andrew, 2005). SD has been studied in a variety of experimental models using triggers such as brief exposures to elevated extracellular K^+, strong synaptic stimulation or inhibitors of plasma membrane Na^+/K^+ ATPase activity, and hypoxia (Somjen, 2001).

Growing evidence suggests that mitochondrial dysfunction contributes to the induction of SD (Bahar et al., 2000; Hashimoto et al., 2000; Gerich et al., 2006). Hypoxia induces a slow progressive mitochondrial depolarization prior to a large and rapid mitochondrial depolarization coincident with SD (Bahar et al., 2000). Since these were not prevented by the removal of extracellular Ca^{2+} (Bahar et al., 2000), we examined the possibility that mitochondrial depolarization prior to SD could also be due to neuronal Zn^{2+} increases. We recently examined mechanisms underlying SD in hippocampal slices (Dietz et al., under review). We used the Na^+/K^+ ATPase inhibitor ouabain and found evidence for a

slow initial mitochondrial depolarization that occurred prior to SD. A significant contributor to this initial mitochondrial depolarization was Zn^{2+}, via L-type channels, although Ca^{2+} -dependent depolarization was also observed. Significantly, selective chelation of Zn^{2+} abolished SD under these conditions.

Both Zn^{2+} and Ca^{2+} are capable of causing mitochondrial depolarization, as a consequence of flux via the uniporter (Nicholls and Chalmers, 2004; Malaiyandi et al., 2005), but recent work has suggested that Zn^{2+} accumulation is substantially more toxic for mitochondria (Sensi et al., 2003). Part of this toxicity is due to inhibition of TCA cycle, and other components (Dineley et al., 2003). In contrast, Ca^{2+} accumulation can significantly stimulate dehydrogenases of the TCA cycle (Pralong et al., 1992; Duchen et al., 1993; McCormack and Denton, 1993; Hajnoczky et al., 1995; Rohacs et al., 1997; Brandes and Bers, 1999; Pitter et al., 2002; Voronina et al., 2002), and such activation is proposed to link neuronal activation with increased mitochondrial metabolism.

In the present study, we have examined mitochondrial redox potential changes that occur prior to SD in acutely-prepared hippocampal slices. SD was evoked by ouabain exposure and mitochondrial redox potential was examined from NADH and flavoprotein autofluorescence measurements. We provide evidence that rapid mitochondrial sequestration of Ca^{2+} influx was responsible for changes in mitochondrial redox potential prior to SD, and Zn^{2+} accumulation was without effect. These results suggest that although both cations may contribute to mitochondrial depolarization, opposing actions on mitochondrial metabolism may underlie susceptibility to SD.

3.3 Materials and Methods

Slice preparation

Male FVB/N mice were obtained from Harlan (Bar Harbor, ME) at 4 weeks of age and were housed in standard conditions (12hr/12hr light/dark cycle) for no more than three weeks before sacrifice. For slice preparation, mice were deeply anesthetized with a mixture of ketamine and xylazine (85mg/ml and 15mg/ml, respectively; 200µl s.c.) and decapitated. Brains were removed and placed in ice cold cutting solution. Cutting solution contained in mM: 3 KCl, 1.25 NaH_2PO_4, 6 $MgSO_4$, 26 $NaHCO_3$, 0.2 $CaCl_2$, 10 glucose, 220 sucrose and 0.43 ketamine). 350µm coronal sections were cut using a Vibratome (Technical Products International, St Louis MO) and slices were transferred into 35^{oC} ACSF (containing in mM: 126 NaCl, 3 KCl, 1.25 NaH_2PO_4, 1 $MgSO_4$, 26 $NaHCO_3$, 2 $CaCl_2$, and 10 glucose, equilibrated with 95%O_2 / 5%CO_2). Cutting and recording solutions were both 315-320 mOsmol. After holding for 1 hour, ACSF was changed, and slices were held at room temperature until used for recording. Individual slices were transferred to the recording chamber, and were superfused with oxygenated ACSF at 2 ml/min. Slices were warmed to 30^{o}C during sharp microelectrode impalement experiments and then to 35^{o}C for Ca^{2+} imaging. NAD(P)H experiments mimicked this protocol by warming the slices to 30^{o}C for at least twenty minutes and then, where appropriate, were warmed to 35^{o}C for 10 minutes prior to the start of experiments.

Extracellular recording

Extracellular measurements of DC potentials were made using borosilicate glass microelectrodes with a tip resistance of ~5MΩ when filled with ACSF. All extracellular measurements were obtained by placing the electrode in stratum radiatum approximately 50μm below the surface of the slice.

Autofluorescence imaging

Detection of NAD(P)H and flavoprotein autofluorescence was performed as described (Shuttleworth et al., 2003) with minor modifications. All imaging was performed after focusing onto the surface of the slice with a 10x water immersion objective (NA 0.3, Olympus) and fluorescence collected after 2x2 binning of the 640 x 480 line image. An acquisition rate of 0.4Hz was used for all experiments. The reduced form of NADH is fluorescent (Ex ~ 360nm, Em ~450nm (Shuttleworth and Connor, 2001) and the oxidized form is non-fluorescent. For NAD(P)H imaging, 360nm excitation was delivered via a fiber optic/monochromator system (Polychrome IV; Till Photonics, Grafelfing, Germany) and reflected onto the slice surface using a dichroic mirror (DMLP 400nm, Chroma Technology, Brattleboro, VT). Fluorescence emission (>410nm) was collected with a cooled interline transfer CCD camera (IMAGO, Till Photonics). Image data was background-subtracted to account for camera noise and presented as the changes in fluorescence intensity/prestimulus fluorescence intensity (ΔF/Fo) from stratum radiatum.

In some experiments flavoprotein autofluorescence was monitored using excitation at 480nm and emission detected using a 535nm (50nm BW) interference filter.

Ca^{2+} Imaging

Ca^{2+} measurements were made from individual CA1 pyramidal neurons. Neurons were impaled with glass microelectrodes, and were microinjected with a fluorescent indicator for Ca^{2+} (Fura-2). The procedures for recording/indicator injection were as described previously (Shuttleworth and Connor, 2001), with some modifications. Impalements were made using the step function of a Sutter manipulator (225, Sutter Instruments), and neurons were visualized and imaged using a water immersion objective (40X, NA 0.8, Olympus). In all experiments, the recording/filling electrode was carefully withdrawn, and the cell allowed to recover for 20 min before ouabain exposure. Fura-2 was excited at 350/380 nm, and emission detected at 510/50 nm using a monochromator-based imaging system (Till Photonics). Estimation of Ca^{2+} concentration, and preparation of figures was as previously described (Shuttleworth et al., 2003).

Reagents and solutions

All reagents were obtained from Sigma (St. Louis, MO) except Fura-2 pentapotassium salt which was from Invitrogen (Carlsbad, CA). Ouabain was prepared as a 500x stock in H_2O. Nimodipine was prepared as a 10mM stock in ethanol. All other chemicals were

diluted in ACSF. Zero-Ca^{2+} experiments used ACSF with the CaCl replaced by $MgSO_4$, and 0.5mM EGTA was added.

Statistics

Significant differences between group data was evaluated using paired or unpaired Student‟s t-tests, with $p<0.05$ considered significant. Bonferroni's multiple comparison test was used for post-hoc analysis where the effects of multiple drug treatments were compared against each other. Dunnett‟s multiple comparison test was used for post-hoc comparisons of multiple time points of single drug treatment, when compared with responses immediately prior to drug treatment. $p<0.05$ was considered significant in all cases.

3.4 Results

Autofluorescence changes prior to SD, and following SD

SD was generated by partial inhibition of Na^+/K^+ ATPase using ouabain. In previous work, we have established conditions under which SD responses were sensitive to inhibition of L-type Ca^{2+} channels (30μM ouabain, 35oC, in the presence of the A1 receptor agonist CPA 300nM) (Dietz et al, under review). These same stimulation conditions were used throughout the present work.

NAD(P)H fluorescence in slice was monitored as previously described (Hashimoto et al., 2000; Shuttleworth et al., 2003). In 8/8 slices at 35°C, 30μM ouabain produced an initial increase in the NAD(P)H fluorescence prior to the arrival of an SD event (6.9±1.0% increase, n=8, **Figure 3.1**). As described previously in vivo and in these preparations, NAD(P)H autofluorescence measurements revealed a propagating wave of fluorescence decrease (Duchen, 1992; Mironov and Richter, 2001; Shuttleworth et al., 2003; Reinert et al., 2004; Brennan et al., 2006), followed by a rapid overshoot. The event propagated at a rate of 3.0±0.35 mm/min (n=8) along the CA1 layer. The initial fluorescence decrease was coincident with the downward deflection of the extracellular recording electrode, within the limitations of the image acquisition rate used in these experiments (0.4Hz).

Flavoprotein (FP) autofluorescence has been used to assess mitochondrial function in neurons. Previous work has shown that a correspondence between NAD(P)H and flavoprotein autofluorescence indicates mitochondrial function changes, with the major difference in these signals being that they are inverted (Basarsky et al., 1998; Andrew et al., 1999; Bahar et al., 2000; Jarvis et al., 2001). To investigate the role of mitochondrial function in the NAD(P)H imaging described above, NAD(P)H and flavoprotein transients were compared with near-simultaneous imaging (switching filter cubes at 0.4Hz). It was found that soon after the onset of ouabain exposure, the NAD(P)H signal began to rise as described above while at the same time, the flavoprotein signal decreased prior to SD (Figure 3.1B, peak 5.3±1.6% decrease, n=7).

A very different relationship between NAD(P)H and flavoprotein autofluorescence was observed during the SD event itself. Both NAD(P)H and flavoprotein autofluorescence signals dropped dramatically with SD. One explanation for these changes is that the initial autofluorescence changes prior to SD (inverted NAD(P)H and FP) are due to mitochondrial redox changes, whereas during and after SD swelling responses dominate (see (Van Harreveld and Khattab, 1967; Kow and van Harreveld, 1972), producing similar sign effects on fluorescence emissions with center wavelengths approximately 100nm apart.

Effects of Ca^{2+} removal

Figure 3.2A shows that Ca^{2+} influx via L-type channels is likely responsible for NAD(P)H fluorescence increases. Slices were pre-exposed to the selective L-type inhibitor nimodipine (10μM), and abolished NAD(P)H increases due to ouabain exposure. Nimodipine alone did not cause significant changes in pre-stimulus NAD(P)H fluorescence levels, and did effectively prevent SD in all preparations tested, as recently shown (Dietz et al., under review).

Figure 3.2B shows that the initial NAD(P)H fluorescence increase prior to SD was abolished by removal of Ca^{2+} from the superfusate. Slices were pre-exposed to Ca^{2+}-free ACSF plus 0.5mM EGTA. This procedure alone did not have a significant effect on NAD(P)H fluorescence prior to ouabain exposure (0.6±0.5% decrease; n=5). In all

preparations tested with Ca^{2+} removal, SD was observed, consistent with previous observations (Dietz et al., under review).

Effects of Zn^{2+} removal

We examined the effects of selective Zn^{2+} removal by pre-exposure of slices to the chelator TPEN (50μM). TPEN alone produced a small, but significant increase in NAD(P)H autofluorescence of 2.1±0.6% (n=6) compared to basal levels. When ouabain was applied in the continued presence of TPEN, there was a further NAD(P)H fluorescence increase (**Figure 3.3**), which trended to a smaller increase than compared with bracketed controls, but was not significantly so. Consistent with our previous findings, application of TPEN blocked SD in all six preparations tested.

Cytosolic Ca^{2+} signals

The evidence above suggests that Ca^{2+} influx via L-type channels was responsible for mitochondrial redox potential changes, including responses in stratum pyramidale. However, we have previously described that there is no change in Ca^{2+} levels in CA1 pyramidal neurons prior to SD during single cell Ca^{2+} measurements (Dietz et al., under review). One possible explanation was that L-type Ca^{2+} entry provided a privileged route of Ca^{2+} entry to mitochondria, that prevented its detection by Ca^{2+}-sensitive indicators in the cytosol. This possibility was tested by partial depolarization of mitochondria with the proton-ionophore FCCP. Cells loaded with the high-affinity indicator Fura-2 were

subjected to 30μM ouabain for 5 minutes before a bolus of FCCP (2.5μM estimated final concentration in bath) was added to the bath (**Figure 3.4**). This procedure resulted in a demonstrable Ca^{2+} increase, after a delay of 2.9±0.1 min (after FCCP addition) (n=5). As described above, this pre-SD Ca^{2+} increase was not observed in slices devoid of FCCP exposure. Furthermore, in slices pre-exposed to nimodipine, there was no Fura-2 increase following the FCCP bolus/ouabain procedure (n=5). These Fura-2 results suggest that there is a selective role for L-type VGCC in the loading of Ca^{2+} into mitochondria prior to SD and provide support for the hypothesis that there is source specific coupling of mitochondrial Ca^{2+} uptake through L-type VGCC.

3.5 Discussion

General

The main conclusions of this study are that there is significant Ca^{2+} influx prior to the onset of SD and that this in turn is responsible for mitochondrial redox potential changes. Since Ca^{2+} influx prior to SD is not readily detectable unless mitochondria are partially depolarized, we suggest that mitochondria normally avidly take up Ca^{2+} before it can interact with cytosolic indicators. In contrast to Ca^{2+} influx, Zn^{2+} accumulation does not significantly influence mitochondrial redox potential, and other effects of Zn^{2+} are likely to contribute to the initiation of SD under these conditions.

Autofluorescence Imaging of SD

Many previous studies have utilized autofluorescence to recorded spreading waves of SD in brain slices and in vivo following ischemia, or with K^+ ejection. The present work with ouabain shows a clear NAD(P)H increase prior to SD, and since this was matched by flavoprotein autofluorescence decreases, these initial responses appear to report changes in mitochondrial redox potential. Coincident with SD, there were large and synchronized decreases in both autofluorescence signals, and this response propagated along the CA1 pyramidal layer, representing the spreading wave of SD. Because both autofluorescence signals change in the same direction after the onset of SD, it is unlikely that these large changes are due to mitochondrial redox potential changes, but rather a consequence of the severe tissue swelling that accompanies SD (VanHarreveld, 1959; Aitken et al., 1998; Basarsky et al., 1998; Andrew et al., 1999). The swelling response has been exploited to study the spread of SD in hippocampal slices, and has been attributed to swelling of neurons and in the case of ouabain exposure, beading of dendrites of CA1 pyramidal neurons make a substantial contribution (Rosenthal and Somjen, 1973; Mayevsky and Chance, 1974; Lothman et al., 1975; Mayevsky and Chance, 1975; Jobsis, 1977; Kreisman et al., 1981; Raffin et al., 1991; Rex et al., 1999; Strong et al., 2000).

It is likely that there are significant effects on mitochondrial redox potential occurring after the establishment of SD, but it is impossible to distinguish them due to the much larger optical consequences of swelling. Thus we have concentrated our efforts here on

events prior to SD, that are likely of mitochondrial origin, and may contribute to the initiation and propagation of the SD, rather than its consequence.

In many previous studies it has been reported that mitochondrial oxidative enzymes become oxidized during SD, in contrast to hypoxia and ischemia, where mitochondrial enzymes become reduced already before the onset of HSD and maximally during HSD (Takano et al., 2007). The present in vitro study is simpler in many respects, since there are not complications of blood flow, and recent work has emphasized the compartmentalization that may occur in relation to capillaries in vivo (Dineley et al., 2003).

Mechanisms underlying initial NAD(P)H fluorescence increases

An increase in NADH fluorescence can be due to a number of factors, first and foremost is inhibition of oxygen consumption. Ouabain inhibits a major consumer of cellular ATP, and even at the submaximal concentration used here, it is possible that O_2 consumption could decrease as a consequence. Additionally, the sequestration of Zn^{2+} by mitochondria may also lead to the inhibition of the electron transport chain (Hansford, 1985; Denton and McCormack, 1990; McCormack et al., 1990). However, Figure 2 shows that when Ca^{2+} influx is prevented, ouabain did not produce an NAD(P)H increase, implying a strict Ca^{2+} dependence of the redox change on Ca^{2+} entry. Ca^{2+}-dependent stimulation of TCA cycle enzymes therefore appears a likely mechanism. Regulation of mitochondrial metabolism by Ca^{2+} was shown in isolated mitochondria,

and with mitochondrial enzymes (Duchen, 1992), and was argued to underlie NAD(P)H increases following depolarization of isolated neurons (Shuttleworth et al., 2003).

We have previously investigated NAD(P)H increases following glutamate receptor stimulation in hippocampal slices, and concluded that although cytosolic Ca^{2+} increases were prominent following stimulation, Ca^{2+} increases were unlikely to underlie NA(P)H increases. In that study we suggested that "while these findings suggest that evoked NAD(P)H transients in slice do not reflect mitochondrial Ca^{2+} dynamics, they do not rule out contributions from Ca^{2+}-dependent regulation of NADH signals under other, more extreme, conditions, e.g. spreading depression or anoxia" (Brown et al., 2000; Gazaryan et al., 2002). The present study suggests that this is indeed the case, but raises the possibility that the routes of Ca^{2+} entry may be even more important than intensity of stimulation in determining whether Ca^{2+} is responsible for coupling of neuronal activity to mitochondrial metabolism. In the present work there seems to be tight coupling between L-type Ca^{2+} entry and mitochondrial NAD(P)H increases, and in the work with glutamate receptor stimulation, cytosolic Ca^{2+} increases were much larger but without Ca^{2+}-dependent mitochondrial activation.

We recently showed that neuronal Zn^{2+} levels increase for approximately 5 min prior to the onset of SD. This is a very similar time frame as the NAD(P)H increases described here, but despite this correlation, Zn^{2+} does not contribute to mitochondrial redox potential changes following ouabain exposure. This observation is consistent with much previous work showing that (in contrast to Ca^{2+}) Zn^{2+} inhibits mitochondrial

dehydrogenases rather than stimulating them (Dineley et al., 2003). We did note a small but significant increase in NAD(P)H levels when Zn^{2+} was chelated, suggesting that there might be some contribution of Zn^{2+} that limits basal TCA activity, however any such effect is greatly overshadowed by Ca^{2+} dependent stimulation during ouabain exposure.

Consequences of Ca^{2+} and Zn^{2+} accumulation on SD

Moderate mitochondrial Ca^{2+} elevations may increase generation of respiratory substrates (NADH and $FADH_2$) in mitochondria, but much greater Ca^{2+} elevations can lead to mitochondrial dysfunction, as a consequence of severe depolarization of the mitochondrial inner membrane, permeability transition, or ROS generation. It is clear from this (and recent Dietz et al.) study that potentially deleterious effects of Ca^{2+} elevations do not contribute to the onset of SD under these conditions, since Ca^{2+} removal did not delay or prevent SD. Since TCA activation could potentially be beneficial to neurons, under conditions where SD is generated, it seems that Ca^{2+} accumulation could counteract to some extent the deleterious effects of Zn^{2+} on mitochondrial function. However, if this effect is operative, it is small, since Ca^{2+} removal alone did not significantly increase sensitivity to SD. This may be different in other tissues, such as retina, where it has been reported that Ca^{2+} removal can increase sensitivity to SD. However in CA1, severe effects of Zn^{2+} influx appear to overwhelm any potentially beneficial effect of Ca^{2+} accumulation on mitochondrial function.

While selective chelation of Zn^{2+} abolished SD, we do not yet know how Zn^{2+} triggers SD. Previous work showed that Zn^{2+} chelation reduced mitochondrial depolarizations prior to SD, suggesting a mitochondrial site of action. Zn^{2+} appears substantially more potent at inhibiting mitochondria than does Ca^{2+}, and leads to mitochondrial depolarization and ROS generation, and possibly inhibition of components of the electron transport chain, in addition to the negative effects on TCA cycle described above (Blaustein and Lederer, 1999). The present work suggests that TCA effects are unlikely to contribute, but leave open effects on these other mitochondrial processes as a possible contributor to SD.

3.6 Figure Legends

Figure 3.1: Mitochondrial redox potential change prior to SD. **A:** Extracellular potential (upper trace), NAD(P)H (blue) and flavoprotein (green) autofluorescence from a single preparation during exposure to ouabain. The rapid voltage deflection indicates the onset of SD, and coincident with this event, rapid decreases in both autofluorescence signals were observed. Prior to SD, NAD(P)H progressively increased, and FP levels showed a progressive decrease over the same time frame. **B:** The upper left image is a bright field image of the hippocampal slice showing the region of interest from which the data was collected (yellow box). The color images are single frames showing changes in NAD(P)H and FP autofluorescence throughout the same slice, with letters corresponding to times on the trace in A. The asterisks in frames c, d, and e show the propagation of the decrease in fluorescence corresponding with SD.

Figure 3.2: Ca^{2+} influx through L-type channels is responsible for initial NAD(P)H increases. **A:** Mean NAD(P)H autofluorescence increases recorded before the onset of SD in control conditions (filled circles) were completely abolished in slices pre-exposed to nimodipine (open circles, 10μM, n=8 each). **B:** In Ca^{2+}-free ACSF, there is no NAD(P)H autofluorescence increase prior to SD (n=6), despite the occurrence of SD in all preparations tested (latter is not shown).

Figure 3.3: Zn^{2+} removal does not alter pre-SD NAD(P)H changes. **A:** Mean NAD(P)H autofluorescence increases recorded before the onset of SD (control, filled circles) recorded following administration of ouabain. Control experiments (closed circles, n=6) were interleaved with experiments where the slice was pre-exposed to TPEN (50μM, open circles, n=6). While control experiments experienced SD, the slices exposed to TPEN did not, despite there being no significant difference in the pre-SD NAD(P)H increases.

Figure 3.4: Mitochondrial accumulation of Ca^{2+} prior to SD. **A:** Ca^{2+} measurements from somata of single CA1 neurons loaded with Fura-2. Traces shown are during exposure to ouabain, and are aligned to the onset of SD in each preparation (at time 0). In control preparations (filled circles), a large Ca^{2+} increase was observed, beginning coincident with the onset of SD in each preparation. However, under control conditions, there was no detectable increase in somatic [Ca^{2+}] prior to SD. In contrast, in cells which received a prior bolus of FCCP, a significant somatic Ca2+ elevation was seen prior to the onset of SD (open circles). The FCCP bolus (2.5μM estimated final concentration,

during 2ml/min flow) was applied after 5 min of ouabain exposure and panel **B** shows that this procedure produced a significant mitochondrial depolarization over a similar time frame. These 6 preparations were loaded with Rh123, to report changes in mitochondrial inner membrane potential, and responses in each preparation were compared to subsequent sustained exposures 1uM FCCP, to completely depolarize mitochondria.

Figure 3.1

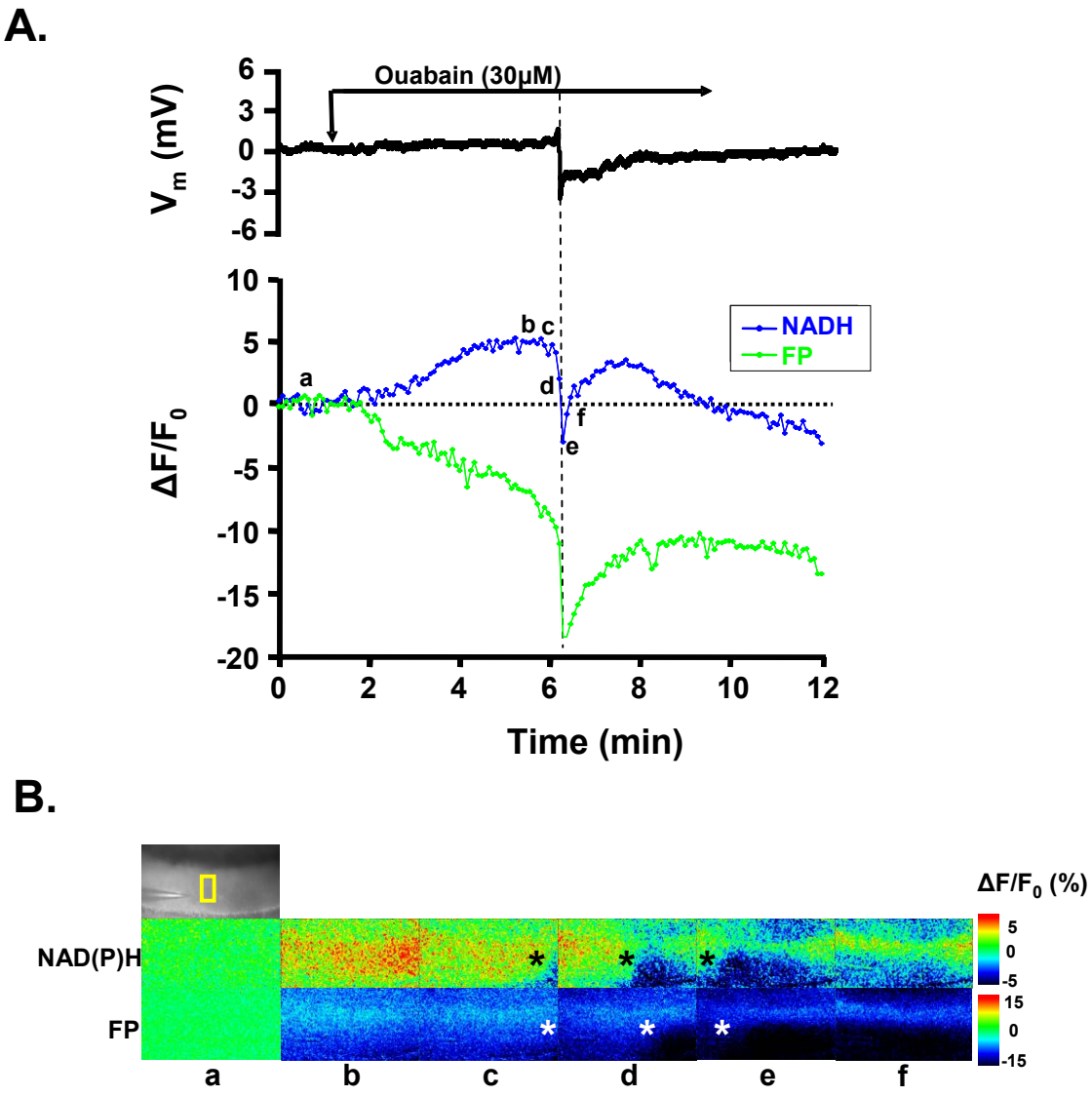

Figure 3.2

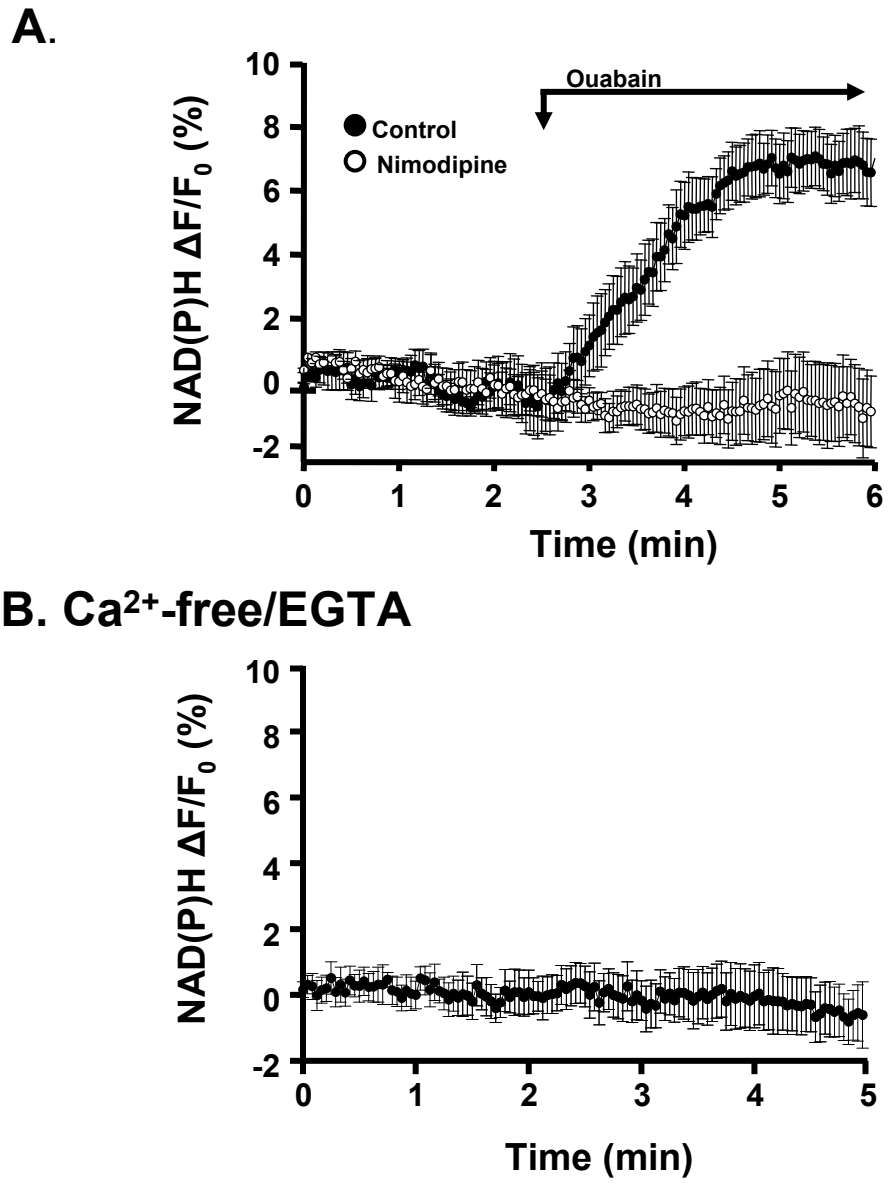

Figure 3.3

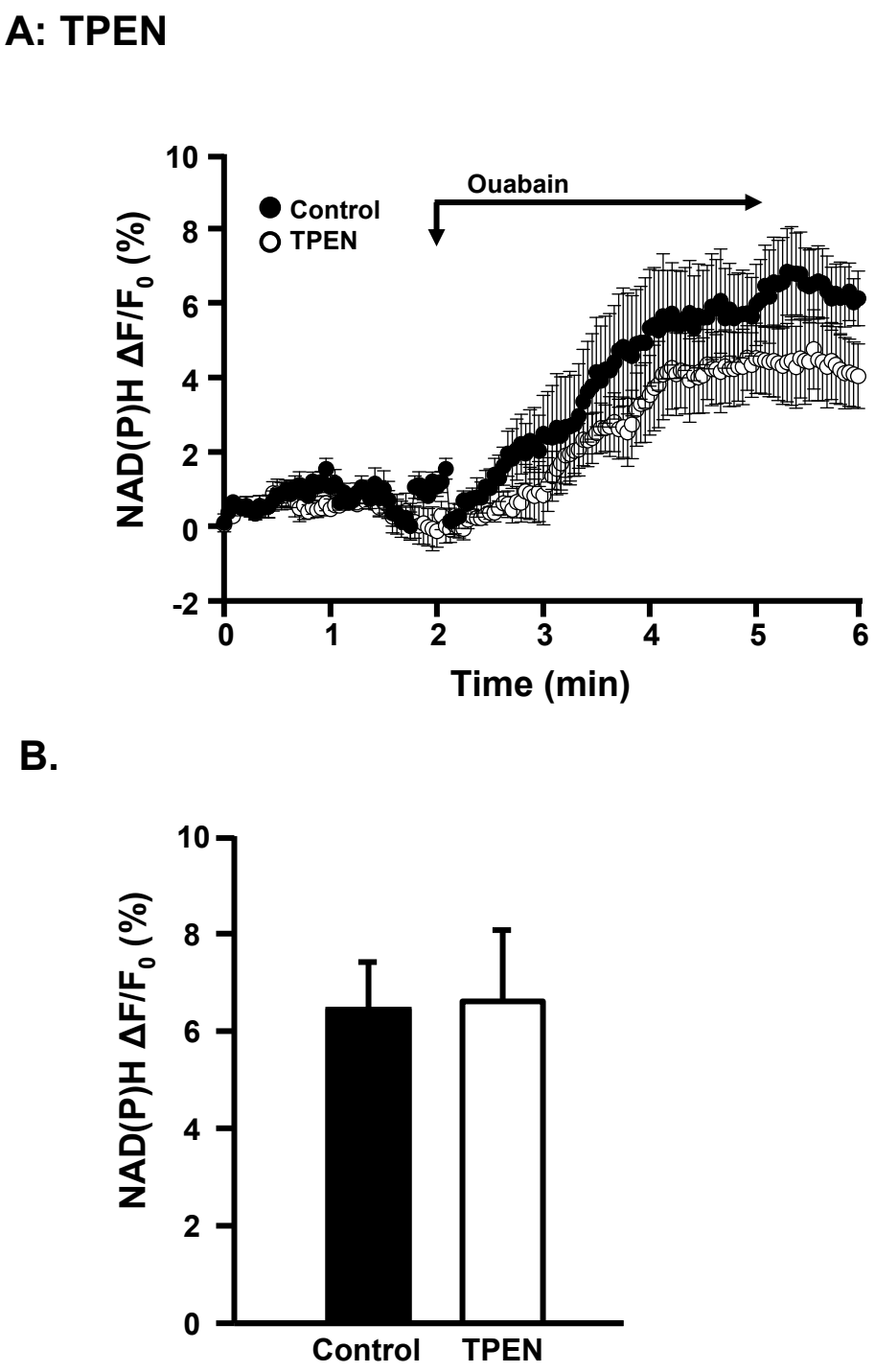

Figure 3.4

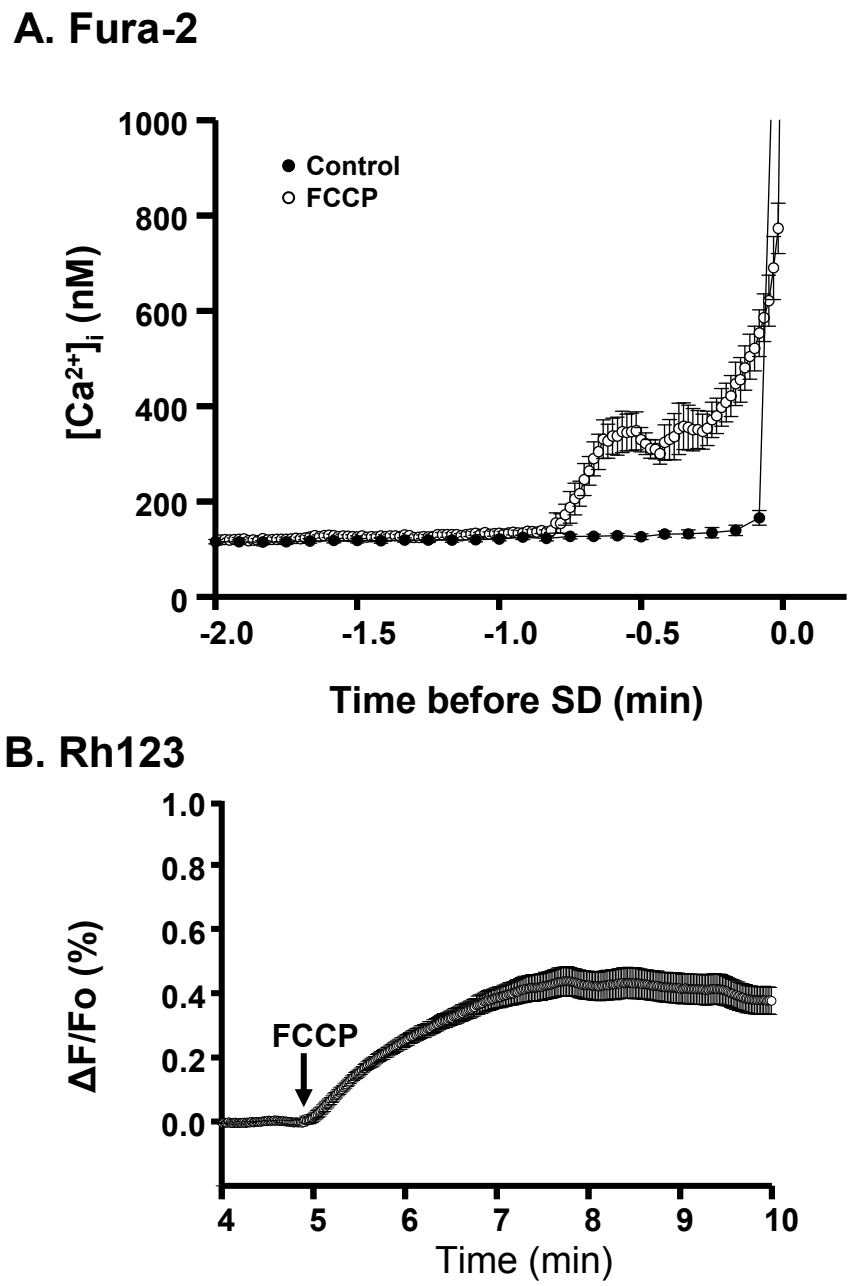

4. Contribution of Na^+/Ca^{2+} exchange to excessive Ca^{2+} loading in dendrites and somata of CA1 neurons in acute slice.

Robert M. Dietz[1], Lech Kiedrowski[2], C. William Shuttleworth[1]

[1]Department of Neurosciences

University of New Mexico School of Medicine

Albuquerque, New Mexico

[2] The Psychiatric Institute

Departments of Psychiatry and Pharmacology

The University of Illinois

Chicago, Illinois

(Published in Hippocampus. 2007;17(11):1049-59)

4.1 Abstract

Multiple Ca^{2+} entry routes have been implicated in excitotoxic Ca^{2+} loading in neurons and reverse-operation of sodium-calcium exchangers (NCX) has been shown to contribute under conditions where intracellular Na^{+} levels are enhanced. We have investigated effects of KB-R7943, an inhibitor of reverse-operation NCX activity, on Ca^{2+} elevations in single CA1 neurons in acute hippocampal slices. KB-R7943 had no significant effect on input resistance, action potential waveform or spike frequency adaptation but reduced L-type Ca^{2+} entry in somata. Nimodipine was therefore included in subsequent experiments to prevent complication from effects of L-type influx on evaluation of NCX activity. NMDA produced transient primary Ca^{2+} increases, followed by propagating secondary Ca^{2+} increases that initiated in apical dendrites. KB-R7943 had no significant effect on primary or secondary Ca^{2+} increases generated by NMDA. The Na^{+}/K^{+} ATPase inhibitor ouabain (30μM) produced degenerative Ca^{2+} overload that was initiated in basal dendrites. KB-R7943 significantly reduced initial Ca^{2+} increases and delayed the propagation of degenerative Ca^{2+} loads triggered by ouabain, raising the possibility that excessive intracellular Na^{+} loading can trigger reverse-operation NCX activity. A combination of NMDA and ouabain produced more rapid Ca^{2+} overload, that was contributed to by NCX activity. These results suggest that degenerative Ca^{2+} signaling can be triggered by NMDA in dendrites, before intracellular Na^{+} levels become sufficient to reverse NCX activity. However, since Na^{+}/K^{+} ATPase inhibition does appear to produce significant reverse-operation NCX activity, this additional Ca^{2+} influx pathway may operate in ATP-deprived CA1 neurons and play a role in ischemic neurodegeneration.

4.2 Introduction

Excessive accumulation of cytosolic Ca^{2+} is central to most hypotheses of excitotoxic neuronal death and it has been suggested that plasma membrane Na^{+}/Ca^{2+} exchange (NCX) regulates cytoplasmic Ca^{2+} levels that contribute to the degree of excitotoxic injury. Three NCX isoforms have been identified (NCX1-3) (Blaustein and Lederer, 1999; Fujioka et al., 2000; Dong et al., 2002) and both beneficial and detrimental effects of NCX activity have been suggested. When operating in the "forward mode", NCX can reduce cytoplasmic Ca^{2+} levels by exchange of either 3 or 4 Na^{+} for $1Ca^{2+}$ (Hartley and Choi, 1989; Andreeva et al., 1991; White and Reynolds, 1995). Forward-operation NCX is thought to limit neuronal death following glutamate stimulation of cultured neurons (Pignataro et al., 2004a) and following middle cerebral artery occlusion in rat brain (Bano et al., 2005). Calpain-mediated proteolysis of NCX is argued to contribute to neuronal death following ischemia, as a consequence of impaired Ca^{2+} extrusion (Kiedrowski et al., 1994).

NCX activity reverses when the plasma membrane potential becomes more positive than the equilibrium potential of NCX, which happens when neurons are depolarized and/or intracellular Na^{+} levels are substantially elevated. Simultaneous Na^{+} and Ca^{2+} measurements suggested a role for reverse-operation NCX following brief glutamate pulses to cerebellar granule cells (Kiedrowski, 1999; Czyz et al., 2002; Kiedrowski et al., 2004), and this Ca^{2+} entry pathway was subsequently concluded to be an important contributor to excitotoxic cell death if these cells are glucose-deprived and depolarized (Matsuda et al., 2001). Inhibiting reverse-operation NCX appears to limit the extent of

ischemic brain damage (Stys et al., 1992; Imaizumi et al., 1997; Li et al., 2000). Reverse-operation NCX is also suggested to contribute to damage in white matter injury in spinal cord preparations (Blaustein and Lederer, 1999; Annunziato et al., 2004).

Classically, inhibition of NCX activity has been achieved by using divalent or trivalent cations (Ni^{2+}, Cd^{2+}, and La^{3+}) and organic compounds such as benzamil and bepridil (Iwamoto and Kita, 2004). Because these inhibitors also influence other ionic fluxes, a number compounds have been identified with increased selectivity for NCX, and furthermore, some of these agents preferentially inhibit the reverse-operation of exchanger activity.

The reverse-operation mode of all three known NCX isoforms is effectively inhibited by KB-R7943 (2-[2-[4-(4-nitrobenzyloxy)phenyl]ethyl]isothiourea methanesulfonate) (Sekizawa and Bonham, 2006; Xu et al., 2006). It is widely used as a tool to study the physiological and pathological roles of NCX, including recent studies in forebrain or brainstem slices (Czyz and Kiedrowski, 2002; Kiedrowski et al., 2004). KB-R7943 has been shown to be protective against Na^+-dependent Ca^{2+} overload in cultured neurons (Schroder et al., 1999; Breder et al., 2000; Martinez-Sanchez et al., 2004). This agent also reduces Ca^{2+} accumulation and injury following oxygen-glucose deprivation in slice culture (Hoyt et al., 1998). Interestingly, in studies of forebrain neurons, KB-R7943 effectively limited Ca^{2+} transients produced by brief pulses of NMDA, but was ineffective against excitotoxic Ca^{2+} accumulation following more extended glutamate exposure in the presence of glucose (Blaustein and Lederer, 1999; Kraev et al., 2001; Li

et al., 2002), suggesting that other pathways were important for these neurotoxic Ca^{2+} elevations.

In addition to NCX, a family of K^+-dependent Na^+/Ca^{2+} exchangers, NCKX 1-4 has also been identified (Kiedrowski et al., 2002) and found to be preferentially expressed in neurons (Czyz and Kiedrowski, 2002). KB-R7943 is ineffective against NCKX-mediated Ca^{2+} entry (Czyz and Kiedrowski, 2002; Kiedrowski, 2004) and no NCKX inhibitors are available. Nevertheless, the contribution of this pathway to Na-dependent Ca^{2+} influx has been estimated using K^+-free solutions in neuronal cultures (Kip et al., 2006). Hippocampal neurons express NCX 1-3 and NCKX 2-4 isoform transcripts (Li et al., 2006; Minelli et al., 2006). The expression of NCX1-3 and NCKX2 proteins have been confirmed in CA1 neurons (Kiedrowski et al., 2004), which also robustly exhibit reverse NCX and NCKX activity, when cytosolic $[Na^+]$ is experimentally elevated (Shuttleworth and Connor, 2001).

The contribution of NCX to Ca^{2+} influx pathway in mature hippocampal CA1 neurons in slices is less well understood. We have examined Ca^{2+} elevations in slice and identified degenerative Ca^{2+} overload that initiates in dendrites and propagates to somata (Iwamoto et al., 1996; Hoyt et al., 1998; Czyz et al., 2002; Ouardouz et al., 2005). Since the contribution of NCX to this Ca^{2+} accumulation is currently unknown, the goals of the present study were to investigate the contribution of NCX on Ca^{2+} elevations in CA1 pyramidal neurons in acute hippocampal slices, with different types of stimuli. KB-R7943 was used to probe NCX involvement, and since this agent has been shown to

inhibit some voltage-dependent Ca^{2+} channels (Sobolevsky and Khodorov, 1999; Czyz et al., 2002), and glutamate receptors (see Shuttleworth and Connor, 2001) part of the study evaluated the possible contribution of these non-specific effects. We show KB-R7943 has inhibitory effects on L-type Ca^{2+} channels on somata, but was without demonstrable effect on voltage-dependent Ca^{2+} entry on dendrites. Excitotoxic Ca^{2+} levels were examined by NMDA exposure and by Na^+/K^+ ATPase inhibition with ouabain. The results suggest a contribution of reverse-operation NCX activity to progressive Ca^{2+} loading, which is most clearly demonstrable when Na^+ accumulation is enhanced by Na^+/K^+ ATPase inhibition, and may involve NCX activity in CA1 dendrites.

4.3 Materials and Methods

Slice preparation and intracellular recording

Male mice (FVB/N) were obtained from Harlan (Bar Harbor, ME) at 4-6 weeks of age and were housed in standard conditions (12hr/12hr light/dark cycle) before sacrifice. Numbers in the study refer to numbers of neurons, each obtained from a different experimental animal for each protocol. For slice preparation, mice were deeply anesthetized with a mixture of ketamine and xylazine (85mg/ml and 15mg/ml, respectively; 200µl s.c.) and decapitated. Brains were removed and placed in ice cold cutting solution. 350µm coronal sections were cut using a Vibratome (Technical Products International, St Louis MO) and slices were transferred into 35ºC ACSF. Cutting and recording solutions were both 315-320 mOsmol. After holding for 1 hour, ACSF was changed, and slices were held at room temperature until used for recording.

Individual slices were transferred to the recording chamber, and were superfused with oxygenated ACSF at 1.7-2.3 ml/min (35^{oC}). Intracellular recordings were made from single CA1 pyramidal neurons using glass microelectrodes, which were advanced using a Nanostepper micropositioner (SPI, Germany). Voltage recordings were made using an Axoclamp 2A amplifier (Axon Instruments, Foster City, CA), digitized (Digidata1322A) and analyzed using PClamp 9.2 (Axon Laboratory).

Cells were accepted for filling and analysis if they had steady resting membrane potentials (RMPs) less than -60mV and generated action potentials greater than 60mV in response to depolarizing current pulses. Input resistance was calculated from responses to small hyperpolarizing current pulses (100pA, 500ms), and spike-driven Ca^{2+} transients evaluated from depolarizing current pulses (100-500pA, 500ms) delivered from -65mV.

In all studies involving NMDA or ouabain application, the filling electrode was withdrawn before stimulating the neuron. This procedure minimized the possibility of Ca^{2+} changes due to changes in impalement quality during intense activation of the slice (Grynkiewicz et al., 1985). In a small number of cases (3/62), electrode withdrawal led to membrane rupture, immediate irrecoverable Ca^{2+} influx and dye loss, and these cells were discarded. All other neurons were allowed to recover for 20 min following electrode withdrawal before drug exposure.

Ca^{2+} measurements

To provide adequate resolution of Ca^{2+} in dendrites, individual neurons were microinjected with a Ca^{2+} indicator. The high-affinity indicator Fura-2 (K_d~225nM in 1mM Mg^{2+}) was used for most experiments. Fura-2 provides sensitive monitoring of Ca^{2+} levels near rest (~100nM) as well as levels up to about 2.5μM (approximately 10 fold above K_d of 225nM in 1mM Mg^{2+}). Levels above this are likely underestimated due to saturation of the indicator, and are represented at >2.5μM in some of the figures. The lower-affinity indicator Fura-6F (K_d~5.3μM) was used for some experiments to assess effects of KB-R7943 on peak Ca^{2+} elevations during NMDA or ouabain exposure. The recording/injection microelectrodes were tip-filled with 10mM indicator in 0.5M KAc/0.5M KCl, and back-filled with 3M KCl. These microelectrodes had resistances of approximately 100MΩ when filled with 3M KCl, and >180MΩ initially when filled with injection mixture. After a stable impalement was made, the indicator was injected by passing hyperpolarizing current (300-500pA) for 10-20 min. Neurons were visualized and imaged using a water immersion objective (40X, NA 0.8, Olympus). The indicator was excited at 350/380nm (100ms duration at each wavelength, Till Polychrome IV) and fluorescence emission (510nm center λ) was detected using a CCD-based system (TiLL Photonics, Grafelfing, Germany). For analysis, data from regions of interest ~2.5x2.5μm for dendrites and ~5.0x5.0μm for somata were first background subtracted in each frame. For figure presentation, images were first background subtracted, then ratio images were generated and then filtered using 3 pixel x 3 pixel averaging. Final images were masked using an image generated from raw 380nm fluorescence images. Conversion to

estimated Ca^{2+} concentrations was done using unfiltered pixel values, as described in (Iwamoto et al., 2004) using in vitro Ca^{2+} concentration standards.

Drugs and Solutions

ACSF contained (in mM): 126 NaCl, 3 KCl, 1.25 NaH_2PO_4, 1 $MgSO_4$, 26 $NaHCO_3$, 2 $CaCl_2$, and 10 glucose, equilibrated with 95%O_2 / 5%CO_2. Cutting solution contained (in mM): 3 KCl, 1.25 NaH_2PO_4, 6 $MgSO_4$, 26 $NaHCO_3$, 0.2 $CaCl_2$, 10 glucose, 220 sucrose and 0.43 ketamine. KB-R7943 was from Tocris (Ellisville, MO). We found that another available inhibitor of reverse-operation NCX1-3 (SN-6 (Hell et al., 1993), Tocris) was not suitable for these experiments because of insufficient solubility in ACSF (turbidity at 30 μM). The Ca^{2+} indicators Fura-2 and Fura-6F were from Invitrogen (Carlsbad, CA). All other reagents were from Sigma-Aldrich (St Louis, MO).

Statistical analysis

Differences between multiple groups were evaluated by one way analysis of variance (ANOVA), with Bonferroni‟s post-hoc test. Significant differences between pairs of data were evaluated by either paired or unpaired Student‟s t-tests. $p<0.05$ was considered significant for all tests. Throughout the study, experiments testing the effects of pharmacological inhibitors were interleaved with “control” responses, using different slices from the same experimental animals.

4.4 Results

Effects of KB-R7943 on CA1 neurons

The effects of KB-R7943 were first examined on Ca^{2+} transients produced by intracellular current injection (**Figure 4.1).** Depolarizing current pulses (100-500pA, 500ms) produced trains of action potentials and Ca^{2+} transients in somata and apical dendrites. A series of current intensities (100-500pA) was tested in each neuron and responses produced by 16-20 action potentials were selected for comparison. Responses in control ACSF were stable over time (10 min intervals shown in Figure 4.1A), but exposure to KB-R7943 (10μM, 10 min) produced a significant reduction in the peak amplitude of Ca^{2+} transients recorded from somata. Responses in the apical dendrite (20μm from somata) were larger than soma responses, but were not affected by KB-R7943 exposure. Representative data from a single neuron is shown in Figure 4.1A and B. These figures also show that KB-R7943 caused no significant change in decay kinetics of either compartment, and no obvious change in action potential waveform. Table 4.1 summarizes data from eight neurons, showing that KB-R7943 had no significant effect on action potential amplitude or duration, input resistance, or numbers of spikes elicited during a 300pA test pulse. Summary data showing the selective inhibition of Ca^{2+} transients in somata is shown for a population of six neurons in Figure 4.1C.

Previous work has established a prominent distribution of L-type Ca^{2+} channels on CA1 somata (Ouardouz et al., 2005), and inhibition of L-type channels by KB-R7943 has

recently been reported (Hochstrate and Schlue, 2001). We therefore examined whether the effects of KB-R7943 described above were mimicked and occluded by nimodipine, an inhibitor of L-type channels. As shown in **Figure 4.2**, nimodipine exposure produced a significant reduction in somatic Ca^{2+} transients, with no effect on responses in an adjacent dendrite segment. Furthermore, pre-exposure to nimodipine completely abolished effects of subsequent KB-R7943 exposure. Since this suggests that the effects of KB-R7943 are due to L-type channel block (see Discussion), nimodipine was included (except where noted) in all subsequent experiments to prevent complication from effects on L-type influx on evaluation of NCX activity.

Effects of KB-R7943 on responses to NMDA exposure

To assess the effects of KB-R7943 on much higher Ca^{2+} loads, such as those that might be involved in excitotoxic injury, we examined responses to NMDA (5μM in modified ACSF lacking Mg^{2+}, and containing nimodipine 10μM) (**Figure 4.3**). NMDA produced an initial transient Ca^{2+} increase throughout neurons, followed by recovery to near-basal levels. After a significant delay, a secondary sustained Ca^{2+} elevation was observed in dendritic processes, that propagated to somata. Initial Ca^{2+} increases occurred following a delay of 14.4±0.9 min (n=20) after the onset of NMDA exposure. Neurons that did not show prompt decreases in Ca^{2+} concentration usually showed a rapid decline in fluorescence indicating increased membrane permeability, and were discarded from the study (2/22 neurons). In the majority of cases, secondary Ca^{2+} increases initiated in distal apical dendrites (18/20), and in the remaining cases, propagating events were initiated in

basal dendrites (2/20). In all cases the Ca^{2+} elevation were sufficient to saturate the high-affinity indicator Fura-2. After propagation throughout dendritic processes, secondary Ca^{2+} increases ultimately arrived at somata 28.3±3.3 min (n=7) after initial transient Ca^{2+} increases. Upon arrival at somata, somatic Ca^{2+} elevated to very high levels and were associated with loss of indicator fluorescence. Figure 4.3A shows a representative example of primary and secondary Ca^{2+} increases following NMDA exposure.

A separate set of studies addressed the possibility that the inclusion of nimodipine could alone significantly modify Ca^{2+} elevations produced by NMDA. When NMDA was applied without nimodipine pre-exposure (5μM, in modified ACSF lacking Mg^{2+}), Ca^{2+} elevations were not impaired, when compared with responses described above. Primary Ca^{2+} increases occurred 13.2±0.9 min (n=4) after NMDA onset, and secondary Ca^{2+} increases initiated in apical dendrites, and arrived at somata 22.3±3.2 min after primary Ca^{2+} increases (n=4). The fact that these parameters were not significantly different from responses recorded in the presence of nimodipine ($p>0.40$), implies that Ca^{2+} entry via L-type Ca^{2+} channels is not a significant contributor to propagating secondary Ca^{2+} increases produced by sustained NMDA exposure. Nimodipine was included in all subsequent studies.

Six preparations were exposed to KB-R7943 for 20 minutes prior to NMDA exposure. The representative example shown in Figure 4.3B shows that the inhibitor did not reduce the amplitude of primary Ca^{2+} increases, nor prevent the initiation and propagation of secondary Ca^{2+} increases from the apical dendrites. **Figure 4.4** shows mean data from

six neurons showing the lack of effect on primary Ca^{2+} transient amplitude (4.4A), interval between primary and secondary Ca^{2+} increases measured in somata (4.4B) or the propagation rate of secondary Ca^{2+} increases from apical dendrite to somata (4.4C). These observations suggest that reverse-operation NCX is not a significant contributor to sustained Ca^{2+} increases in dendrites and somata, produced by sustained NMDA exposure.

The high Ca^{2+} affinity of Fura-2 is useful for assessing the advancing front of propagating dendritic Ca^{2+} elevations, but results in saturation at locations behind the front. To test the hypothesis that KB-R7943 may affect ultimate levels during primary and secondary Ca^{2+} increases, a set of studies was repeated using the low affinity indicator Fura 6F. Estimates of amplitudes of primary and secondary Ca^{2+} elevations in both somata and apical dendrite segments were not significant influenced by KB-R7943 (n=5 for each group, **Table 4.2**).

K^+-free ACSF

Since KB-R7943 does not block K^+-dependent Na^+/Ca^{2+} exchangers (NCKX), possible contributions of NCKX to Ca^{2+} elevations were examined by exposure to K^+-free ACSF (see Introduction). In initial experiments, four neurons were exposed to K^+-free ACSF (without concomitant NMDA exposure) for over 50 min each and no change in Ca^{2+} levels were observed ($[Ca^{2+}]_i$=98.4±2.71nM during the first minute and 99.2±3.55nM at the 50th minute). In subsequent experiments, K^+-free ACSF was applied after initial Ca^{2+}

transients elicited by NMDA, to determine whether NCKX was involved in degenerative Ca^{2+} transients propagating along apical dendrites. If NCKX was a significant contributor to propagating events, we would expect a slowing of events, and an increase in interval between primary and secondary Ca^{2+} increases. However, when this was attempted in slice, secondary Ca^{2+} increases were significantly accelerated, rather than inhibited (n=7, Figure 4.4). The acceleration was prevented by a pre-exposure to KB-R7943. Most likely, the accelerating effect of K^+-free medium is due to inhibition of Na^+/K^+ ATPase activity (Kiedrowski, 2004). When Na^+/K^+ ATPase is inhibited, cytosolic $[Na^+]$ increases at a faster rate which causes NCX reversal more quickly, and the latter is inhibited by KB-R7943

Na^+/K^+ ATPase inhibition results in reverse-operation NCX

A Na^+/K^+ ATPase inhibitor (ouabain 30μM, in the presence of nimodipine 10μM), was used to assess Ca^{2+} responses to progressive intracellular Na^+ loading (**Figure 4.5**). The concentration of ouabain was chosen as it partially inhibits the Na^+/K^+ ATPase producing a response temporally similar to the NMDA response discussed above. Ouabain produced an initial Ca^{2+} transient 8.3±1.8 min (n=6) after onset of drug application, followed by recovery to near basal levels. A second, irrecoverable Ca^{2+} increase then occurred, which originated in the basal dendrites of all neurons studied (6/6). The secondary Ca^{2+} increase then invaded the soma, and spread into the apical dendrite in 4/6 neurons. In 2/6 neurons secondary Ca^{2+} elevations were observed in both apical and basal dendrites, but the somata was invaded first by events initiated in a basal dendrite. Figure

4.5A shows a representative example, illustrating basal dendrite involvement. Figure 4.5B shows population data. KB-R7943 significantly decreased initial Ca^{2+} increases produced by ouabain (Figures 4.5B and C). There was also a significant increase in the time required for propagating secondary responses to invade somata (Figure 4.5D).

An additional set of experiments examined the combined effects of NMDA and ouabain. Neurons were first exposed to NMDA (5μM) until a primary Ca^{2+} increase occurred and then ouabain (30μM) was applied in the continued presence of NMDA. As would be expected from the observations above, inhibition of Na^+/K^+ ATPase accelerated dendritic secondary responses with the secondary Ca^{2+} increase arriving at the somata 8.96±0.6 min after ouabain application. KB-R7943 reversed this effect, and the delay to secondary Ca^{2+} increases was increased to 11.1±0.8 min ($p<0.05$).

In a final set of experiments, K^+-free ACSF was tested with ouabain to study the role of NCKX when the Na^+/K^+ ATPase is inhibited. The perfusate was switched to K^+-free ASCF prior to ouabain exposure. In K^+-free ACSF the time to non-recoverable Ca^{2+} increases following ouabain exposure was decreased (9.69±0.6 min), compared with ouabain alone (21.30±2.3 min). From these data it appears that, in slice, a role for NCKX cannot be studied using the K^+-free medium method that has been described in cultured neurons (Iwamoto et al., 1996).

4.5 Discussion

This study combined single-neuron Ca^{2+} imaging and electrophysiological studies to assess the possible contribution of NCX to excitotoxic Ca^{2+} loading in CA1 neurons in

acute slices. The reverse-operation NCX inhibitor KB-R7943 decreased Ca^{2+} influx via L-type channels, but when this effect was taken into account, a role for reverse-operation NCX could be demonstrated. In slice, degenerative Ca^{2+} increases were observed to initiate in dendritic processes, and then propagate throughout neurons, resulting in irrecoverably high Ca^{2+} levels throughout cells. Reverse-operation NCX appears to contribute to these events, when triggered by excessive Na^+ loading. However, other Ca^{2+} entry routes may be more significant during NMDA exposures, when applied without concomitant inhibition of Na^+/K^+ ATPase activity. The possible contribution of K^+-dependent Na^+/Ca^{2+} exchangers (NCKX) as one of these contributing pathways proved difficult to assess in acute slices, without the availability of selective pharmacological agents.

Effects of KB-R7943 on spike-driven Ca^{2+} transients

Short trains of action potentials resulted in brief Ca^{2+} transients in somata and proximal dendrite segments in CA1 neurons. These responses involve multiple types of voltage-dependent Ca^{2+} channels (VDCCs, see below) and reverse-operation Na^+/Ca^{2+} exchange appears unlikely to make a significant contribution in either somatic or dendritic compartments to Ca^{2+} elevations produced by these stimuli. KB-R7943 has little or no demonstrated interaction with many ion channels and transporters (Iwamoto et al., 1996), and had no significant effect on active or passive membrane properties in the present study. However, a significant reduction of somatic Ca^{2+} entry was observed, and attributed to inhibition of L-type Ca^{2+} channels, rather than inhibition of NCX activity.

Somatic action potential-driven Ca^{2+} entry was reduced by KB-R7943 just as effectively as was observed with a selective L-type channel blocker (nimodipine), and nimodipine fully occluded the effects of KB-R7943 on somatic Ca^{2+} entry. An inhibitory effect of KB-R7943 on L-type channels was initially reported in cardiac muscle (Hoyt et al., 1998; Matsuda et al., 2001; Czyz and Kiedrowski, 2002; Ouardouz et al., 2005). Subsequent studies suggest that KB-R7943 may bind to, and act in a dihydropyridine manner to stabilize the inactivated conformation of these channels (Papa et al., 2003). However, the lack of effect of KB-R7943 on dendritic Ca^{2+} transients implies that other VDCCs are not affected, allowing studies of reverse-operation NCX in dendrites following more excessive stimulation (see below), without the complication of VDCC block.

CA1 neurons express NCX1, NCX2 and NCX3 mRNA, and protein expression in apical dendrites was suggested from immunohistochemical localization of these three isoforms in CA1 stratum radiatum (Minelli et al., 2006; Lorincz et al., 2007). Consistent with this suggestion, recent electron microscopic studies have demonstrated immunoreactivity for NCX1-3 in dendritic shafts and spines in this region (Scheuss et al., 2006; Lorincz et al., 2007). Forward-operation NCX activity has recently been shown to contribute to Ca^{2+} extrusion from dendritic shafts and/or spines of CA1 neurons following synaptic stimulation (Iwamoto and Shigekawa, 1998).

To test the hypothesis that reverse-operation NCX can contribute to Ca^{2+} influx in CA1 neurons, all three NCX isoforms have to be down-regulated. We achieved this goal using KB-R7943, as the drug inhibits NCX1, NCX2 and NCX3 reversal (Matsuda et al., 2001).

In contrast, SEA0400 (Iwamoto and Kita, 2004) inhibits NCX1 reversal with high affinity, but fails to inhibit NCX3, and relatively weakly inhibits NCX2 reversal (Pignataro et al., 2004b; Boscia et al., 2006). We also considered that the overall NCX activity in CA1 neurons could be compromised by a simultaneous knockdown of all three NCX isoforms (using RNA interference or antisense oligonucleotide strategy (Connor and Cormier, 2000). However, considering that the chances of success in such knockdown are small and would also remove possible beneficial effects of forward-operation NCX activity, we did not attempt this strategy.

NCX does not contribute significantly to Ca^{2+} elevations during extended NMDA exposure

NMDA exposure in slice produced transient primary Ca^{2+} increases, followed by non-recoverable secondary Ca^{2+} rises that initiated in apical dendrites and propagated throughout neurons. After invasion of somata, secondary Ca^{2+} increases remained irrecoverably high. The propagation of events along apical dendrites was similar to that previously described with glutamate iontophoresis (Shuttleworth and Connor, 2001) or kainate stimulation (Thompson et al., 2002) in slice. In the present study, secondary responses to NMDA initiated in apical dendrites, likely due to the predominant distribution of NMDA receptors in this compartment (Shuttleworth and Connor, 2001). The lengthy delays between primary and secondary Ca^{2+} increases recorded in somata appear to be explained, at least in part, by the time taken for Ca^{2+} overload to progress from remote initiation sites to the soma. As described previously, somatic Ca^{2+}

elevations did not increase before the arrival of excessive Ca^{2+} increases from a dendritic process (Tymianski et al., 1993; Rajdev and Reynolds, 1994; Nicholls and Budd, 2000). Long delays before secondary Ca^{2+} increases in somata have been investigated extensively using somatic Ca^{2+} measurements in neuronal cultures (Connor et al., 1988), and responses involving NMDA may involve mitochondrial dysfunction and generation of reactive oxygen species. The reasons why Ca^{2+} overload occurs first in fine distal dendrites and propagates slowly throughout neurons in slice is not yet known, but may include these mechanisms, and/or localized modification of voltage-dependent Ca^{2+} entry via kinase mechanisms (Shuttleworth and Connor, 2001).

Previous work showed that influx of Ca^{2+} from the extracellular space was responsible for propagating dendritic Ca^{2+} increases (Magee and Johnston, 1995; Kavalali et al., 1997), but the Ca^{2+} entry routes are currently unknown. Results from the present study show that entry via L-type VDCCs is not a significant contributor to spike-driven Ca^{2+} entry, or initiation and propagation of secondary Ca^{2+} elevations along dendrites. Likewise, the lack of effect of KB-R7943 on NMDA primary or secondary Ca^{2+} increases, suggests little contribution from reverse-operation NCX activity. Alternative pathways include flux via NMDA receptors, other (non-L-type) VDCCs found in dendrites of CA1 neurons (Kiedrowski, 2004), and also K^+-dependent Na^+/Ca^{2+} exchangers (NCKX) (Kiedrowski, 2004). KB-R7943 does not inhibit reverse-operation NCKX and pharmacological inhibitors are not yet available. A contribution of NCKX to Ca^{2+} influx was previously tested in neuronal cultures by comparing the effects of K^+-free versus K^+-containing medium on the rate of Ca^{2+} influx in the presence of 1 mM ouabain

(Hoyt et al., 1998; Sobolevsky and Khodorov, 1999; Czyz et al., 2002). In slice preparations, unlike in cell cultures, a studied neuron is embedded 15-55 µm underneath the surface and does not have a direct contact with the superfusate. If Na^+/K^+ ATPase operation is compromised, K^+ efflux from cells within the slice (neurons and glia) elevates external $[K^+]$ within the slice, even if the medium with which the slice is being perfused is K^+-free. Although these experiments can not be used to assess the contribution of NCKX in Ca^{2+} elevations in CA1 neurons in slice, they do suggest that reverse-operation NCX activity is activated when Na^+/K^+ ATPase operation is compromised either by ouabain or K^+-free medium or both.

Inhibition of NMDA receptors by KB-R7943 has been a controversial subject (Sobolevsky and Khodorov, 1999), but the lack of effect of 10µM KB-R7943 on primary or secondary Ca^{2+} increases suggests that there was not significant NMDA receptor block in the present experiments. It is possible that NMDA receptors with differential sensitivity to KB-R7943 exist, as discussed by Sobolevsky and Khodorov (Hochstrate and Schlue, 2001) and contribute to differences between reports.

Responses to ouabain

Ouabain inhibits Na^+/K^+ ATPase activity, and can elevate neuronal cytosolic Ca^{2+} levels as a consequence of depolarization and influx via VDCCs (Blaustein and Lederer, 1999). It has also been clear for several decades from studies including atrial muscle and squid axons that Na^+/Ca^{2+} exchange provides an additional route of Ca^{2+} entry during ouabain application, due to Na^+ accumulation and depolarization (Kiedrowski et al., 2004). In

previous work with cultured forebrain neurons, it was concluded that high intraneuronal Na^+ loads produced by ouabain were responsible for reverse-operation NCX (Czyz and Kiedrowski, 2002; Kiedrowski et al., 2004). In the present study, ouabain produced primary Ca^{2+} elevations, followed by secondary Ca^{2+} responses that were similar in some respects to responses observed with NMDA. In contrast to NMDA responses, propagating Ca^{2+} elevations following ouabain exposure were often initiated in basal dendrites, and propagated relatively quickly into somata. Differences between NMDA and ouabain responses could be due to differences in dimensions of apical dendrites versus the finer basal dendrites, if pump inhibition was the same in all locations, or alternatively, the difference could arise from the differential distribution of NMDA receptors.

Primary Ca^{2+} responses in ouabain were greatly reduced by KB-R7943, suggesting that Na^+ accumulation and NCX activity is a predominant contributor to this initial event. Secondary Ca^{2+} responses were significantly reduced, but not blocked by KB-R7943. Since the interval before invasion of somatic compartments was delayed by NCX inhibition, it is possible that propagation is due in part to NCX-mediated Ca^{2+} influx in dendrites. If this is the case, then localized Na^+/K^+ ATPase inhibition (as may occur during ischemia or other insults) may involve dendrites as initiation sites for Ca^{2+}-dependent injury by this mechanism. This possibility remains to be investigated, once the Ca^{2+} influx pathways involved in dendritic Ca^{2+} elevations are fully elucidated.

Combined application of ouabain and NMDA

The fact that ouabain potentiated the effects of NMDA by increasing secondary Ca^{2+} responses was not unexpected, given this additional route of Ca^{2+} influx as well as other possible consequences of ouabain-induced membrane depolarization. Previous work has concluded that reverse-operation NCX and NCKX contribute to Ca^{2+} influx and excitotoxicity when NMDA application is combined with Na^+/K^+ ATPase inhibition (Kiedrowski et al., 2004).

An interaction of ouabain and NMDA may explain the differences in reported involvement of NCX. For example, it was shown that NMDA-mediated reversal of NCX contributes to excitotoxicity in cultured forebrain neurons when ouabain is present (Hoyt et al., 1998), but not if ouabain is absent (Kiedrowski et al., 2004). It was suggested by Kiedrowski, *et al*. (Leao, 1944) that an active Na^+/K^+ ATPase counteracts Na^+ accumulation brought on by NMDA application and limits NCX reverse operation. The results of the current study support this suggestion as a role for NCX is evident when the pump is inhibited by ouabain and presumably K^+ removal.

Conclusion

Ca^{2+} overload in neurons in slice originates in small dendritic compartments and propagates relatively slowly to the soma. The basis of this regional Ca^{2+} overload is not well understood, but it is possible that this involves (in part) reverse-operation NCX,

particularly when Na^+/K^+ ATPase is inhibited by ouabain (or compromised by ATP depletion). Ca^{2+} influx via reversed NCKX may also be involved, but this pathway could not be assessed from these experiments. In the absence of Na^+/K^+ ATPase inhibition, other Ca^{2+} influx pathways, such as VDCCs and NMDA channels, may be more important in producing propagating Ca^{2+} overload triggered by activating NMDA receptors. The demonstration of reverse-operation NCX activity does suggest that this pathway may be more predominant in dendrites under pathological conditions, where glutamate receptor activation is combined with ATP depletion and Na^+/K^+ pump failure.

4.6 Figure Legends

Figure 4.1: KB-R7943 reduced evoked Ca^{2+} responses in soma but not dendrites. A: Representative example of intracellular Ca^{2+} response in CA1 pyramidal neuron, showing that KB-R7943 (10μM, 10 min, open triangle) reduced the peak response in the soma, but not in the proximal apical dendrite. Sequential sets of control responses were measured at 10 minutes intervals (closed circles and squares). The bar below each trace indicates the duration of intracellular current injection. **B:** Representative trains of action potentials evoked by current injection (200pA, 500ms from -65mV). Neurons show spike frequency adaptation under control conditions and following KB-R7943 exposure. A and B are from the same cell. **C**: Mean peak Ca^{2+} transients from experiments as illustrated in A (n=5), * $p<0.05$, ANOVA with Bonferroni"s post-hoc test. Scale bars; 200ms, 20mV.

Figure 4.2: Nimodipine mimicked and occluded the effects of KB-R7943. A&B: Representative responses from the soma and proximal apical dendrite of a CA1 pyramidal neuron following intracellular current injection. Nimodipine (10μM, 10 min, open circles) selectively reduced the amplitude of Ca^{2+} transients recorded in soma, but not proximal dendrite. Subsequent addition of KB-R7943 (10μM, open triangles) produced no additional effect on Ca^{2+} transients in either compartment. The bar below each trace indicates the duration of current injection. **C:** Mean peak intracellular Ca^{2+} responses, from 6 experiments as illustrated in A.

* $p<0.05$, ANOVA with Bonferroni‟s post-hoc test. Scale bars; 200ms, 20mV.

Figure 4.3: KB-R7943 did not prevent Ca^{2+} responses produced by NMDA. A: Representative example of Ca^{2+} transient in response to continuous bath application of NMDA (5μM). The far left panel shows Fura-2 excited at 380nm and the following panels (*1-7*) show estimated Ca^{2+} concentrations as false color images (scale at right). The plot shows somatic Ca^{2+} levels. Pre-stimulus Ca^{2+} levels are indicated by the dotted line and the numbers refer to individual color images above. NMDA produced a primary Ca^{2+} increase (2) followed by a recovery to near resting levels (3). Following a delay, an irrecoverable secondary Ca^{2+} increase initiated in the apical dendrite and propagated (*arrows*) along the apical dendrite and ultimately involved the soma (4-7). **B:** Representative example of a CA1 pyramidal neuron that was exposed to KB-R7943 (10μM) for 20 minutes prior to NMDA application. The details are otherwise as described above for A. KB-R7943 pre-exposure did not prevent primary or secondary

Ca^{2+} increases produced by NMDA. Nimodipine (10μM) was present throughout, in all panels. Scale bars, 10μm.

Figure 4.4: Population data from experiments illustrated in Figure 4.3. A: Peak primary Ca^{2+} transients in neurons exposed to NMDA (black, n=7) and neurons pre-exposed to KB-R7943 prior to NMDA application (white, n=6). **B:** Mean interval between primary and secondary Ca^{2+} increases produced by NMDA. Pre-exposure to KB-R7943 (n=6) prior to NMDA application had no effect on interval, compared with bracketed control values (n=7). K^+ reduction (see Methods) decreased the interval between primary and secondary Ca^{2+} increases (n=7). The effect of K^+-free ACSF was prevented by KB-R7943 pre-exposure (n=6). * $p<0.05$, ANOVA with Bonferroni‟s post-hoc test. **C**: Mean propagation rates of secondary Ca^{2+} responses along apical dendrites. K^+-free ACSF increased propagation rates, and this effect was prevented by KB-R7943. * $p<0.05$, ANOVA with Bonferroni‟s post-hoc test. Nimodipine (10μM) was present throughout.

Figure 4.5: Effects of Na^+/K^+ ATPase inhibition. A: Representative example of effects of ouabain exposure (30μM). The far left panel shows Fura-2 excited at 380nm and the following panels show estimated Ca^{2+} concentrations as false color images (scale at right). The numbers indicate the time (in min) relative to onset of ouabain application. After a transient primary Ca^{2+} increase, a secondary Ca^{2+} increase initiated in a basal dendrite (*arrows*, 16 min), which subsequently invaded the soma and spread throughout apical dendrites. Scale bar, 10μm. **B:** Population soma Ca^{2+} data, showing cells exposed

to ouabain alone (*black*), and bracketed cells pre-exposed to KB-R7943 before ouabain onset (*red*). Note that transient, primary Ca^{2+} increases were decreased, and secondary Ca^{2+} increases were delayed by the NCX inhibitor. The asterisk indicates the plot corresponding to the cell in A. **C.** Significant decrease in primary Ca^{2+} transient amplitude. Control, n=7, KB-R7943 n=6. * $p<0.01$, unpaired Student‟s t-test. **D:** Increased interval between primary and secondary Ca^{2+} increases during ouabain exposure Control, n=7; KB-R7943, n=6, * $p<0.05$, unpaired Student‟s t-test. Nimodipine (10μM) was present throughout, in all panels.

Table 4.1: Lack of effect of KB-R7943 on CA1 membrane properties. Data are expressed as mean ± SEM and were obtained from seven preparations exposed to KB-R7943 (10μM). RMP, resting membrane potential; AP, action potential; Adaptation, spike frequency adaptation (interval between 9^{th} and 10^{th} spikes compared with the interval between 1^{st} and 2^{nd} spikes) during an action potential train. KB-R7943 exposure did not result in significant differences for these parameters (paired Student‟s t-tests).

Table 2: Lack of effect of KB-R7943 on peak Ca^{2+} elevations during NMDA exposure. Data are expressed as mean ± SEM (n=5 each) and indicate peak Ca^{2+} elevations (μM) generated by NMDA, and measured using the low affinity Ca^{2+} indicator Fura 6F. KB-R7943 had no effect on either primary or secondary Ca^{2+} elevations in either the somatic or dendritic compartments (unpaired Student‟s t-tests). Nimodipine (10μM) was present throughout.

Figure 4.1

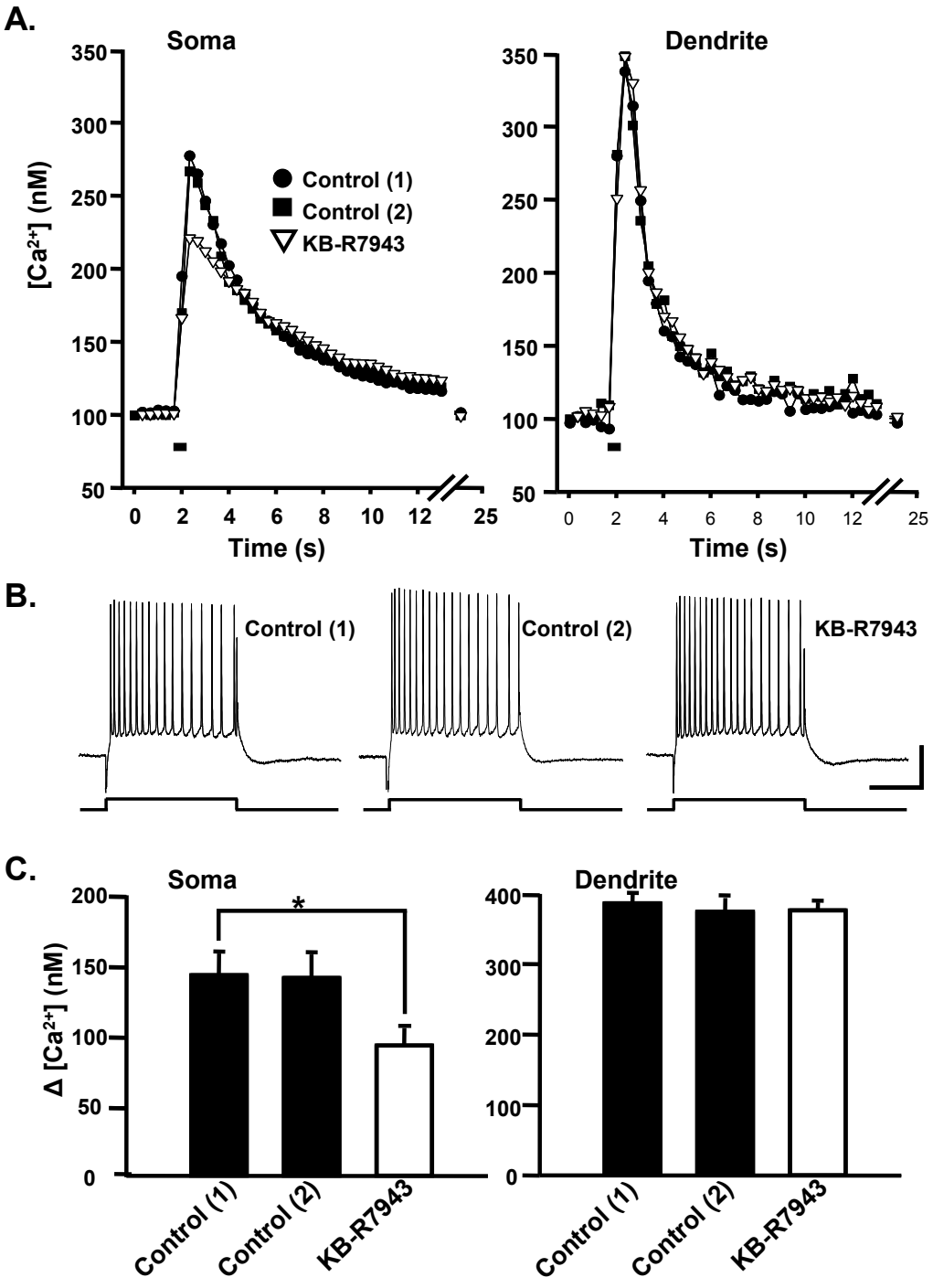

Figure 4.2

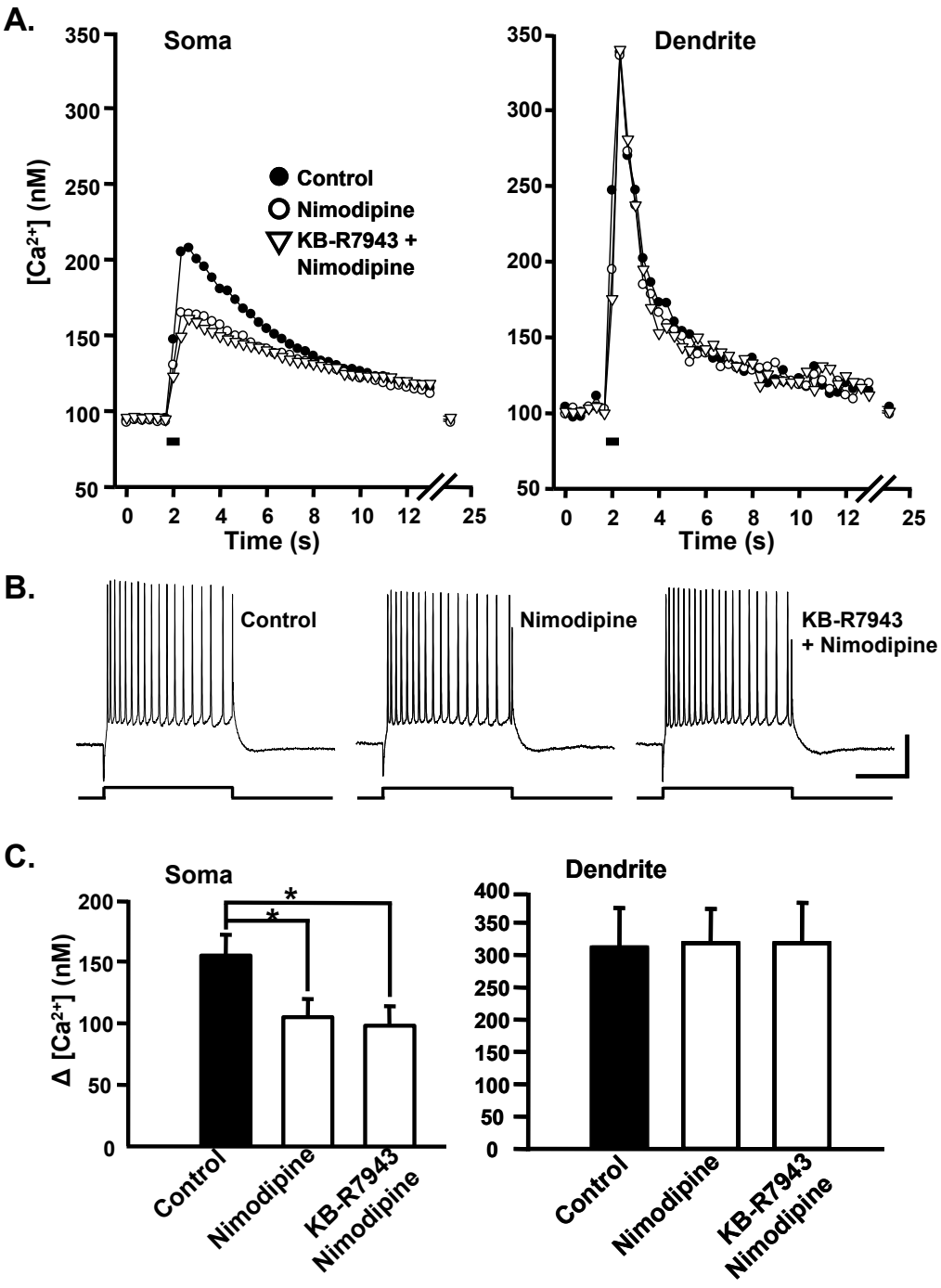

Figure 4.3

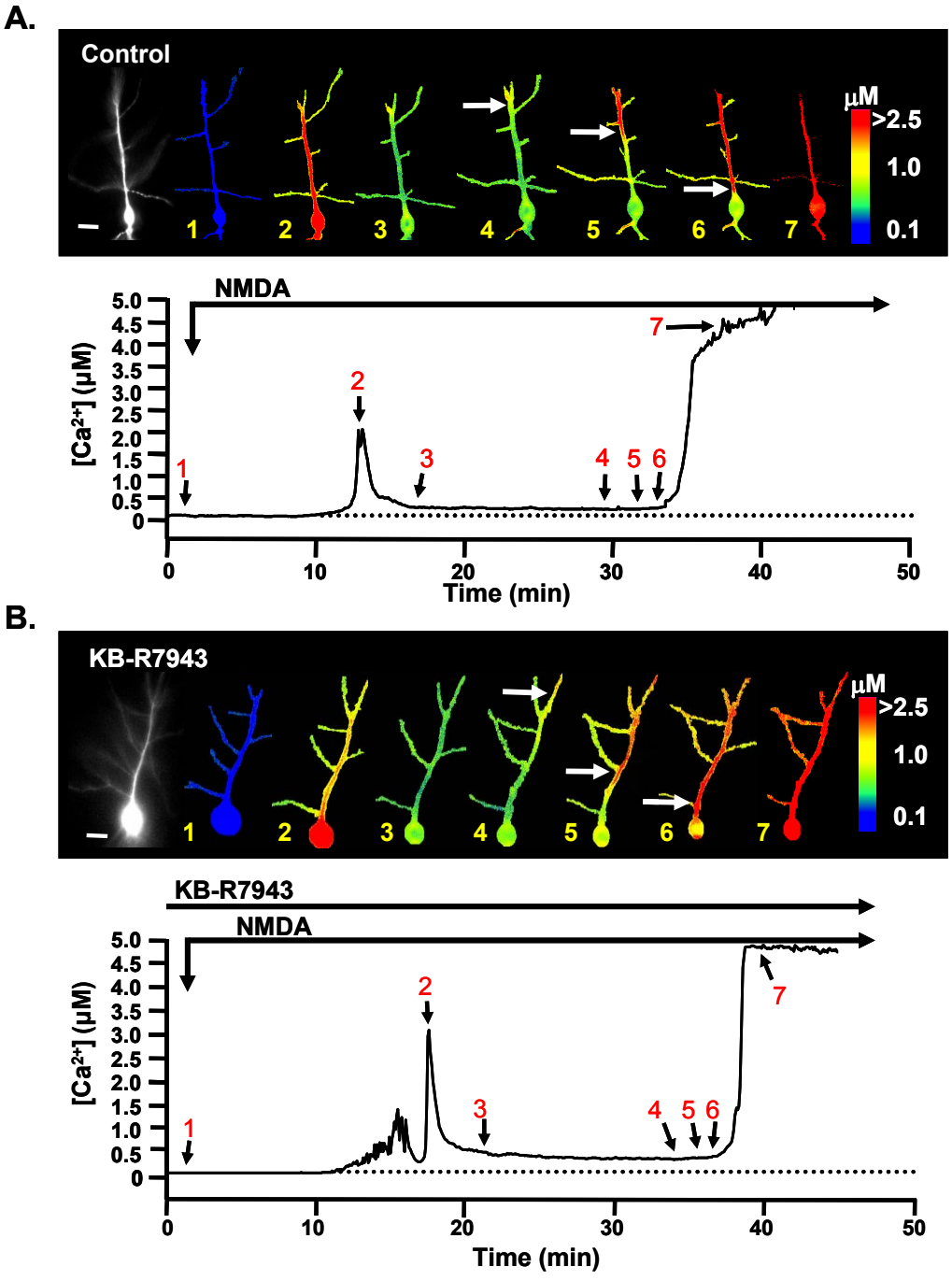

Figure 4.4

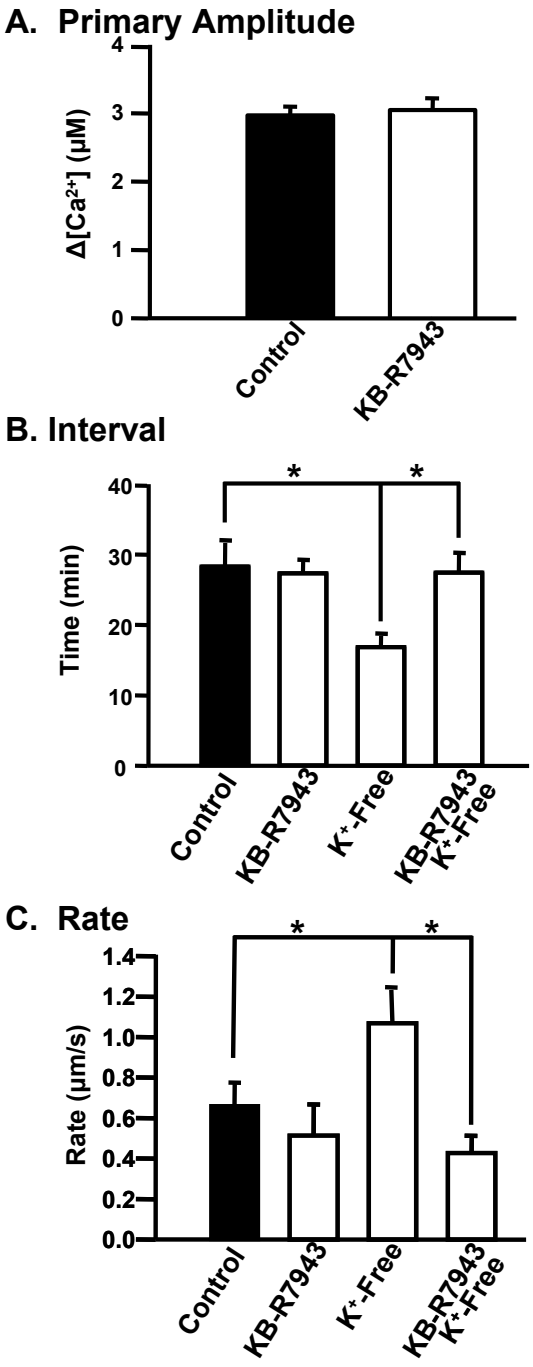

Figure 4.5

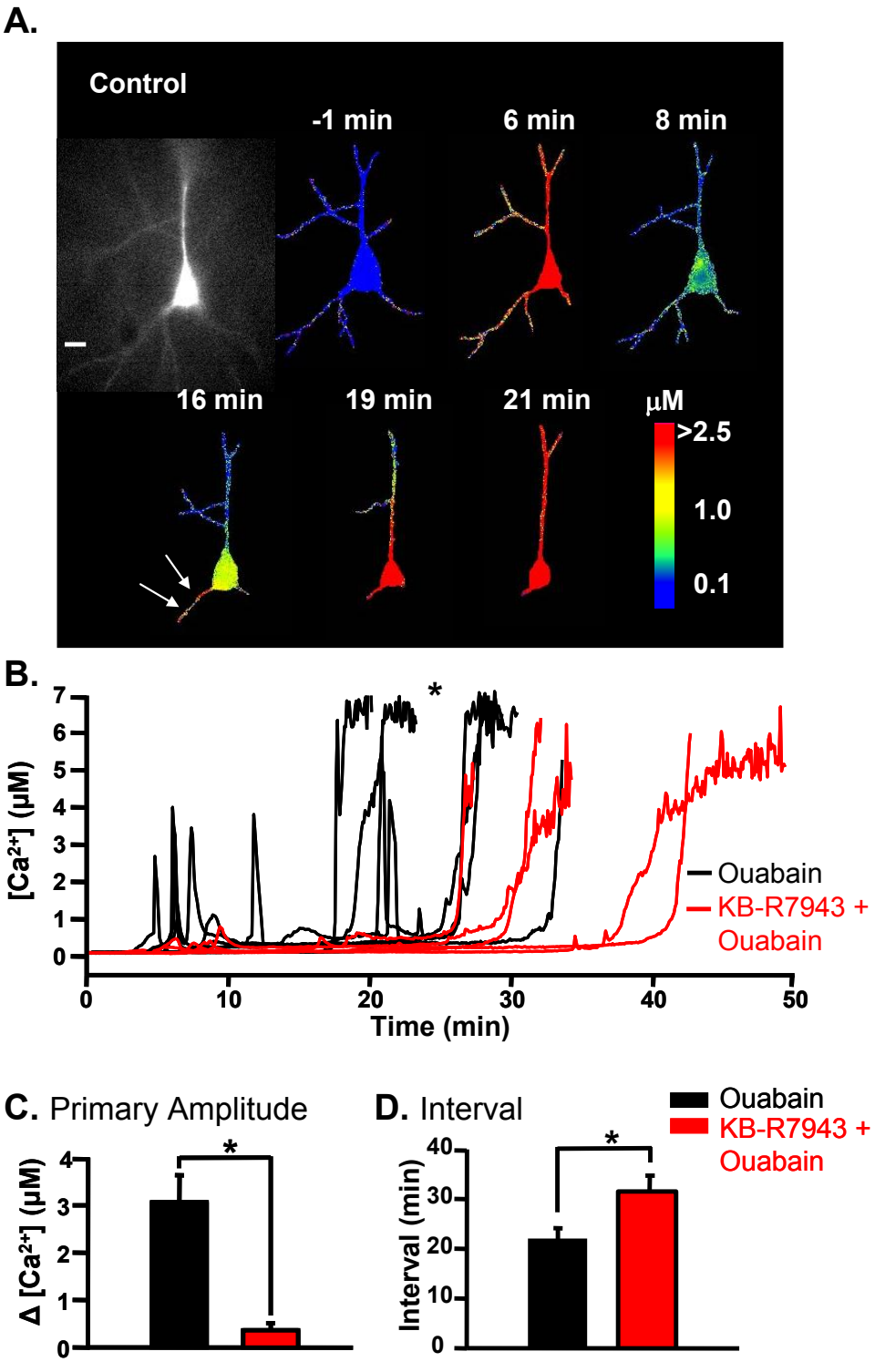

Table 4.1

	Control	**KB-R7943**
RMP (mV)	-65.0±0.1	-65.0±0.03
Input Resistance (MΩ)	99.5±15.0	108.1±17.1
AP amplitude (mV)	68.3±2.5	69.6±3.2
AP Duration (ms)	1.36±0.05	1.35±0.04
Adaptation (%)	244.5±42.5	224.6±13.3

Table 4.2

	NMDA	KB-R7943 NMDA
Soma		
Primary	9.2±1.3	9.5±1.8
Secondary	28.6±3.5	27.8±2.8
Dendrite		
Primary	6.2±1.3	8.9±1.9
Secondary	26.4±3.2	26.3±3.1

5. Different Contributions of Zn^{2+} and Ca^{2+} to Spreading Depression

R.M. Dietz[1], J. H. Weiss[2] & C.W. Shuttleworth[1]

[1]Department of Neurosciences

University of New Mexico School of Medicine

Albuquerque NM 87131

[2]Departments of Neurology & Anatomy and Neurobiology

University of California Irvine,

Irvine, CA 92697

5.1 Abstract

Spreading depression (SD) has been associated with a range of CNS disorders. While the characteristics of SD generated by diverse stimuli appear quite similar, the intracellular mechanisms responsible for triggering SD are likely to be different. We recently showed that intracellular accumulation of Zn^{2+} was critical for initiation of SD generated by the Na^+/K^+ ATPase inhibitor ouabain, whereas Ca^{2+} accumulation was not required. We examined here whether the same was true for SD generated in an *in vitro* ischemia model (oxygen/glucose deprivation (OGD)) and for SD generated by high K^+ application to hippocampal slices. Both types of stimuli produced SD with similar extracellular voltage changes and propagation rates. Single neuron Ca^{2+} studies showed that OGD/SD produced an irrecoverable Ca^{2+} increase in CA1 neurons, but high K^+/SD produced a smaller, transient Ca^{2+} increase that recovered quickly. Removal of extracellular Ca^{2+} did not prevent OGD/SD, but abolished the propagation of high K^+/SD. Extracellular Zn^{2+} levels increased dramatically following SD generated by both stimuli, and an extracellular Zn^{2+} decrease was also noted prior to the onset of OGD/SD. Zn^{2+} chelation with TPEN abolished OGD/SD, but did not influence the initiation or propagation of high K^+/SD. These results reveal a critical distinction between the ionic mechanisms involved in the generation of different forms of SD and suggest Zn^{2+} as a novel target for limiting severe depolarizations associated with ischemic injury.

5.2 Introduction

The term spreading depression (SD) refers to a wave of severe depolarization which propagates through a brain region, leading to temporary silencing of synaptic activity.

SD was originally described following electrical stimulation of the cortical surface (see Leao, 1944), and has since been evoked *in vivo* using a wide range of other stimuli, including localized K^+ applications, mechanical stimulation, and focal ischemia. SD can also be generated in *in vitro* brain slice preparations, and the CA1 region of the hippocampus has emerged as one of the most susceptible regions for SD, and has been widely used to investigate SD mechanisms (Somjen, 2001).

Under some conditions, the consequences of SD appear quite reversible, for example when SD is triggered by brief exposures to elevated K^+ concentrations. After a period of inhibition (typically in the order of 10s of minutes), synaptic activity returns and SD can then be initiated by another K^+ stimulus. This has led to the conclusion that, in an otherwise normal brain, K^+-induced SD does not result in neuronal injury (Nedergaard and Hansen, 1988). It is possible that such SD is involved in phenomena such as migraine, which does not lead to overt cell death (Welch, 1993; Flippen and Welch, 1997; Bowyer, 1999; Cao et al., 1999; Bramanti et al., 2005). In contrast, SD is thought to be an important contributor to injury following stroke or traumatic brain injury (Hossmann, 1996; Obeidat and Andrew, 1998; Hartings et al., 2003; Church and Andrew, 2005; Strong et al., 2007). Events similar to SD are observed to initiate at the margins of ischemic infarcts and propagate throughout adjacent tissue (Nedergaard and Astrup, 1986). These events (termed peri-infarct depolarizations) are thought to produce very large and repetitive metabolic burdens on surrounding tissue, which leads to neuronal death and increase in infarct volume (Mies et al., 1993; Busch et al., 1996; Hossmann, 1996). Selectively preventing peri-infarct depolarizations in the hours following an insult

may be of great value in improving clinical outcomes, but no selective inhibitors are yet available.

Although the measured characteristics of SD triggered by either ischemia or localized high K^+ applications are very similar, the events involved in these forms of SD may be very different (Tegtmeier, 1993; Somjen, 2001). Understanding these initial mechanisms might well suggest ways to selective target SD arising in distinct circumstances. We recently found evidence for a critical role of intracellular Zn^{2+} accumulation, prior to SD triggered by the Na^+/K^+ ATPase inhibitor ouabain. Ouabain reliably produces SD in hippocampal slices (LaManna and Rosenthal, 1975; Basarsky et al., 1998; Balestrino et al., 1999) and we showed that Zn^{2+} influx via L-type Ca^{2+} channels was required for this effect. In that model, Ca^{2+} influx was not required for the initiation or propagation of SD. The present study addresses the question of whether Zn^{2+} is involved in SD generated by other stimuli, that model more directly CNS pathologies. We examined SD produced in an *in vitro* model of ischemia (oxygen glucose deprivation, OGD) and compared this with a non-injurious SD triggered by localized high K^+ exposures. We confirm that these disparate stimuli both produce a similar SD, but show for the first time these different types of SD can be clearly distinguished by dependence on either Ca^{2+} or Zn^{2+} dynamics.

5.3 Materials and Methods

Slice preparation and intracellular recording

Male mice (FVB/N) were obtained from Harlan (Bar Harbor, ME) at 4 weeks of age and were housed in standard conditions (12hr/12hr light/dark cycle) for no longer than 2 weeks before sacrifice. Numbers in the study refer to numbers of slices, each obtained from a different experimental animal for each protocol. For slice preparation, mice were deeply anesthetized with a mixture of ketamine and xylazine (85mg/ml and 15mg/ml, respectively; 200µl s.c.) and decapitated. Brains were removed and placed in ice cold cutting solution. 350µm coronal sections were cut using a Vibratome (Technical Products International, St Louis MO) and slices were transferred into 35ºC ACSF. Cutting and recording solutions were both 315-320 mOsmol. After holding for 1 hour, ACSF was changed, and slices were held at room temperature until used for recording. Individual slices were transferred to the recording chamber, and were superfused with oxygenated ACSF at ~2 ml/min (32^{o}C). Voltage recordings were made using an Axoclamp 2A amplifier (Axon Instruments, Foster City, CA), digitized (Digidata1322A) and analyzed using PClamp 9.2 (Axon Laboratory).

Ca^{2+} measurements

To provide adequate resolution of Ca^{2+} in dendrites, individual neurons were microinjected with a low-affinity Ca^{2+} indicator Fura-6F. The recording/injection microelectrodes were tip-filled with 10mM indicator in 0.5M KAc/0.5M KCl, and back-

filled with 3M KCl. These microelectrodes had resistances of approximately 100MΩ when filled with 3M KCl, and >180MΩ initially when filled with injection mixture. After a stable impalement was made, the indicator was injected by passing hyperpolarizing current (300-500pA) for 10-20 min. In all studies involving Ca^{2+} imaging, the filling electrode was withdrawn before stimulating the neuron. This procedure minimized the possibility of Ca^{2+} changes due to changes in impalement quality during intense activation of the slice. All neurons were allowed to recover for 20 min following electrode withdrawal before applying the SD stimulus. These loading conditions provided adequate resolution of apical dendrites, and the final indicator concentration was verified to be less than 200μM from comparisons with neurons loaded via patch electrodes (15-20min dialysis) and then imaged under identical conditions (see Petrozzino and Connor, 1994). Neurons were visualized and imaged using a water immersion objective (40X, NA 0.8, Olympus). The indicator was excited at 350/380nm (100ms duration at each wavelength, Till Polychrome IV) and fluorescence emission (510nm center λ) was detected using a CCD-based system (TiLL Photonics, Grafelfing, Germany). Image pairs were acquired at 3Hz for experiments shown in Figures 1&2 and 0.2Hz for all other studies. For analysis, data from regions of interest ~2.5x2.5μm for dendrites and ~5.0x5.0μm for somata were first background subtracted in each frame. For figure presentation, images were first background subtracted, then ratio images were generated and filtered using 3 pixel x 3 pixel averaging. Final images were masked using an image generated from raw 380nm fluorescence images. Conversion to Ca^{2+} concentrations was done using unfiltered pixel values, using an equation described in (Grynkiewicz et al., 1985) $[Ca^{2+}] = K_D(R-R_{min}/R_{max}-R)(S_{f2}/S_{b2})$, where R_{min} and R_{max} are

ratios at zero and saturating Ca^{2+} levels, and S_{f2}/S_{b2} is the ratio of calcium-free to calcium bound fluorescence at 380nm excitation. R_{min}, R_{max} and S_{f2}/S_{b2} values were determined from calibration solutions (containing 1mM Mg^{2+}, C-3722, Invitrogen, Carlsbad, CA) that were loaded into thin walled capillary tubes to prevent quenching effects, and imaged within the recording chamber with the same water-immersion objectives as used for neuronal recordings. A K_D of 5.6μM was assumed for Fura-6F (Invitrogen). Because of the assumptions made in using these values, the calculated values should only be considered estimates of intracellular Ca^{2+} concentrations.

Extracellular Zn^{2+} fluorescence imaging

To examine relative changes in extracellular Zn^{2+} content the Zn^{2+}-sensitive indicator FluoZin-3 was present in the ACSF at a concentration of 2μM. The slow Zn^{2+}-chelator CaEDTA (200μM) was included to reduce basal fluorescence (Qian and Noebels, 2005). FluoZin-3 was excited at 495 nm, and emission detected at 535/50nm using a 10X objective (NA 0.3, Olympus). For figure presentation, images were first background subtracted, then $\Delta F/F_0$ images were generated and filtered using 3 pixel X 3 pixel averaging. Slices were exposed to FluoZin-3 for 15 minutes and CaEDTA for 10 minutes prior to application of stimulus.

Drugs and Solutions

ACSF contained (in mM): 126 NaCl, 2 KCl, 1.25 NaH_2PO_4, 1 $MgSO_4$, 26 $NaHCO_3$, 2 $CaCl_2$, and 10 glucose, equilibrated with 95%O_2 / 5%CO_2. Cutting solution contained (in mM): 3 KCl, 1.25 NaH_2PO_4, 6 $MgSO_4$, 26 $NaHCO_3$, 0.2 $CaCl_2$, 10 glucose, 220 sucrose and 0.43 ketamine. We have previously found that the level of adenosine receptor activation in a slice can be important in determining the contribution of Ca^{2+} channels during SD and can vary between slices and animals (see Results). Therefore, in this study, the adenosine A1 receptor agonist N^6-cyclopentyladenosine (CPA, 300nM) was present in all experiments to clamp A1 activation at a high level. OGD solution was the same as ACSF except that glucose was replaced with equimolar sucrose and equilibrated with 95%N_2 / 5%CO_2. KCl (1M) was ejected from a microelectrode, by using brief pressure pulses (10psi, 100ms, Picrospritzer II). The microelectrode (3-5MΩ) was placed on the surface of the slice, ~350μm from the recording electrode). Ca^{2+}-free solutions were the same as ACSF above except that $CaCl_2$ was replaced by $MgSO_4$. The Ca^{2+} indicator Fura-6F, Zn^{2+} indicator FluoZin-3 and Zn^{2+} chelator TPEN were from Invitrogen (Carlsbad, CA). All other reagents were from Sigma-Aldrich (St Louis, MO).

Statistical analysis

Differences between multiple groups were evaluated by one way analysis of variance (ANOVA), with Bonferroni‟s post-hoc test. Significant differences between pairs of data were evaluated by either paired or unpaired Student‟s t-tests. $p<0.05$ was considered

significant for all tests. Throughout the study, experiments testing the effects of pharmacological inhibitors were interleaved with "control" responses, using different slices from the same experimental animals.

5.4 Results

Characterization of SD responses

SD was reliably produced using either deprivation of oxygen and glucose (OGD) or microinjection of 1M KCl into the hippocampal slice. **Figure 1A** shows that both stimuli elicited negative shifts in extracellular potential which were similar in waveform and amplitude (3.6±0.3 mV for OGD vs. 3.8±0.5 mV for K^+; p=0.68, n=6 each). Propagation of the spreading events was determined using NAD(P)H autofluorescence imaging (Figure 1B) (Jing et al., 1993). SD, whether by either OGD or K^+, induced a spreading wave of decreased fluorescence which propagated throughout the slice at a rate of 4.8±0.6 mm/min for OGD (n=6) and 4.6±0.5 mm/min for K^+-induced SD (n=5; p=0.85, t-test, Figure 1C). In every case, the extracellular voltage shift was completely coincident with the arrival of the autofluorescence decrease at the recording electrode, confirming the validity of the optical marker. Optical signals following the onset of SD were not assessed further, due to complications of tissue swelling due to SD (Aitken et al., 1999; Andrew et al., 1999) and significant differences in pre-stimulus levels of fluorescence immediately prior to SD under the two conditions (Sick and Perez-Pinzon, 1999; Brennan et al., 2007).

A major difference between the two stimuli was the latency to SD. Following the onset of OGD exposure, it took 10.2±0.8 min (n=6) until SD was observed. In contrast, SD occurred 0.16±0.02 min (n=6) after K^+ application. We have therefore considered that different mechanisms may play a role in the initiation of these different spreading events and explore the role of Ca^{2+} and Zn^{2+} using these different stimuli throughout the rest of this study.

Neuronal Ca^{2+} response differences dependent on stimulus

Figure 2 shows a representative example of single-neuron Ca^{2+} signals produced by OGD exposure. We used the low affinity indicator Fura-6F so that we could estimate the ultimate levels of Ca^{2+} during this event. Prior to SD there was no detectable increase in Ca^{2+} in six neurons. However, the arrival of SD was associated with a large, irrecoverable Ca^{2+} increase that originated in somata and rapidly progressed toward apical dendrites in all neurons tested. Somatic Ca^{2+} elevations were estimated at 24.1±1.1 μM, and Ca^{2+} elevations throughout the neuron showed no indication of recovery after the SD was generated. Furthermore, there was a large decrease in the fluorescence of the Ca^{2+} indicator, despite the fact that the ratio remained high after SD. In 4 neurons where the indicator loss was assessed, 81.8±3.2% (n=4) of fluorescence was lost in the 10 minutes immediately following the SD, as compared to only 4.8±1.7% in the 10 minutes prior to SD. This large loss after SD was interpreted as a loss of membrane integrity, associated with the sustained very high cytosolic Ca^{2+} accumulation.

As seen in **Figure 3**, the spatial and temporal Ca^{2+} dynamics during SD evoked by high K^+ were quite different. Instead of experiencing an irrecoverable Ca^{2+} increase, the neurons instead underwent a transient Ca^{2+} elevation (average increase 7.8±1.9μM in soma and 25.3±2.6μM measured in apical dendrite 40μm from soma) which lasted less than 5 seconds. Following this transient Ca^{2+} increase, an advancing front of high Ca^{2+} traveled from distal dendritic sites toward the soma. The advancing front of Ca^{2+} never fully involved the soma but instead quickly retreated out along the dendrites toward their sites of origin. Within an average of 1.7±0.2 min, intracellular Ca^{2+} had recovered to near resting levels. Intracellular Ca^{2+} concentrations were estimated at 109±6 nM five minutes after SD and at 112±8 nM 40 minutes after SD (n=6). These values were not significantly different than basal Ca^{2+} concentrations (104±5 nM, n=6). In three neurons, high K^+ solution was applied a second time approximately 45 minutes after the first exposure. SD was registered again and the Ca^{2+} response was similar to the first with an average Ca^{2+} increase of 6.8±1.2μM (n=3) which recovered within an average of 1.9±0.4 min. The complete recovery of cytosolic Ca^{2+} levels, and the similarity of the second event to the first imply that the SD produced by K^+ is not terminal.

Removal of Extracellular Ca^{2+}

Because there appears to be a clear difference in Ca^{2+} homeostasis associated with the two types of SD, we next examined the effects of removing extracellular Ca^{2+}. In slices subjected to OGD, removal of Ca^{2+} did not prevent the generation of SD (**Figure 4**), nor

did it change the propagation of the spreading event in interleaved experiments (4.0±0.2 mm/min vs. 4.1±0.4 mm/min control; n=6 each; p=0.75, t-test).

In contrast to the OGD experiments, removing extracellular Ca^{2+} caused a profound inhibition of the propagation of SD evoked by K^+ application, in all preparations tested (0/6 slices). Autofluorescence imaging showed that there was still a substantial NAD(P)H decrease in the proximity of the K^+ pipette, followed by an NAD(P)H fluorescence overshoot, indicative of strong localized depolarization (Shuttleworth et al., 2003). However, the response decayed steeply from the K^+ pipette, and there was no evidence of a propagating front of depolarization that could be detected by the extracellular recording electrode, positioned ~300-400 μm away.

Extracellular Zn^{2+} measurements and Zn^{2+} chelation

Figure 5 shows extracellular Zn^{2+} measurements, using the high-affinity Zn^{2+} indicator FluoZin-3 added to the superfusate. During SD elicited by either OGD or K^+, a wave of high extracellular Zn^{2+} swept across CA1 at propagation rates no different than seen in the NAD(P)H fluorescence above (3.5±0.4 mm/min for OGD, 3.8±0.3 for K^+). Figures 4C and D show that this wave of Zn^{2+} peaked immediately after SD and recovered to near pre-SD levels within 2.6±0.5 min for OGD and 2.9±0.7 min for K^+ (time to 90% recovery, n=6 each).

Because of the possibility that intracellular Zn^{2+} accumulation may contribute to the onset of SD (see below), we also evaluated extracellular FluoZin-3 fluorescence prior to the onset of SD. Following the onset of OGD applications, there was a significant decrease in FluoZin-3 fluorescence (13.8±3.0%), which could be due to translocation of Zn^{2+} from the extracellular space into neurons and/or glia. However, there was no such change in FluoZin-3 fluorescence detectable in the brief interval between K^+ injection and the onset of K^+-induced SD.

Figure 6 summarizes experiments showing that pre-exposure to the Zn^{2+} chelator TPEN (50μM) abolished OGD/SD in all slices tested (6/6 slices). In contrast, high K^+/SD was unaffected by TPEN. High K^+/SD still occurred in all slices tested (6/6) and the time before SD onset was not significantly delayed 0.17±0.04 vs. 0.15±0.08 min (control and TPEN respectively, n=6 each, p=0.75).

5.5 Discussion

General

SD can be initiated in hippocampal slices by diverse stimuli and once initiated, propagate throughout the preparation in a similar manner, producing profound depolarization of CA1 neurons. However, the results here provide the first evidence for a clear ionic distinction between SD produced by two different types of stimuli. Zn^{2+}, rather than Ca^{2+} was a critical contributor to SD produced in an *in vitro* ischemia model, but the converse was true for SD initiated by high K^+ applications. Thus removal of extracellular Ca^{2+}

prevented propagation of high K^+ SD whereas selective chelation of Zn^{2+} effectively abolished SD produced by oxygen-glucose deprivation. These findings imply different mechanisms for SD induction and suggest very different therapeutic strategies for mitigation of deleterious consequences of SD produced under different pathologic conditions.

High K^+ induced SD

While Ca^{2+} removal completely prevented high K^+/SD being recorded by a remote extracellular electrode, the autofluorescence imaging provided evidence of a strong depolarization that was restricted to the region of the K^+ source electrode (Shuttleworth et al., 2003). The lack of propagation of the event across the slice is reminiscent of previous work with non-selective Ca^{2+} channel blockers Ni^{2+} or Co^{2+}, which also prevented the spread of high K^+/SD in hippocampal slices (Jing et al., 1993). In contrast to recent observations with ouabain (Dietz et al., under review) and OGD (present study), the lack of effect of Zn^{2+} chelation on the ability to generate SD implies involvement of a strictly Ca^{2+}-dependent mechanisms in SD initiation and/or propagation.

Previous work has implicated Ca^{2+} flux via P/Q type Ca^{2+} channels in SD generated by high K^+ or brief electrical stimulation. Genetic alterations that reduce P/Q-type Ca^{2+} channel activity increase the threshold for high K^+/SD in mouse cortex (Ayata et al., 2000) and in hippocampal slice cultures, selective P/Q channel blockers prevented SD generated by strong synaptic stimulation (Kunkler and Kraig, 2004). Presynaptic

inhibition of glutamate release is a likely candidate mechanism for these effects, since P/Q-type channels are important for release of the excitatory neurotransmitter glutamate, and glutamate receptor antagonists can reduce the incidence of SD evoked by electrical or high K^+ stimulation SD (Somjen, 2001; Kunkler and Kraig, 2004).

High K^+/SD in otherwise normal tissue often recovers within 30 minutes with no apparent lasting effects (Buresova and Bures, 1969; Nedergaard and Hansen, 1988) and this reversibility has been taken to suggest that this brief localized stimulus serves to model aspects of SD related to migraine aura, and possibly even the headache associated with migraine (Dalkara et al., 2006; Cutrer and Huerter, 2007). Interestingly, P/Q channel mutations of have been found in patients with inheritable migraine diseases where Ca^{2+} flux is increased (Ophoff et al., 1996), which may be consistent with this hypothesis. Taken together, these observations suggest that targeting Ca^{2+}-, but not Zn^{2+}-dependent mechanisms may be effective for development of interventions to reduce migraine aura.

OGD-induced SD

Previous work has shown that Ca^{2+} removal does not reliably prevent SD produced by hypoxia or OGD (Young and Somjen, 1992; Bahar et al., 2000), and this is confirmed in the present work. Instead, these results provide the first evidence that effects of endogenous Zn^{2+} can be a critical causative agent for the initiation and propagation of SD with OGD.

The mechanisms by which Zn^{2+} may contribute to OGD-induced SD are not yet known. The consistent decrease in extracellular Zn^{2+} measured prior to the onset of SD is consistent with the possibility that Zn^{2+} translocates from the extracellular space (Frederickson, 1989) and contributes to SD onset (Figure 4). However it is also possible that Zn^{2+} could be released from intracellular binding sites, in response to metabolic compromise (Aizenman et al., 2000; Lee et al., 2003; Sensi et al., 2003; Bossy-Wetzel et al., 2004). A range of deleterious effects of Zn^{2+} accumulation have been described, including effects on mitochondrial function, glycolytic energy production, and effects on gap junctions that could contribute to SD (Chappell et al., 2003; Dineley et al., 2003). Additionally, it has been reported that Zn^{2+} can activate extramitochondrial ROS and NO generating pathways which could be detrimental to the cell (Kim et al., 1999; Noh et al., 1999; Kim and Koh, 2002). The relative contributions of these or other possible mechanisms to the initiation and/or propagation of SD remain to be investigated.

These findings suggest that deleterious effects of Zn^{2+} could be important for the initiation of periinfarct depolarization (PIDs, see Introduction) following *in vivo* ischemic insults. PIDs have been closely associated with tissue damage, and recent studies suggest that they are an important contributor to the progressive increase in infarct size in the days following ischemic injuries (Hartings et al., 2003; Strong et al., 2007). This is of particular interest, since chelation of Zn^{2+} has been found to be effective at limiting the size of infarcts when given prior to global ischemia in rats (Koh et al., 1996), and indeed

when given many hours following the injury (Calderone et al., 2004), at a time when PIDs are expected to be very prominent (Hartings et al., 2003).

Recording conditions

In recent work, we found that Zn^{2+} chelation could effectively prevent SD produced by the Na^+/K^+ ATPase inhibitor ouabain. In that case, the degree of adenosine A1 receptor activation was important for determining the relative importance of Ca^{2+} channels as influx routes, and L-type flux was a more prominent entry route when the A1 agonist N^6-cyclopentyladenosine (CPA) was present (Dietz et al., under review). The degree of endogenous A1 receptor activation varies somewhat between slices, and in the present study the A1 agonist was included throughout, to provide a uniform level of A1 activation. This approach mimics an important aspect of *in vivo* ischemia, where extracellular adenosine levels increase substantially (Dunwiddie and Masino, 2001). However, A1 activation will minimize presynaptic transmitter release (Dunwiddie and Masino, 2001) and could therefore underestimate the contribution of presynaptic mechanisms. Thus while it is possible that under conditions were A1 tone is lowered, presynaptic Ca^{2+} effects could make some contribution to OGD/SD propagation. We note that in studies without A1 activation, Zn^{2+} chelation still effectively prevents OGD/SD (data not shown), implying that Zn^{2+} dependent mechanisms are still major contributors to the process.

Ca^{2+} accumulation following the onset of SD

Because of the established link between Ca^{2+} overload and neuronal injury, there has been considerable interest in neuronal Ca^{2+} accumulation following SD. Previous work has shown Ca^{2+} elevations in hippocampal slices following SD, but with bulk-loading indicator approaches, it was difficult to distinguish the pattern of Ca^{2+} accumulation within single CA1 neurons (Basarsky et al., 1998). The single-neuron Fura-6F loading done here provides the first description of Ca^{2+} elevations during OGD/SD. Ca^{2+} levels rose from sites in the soma or near soma, and then rapidly spread throughout the entire neuron. The sustained high Ca^{2+} levels were accompanied by prompt indicator loss, implying compromise of the plasma membrane and neuronal injury. Despite the fact that the SD generated by high K^+ appeared very similar to the OGD event, the consequences on neuronal Ca^{2+} dynamics were completely different where Ca^{2+} elevations were highest in apical dendritic processes, and recovered relatively quickly to baseline levels following the passage of the SD. Recent work with single neuron filling has been done with SD evoked by synaptic stimulation, and showed a very similar profile as described here for high K^+/SD (Kunkler and Kraig, 2004), reinforcing the idea that the responses observed with high K^+ and brief synaptic stimulation may involve similar mechanisms.

Thus, the different Ca^{2+} responses seen with the two stimuli used here may account for the differences in the ultimate fate of the neurons following SD. The transient nature of Ca^{2+} elevations following high K^+/SD is likely a consequence of relatively unaltered metabolism preceding the event (Bahar et al., 2000) and results in a recoverable form of

SD (Buresova and Bures, 1969; Nedergaard and Hansen, 1988). Alternatively, sustained Ca^{2+} loads for extended periods of time lead to cell death (Siesjo and Bengtsson, 1989; Lipton, 1999; Arundine and Tymianski, 2003; Deshpande et al., 2007) and OGD induces what has been termed "terminal" SD (Tanaka et al., 1997; Obeidat and Andrew, 1998). The terminal nature of this form of SD is likely due to the metabolic disruption which occurs prior to SD (Bahar et al., 2000; Allen et al., 2005) and subsequent inability of the neurons to clear Ca^{2+}. In previous work, 75% reductions of extracellular Ca^{2+} concentration substantially improved recovery of orthodromic population spikes following anoxia (Roberts and Sick, 1988). Additionally, it appears that if intracellular Ca^{2+} levels can be reduced within 1.5 minutes of SD by reduction of extracellular Ca^{2+}, complete recovery of function can be regained during OGD (Tanaka et al., 1999). Similar studies showing the critical nature of Ca^{2+} during OGD-induced SD have been described (Rader and Lanthorn, 1989; Yamamoto et al., 1997).

This study also provides evidence for a substantial liberation of Zn^{2+} following the onset of SD (Figure 4), and it is possible that this contributes together with Ca^{2+} to neuronal damage observed under the conditions of OGD.

Conclusion

Because of the similarity of SD generated by different stimuli, it has been difficult to distinguish between different types of SD and find blockers that may be suitable for different pathologic conditions. These results show that Ca^{2+} and Zn^{2+} play critical roles

in different forms of SD, and identify Zn^{2+} as a candidate for inhibition of repetitive depolarizations following brain injury.

5.6 Figure Legends

Figure 5.1: Similarities of spreading depression characteristics. A: Representative records showing the sharp voltage deflection characteristic of SD was recorded with an extracellular electrode placed in stratum radiatum evoked by OGD (top trace) and K^+ (bottom trace). **B:** NAD(P)H traces showing propagation of NAD(P)H autofluorescence across the slice during SD in response to OGD (top) and high K^+ (bottom). **C.** Mean data showing that the propagation of NAD(P)H autofluorescence during SD whether evoked by OGD or K^+ is not different.(n=6 each). Scale bar: 100μm.

Figure 5.2: Ca^{2+} kinetics following OGD/SD. Single CA1 neuron loaded with Ca^{2+} indicator Fura-6F via sharp microelectrode exposed to OGD. The first panel shows raw 380nm fluorescence and subsequent panels are pseudocolor images that represent intracellular $[Ca^{2+}]$. Intracellular Ca^{2+} levels stay near basal levels until SD hits approximately 11.5 min after OGD exposure. Concurrent with SD, excessive Ca^{2+} loading is evident first in the soma, and then progresses throughout dendritic processes. Simultaneous extracellular voltage recording and somatic (black) and dendritic (red) $[Ca^{2+}]$ from the preparation are shown below. $[Ca^{2+}]$ stays high until recording is stopped. Times in the panels are relative to onset of stimulus. Scale bar: 10μm.

Figure 5.3: Ca^{2+} kinetics following K^+-induced SD. Single CA1 neuron loaded with Ca^{2+} indicator Fura-6F via sharp microelectrode in response to application of high K^+.

The first panel shows raw 380nm fluorescence and subsequent panels are pseudocolor images that represent intracellular [Ca^{2+}]. Ca^{2+} kinetics are very different in response to SD induced by high K^+ than OGD (figure 2). Approximately 8 sec after K^+ application, Ca^{2+} in the entire neuron goes to low micromolar levels, but the soma quickly recovers. This is followed by high Ca^{2+} levels arising in distal dendrites that approach the soma, but retreat before reaching the cell body. The Ca^{2+} within the cell returns to near basal levels. Simultaneous extracellular voltage recording and somatic (black) and dendritic (red) [Ca^{2+}] from the preparation are shown below. Times in the panels are relative to onset of stimulus. Scale bar: 10μm.

Figure 5.4: Effects of Ca^{2+} removal on SD. A: Group data showing the incidence (white bars) of SD evoked by either OGD or K^+. OGD-induced SD showed no effect of Ca^{2+}-removal, but SD elicited by K^+ was blocked by Ca^{2+}-free media. Removal of Ca^{2+} had no effect on the rate of propagation (filled bars) in SD elicited by OGD. **B:** Effects of Ca^{2+} removal on SD elicited by high K^+ assessed by NAD(P)H imaging. The first frame shows a bright field image of the slice and subsequent images illustrate the progression of the spreading event along the CA1 pyramidal cell layer under control conditions (top). When Ca^{2+} was removed from the ACSF (bottom), there was a decrease in NAD(P)H autofluorescence in tissue directly surrounding the tip of the K^+ electrode, but this did not spread as under control conditions. K^+, position of K^+-filled electrode; R, position of recording electrode. **C:** Regions of interest were placed 0, 150, and 300μm from the K^+ filled electrode from the preparations in B to show the progression of the spread under control conditions but not when Ca^{2+} was removed.

Figure 5.5: Extracellular Zn^{2+} kinetics during SD. A & B: Examples of propagation of extracellular Zn^{2+} as recorded by FluoZin-3 in the ACSF in response to OGD (Panel A.) and K^+ (Panel B.). The first box shows a bright field image showing the placement of the recording electrode and a region of interest from which data was collected. The subsequent images are sequential and show that a wave of extracellular Zn^{2+} increase propagates across the slice. **A' & B':** Mean graphs showing the kinetics of extracellular Zn^{2+} with respect to SD. Since SD occurred at different times, the SD events were aligned at time 0. Panel C. shows that there is a slight dip in extracellular Zn^{2+} prior to the large increase associated with SD. There is no such decrease prior to SD evoked by K^+ (Panel D) but the large increase is similar in response to SD.

Figure 5.6: Effects of Zn^{2+} chelation on SD. Group data showing the incidence of SD evoked by either OGD (left) or K^+ (right). Control responses (black bars) show that SD was readily evoked by either stimulus, but the application of TPEN (white bars) blocked OGD-induced SD, but had no effect on the incidence of SD evoked by K^+.

Figure 5.1

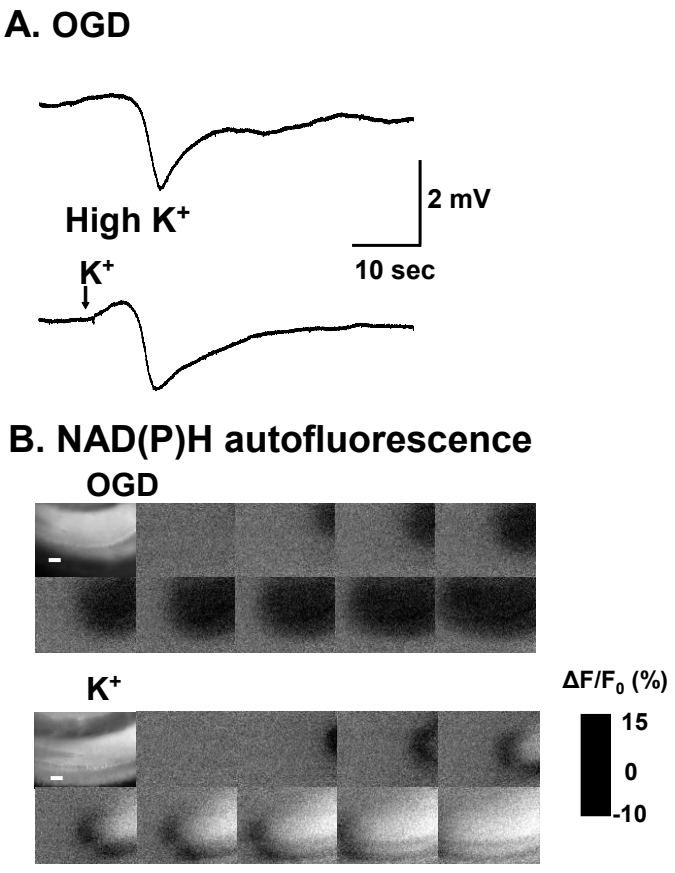

Figure 5.2

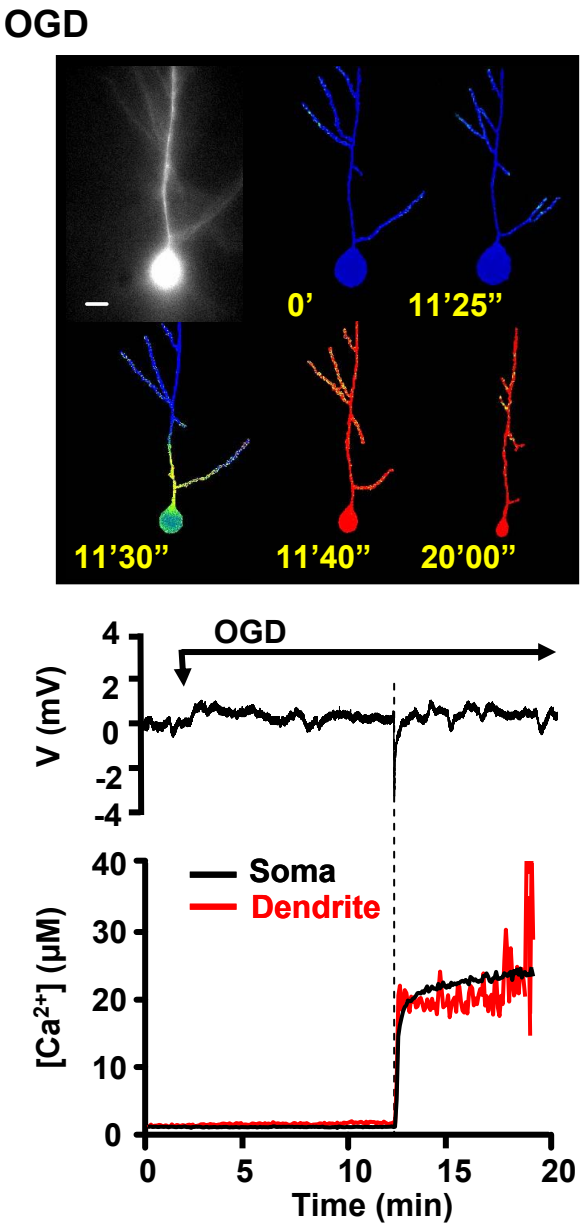

Figure 5.3

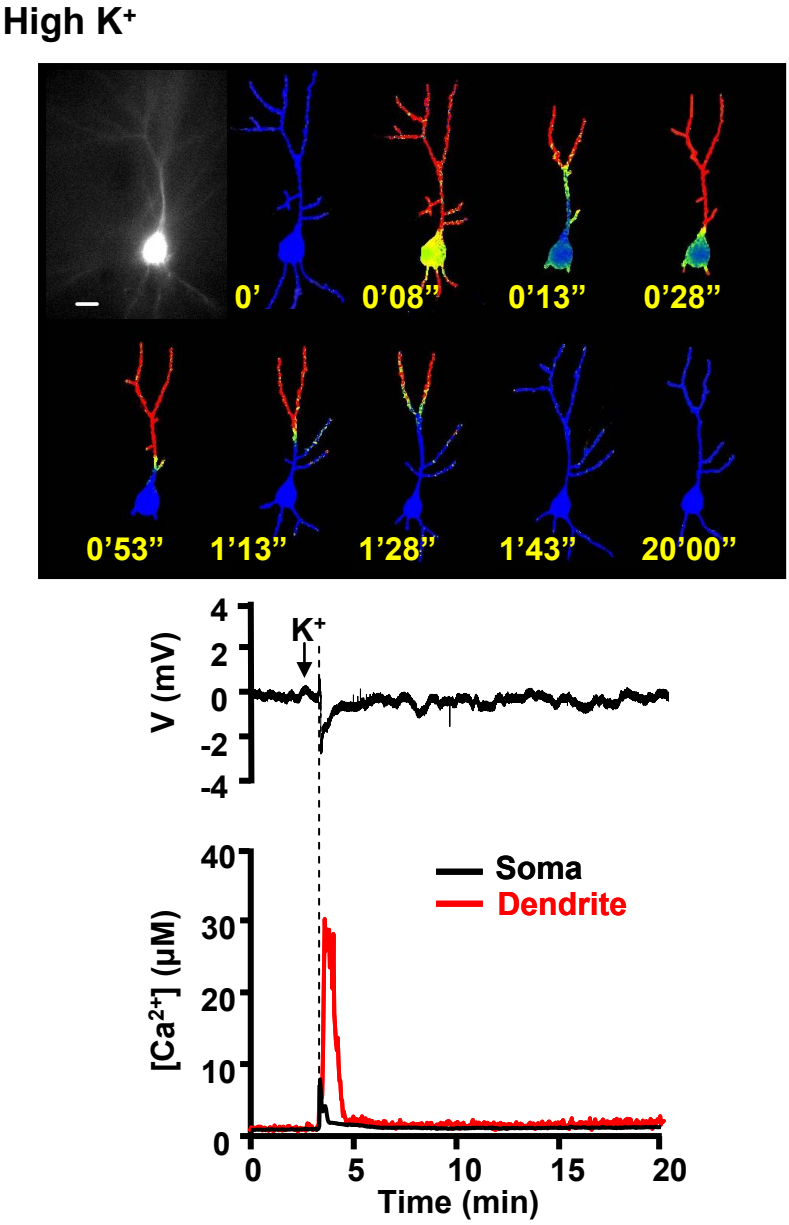

Figure 5.4

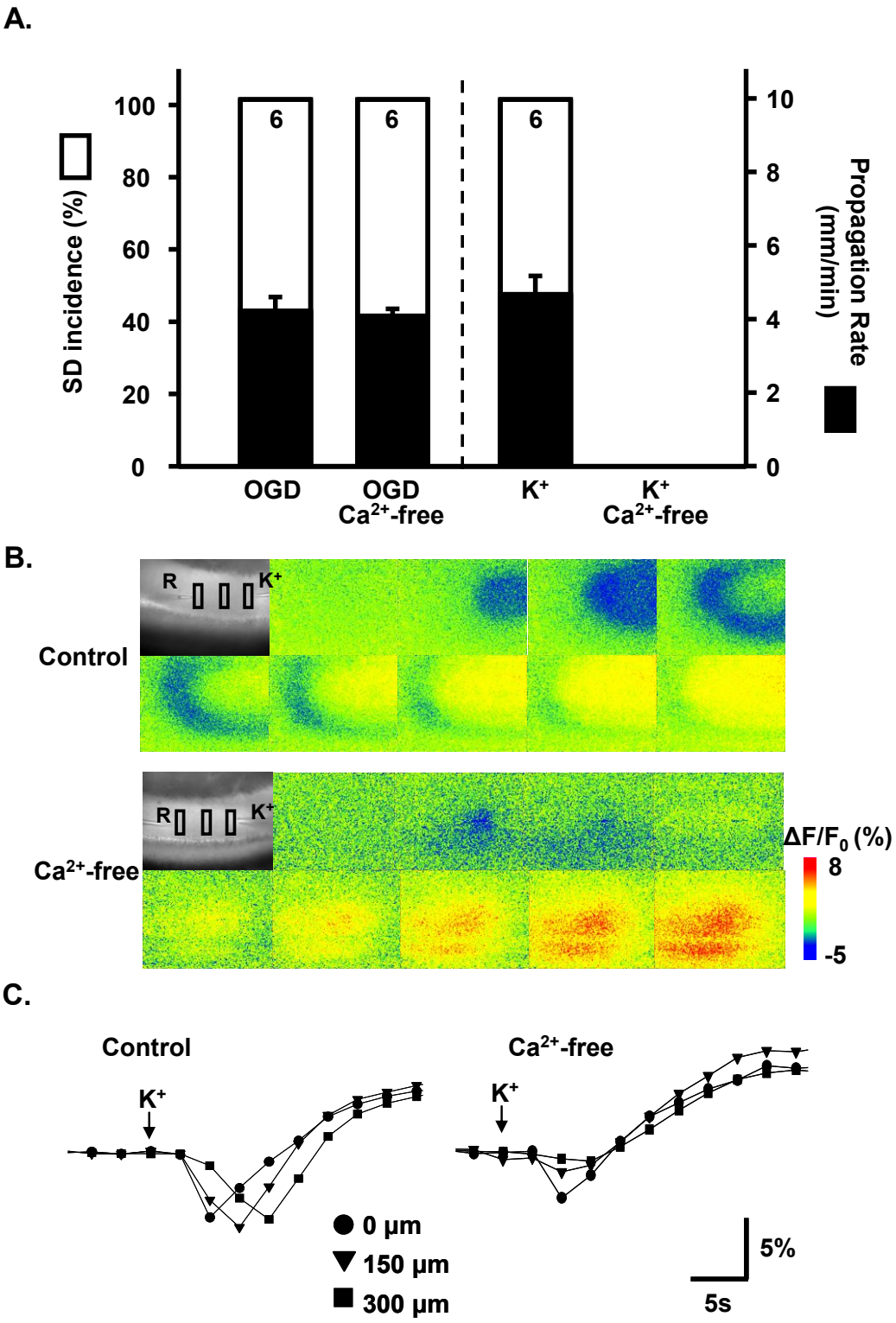

Figure 5.5

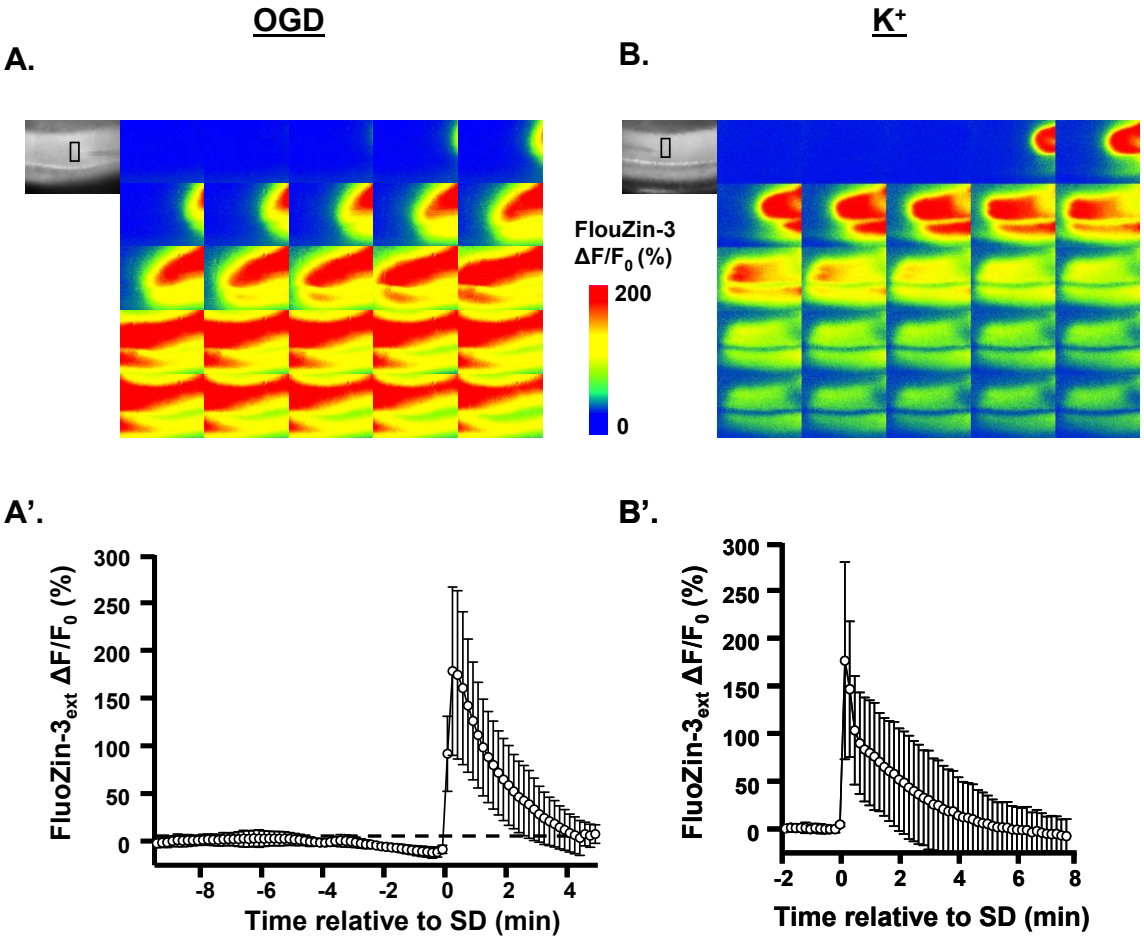

Figure 5.6

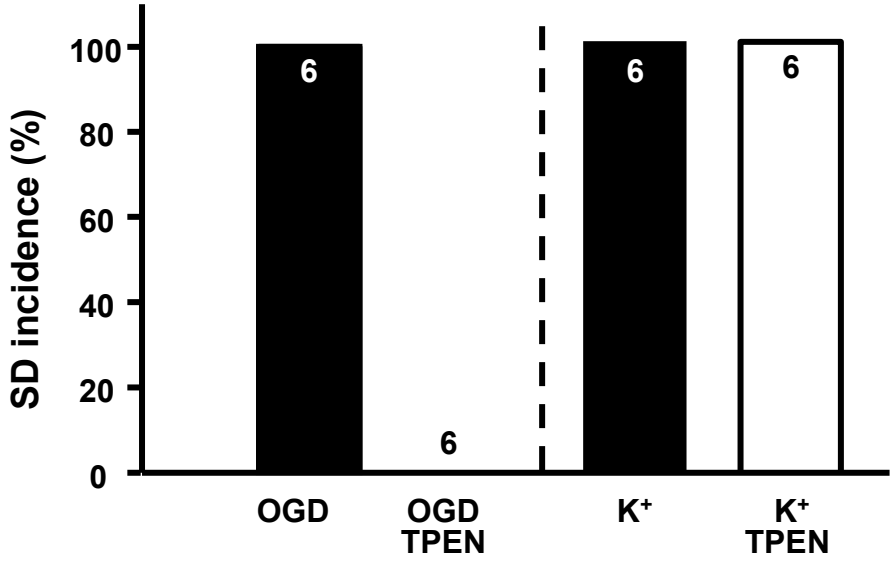

6. Discussion

6.1 Discovery of distinct SD mechanisms

Spreading depression (SD) has intrigued neurophysiologists and neurologists for over 60 years, but approaches to limit SD have been severely hampered by a lack of understanding of the cellular mechanisms that are involved in the initiation of the event. The work in this thesis suggests that a large part of this frustration may be attributable to a trend to treat all forms of SD as the same, and searching for a single unifying hypothesis. Many different types of stimuli can trigger SD, and once evoked, the general characteristics of the event do appear quite similar, regardless of the stimulus. However, the previous chapters show, for the first time, that the ionic mechanisms involved in the initiation of SD can be strikingly different. Specifically, the distinctive roles of Zn^{2+} and Ca^{2+} accumulation in SD can be used to distinguish between SD that is degenerative, and SD that does not lead to irreversible neuronal injury. This provides the first suggestion that targeting Zn^{2+} dependent mechanisms could be used to selectively prevent neuronal injury that is caused by SD-like events following ischemic injuries. As discussed below,

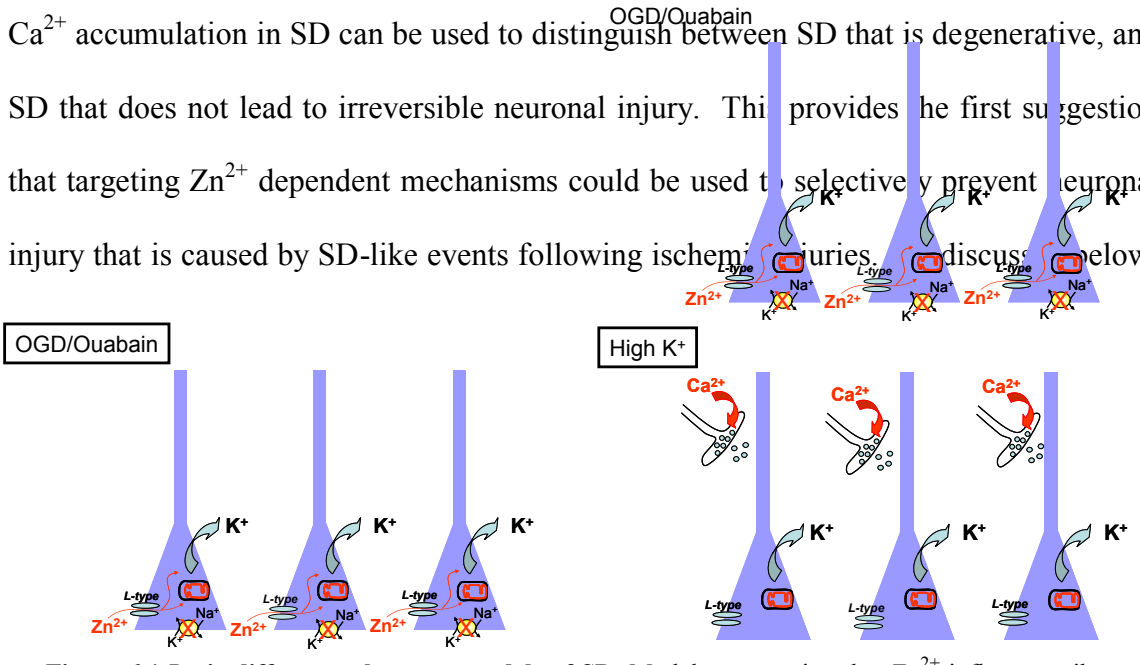

Figure 6.1 Ionic differences between models of SD. Model representing that Zn^{2+} influx contributes in SD models where mitochondrial compromise likely occurs as in OGD or ouabain models. Alternatively, Ca^{2+} likely contributes in the propagation of SD by promoting neurotransmitter release in models where SD is recoverable, such as high K^+.

this new ability to distinguish different types of SD based on differential cation sensitivity should be very helpful for advancing the understanding and treatment of different types of SD, and clarifying the sometimes confusing inconsistencies in the large SD literature.

6.2 Mechanisms of Zn^{2+} in Spreading Depression

The concept that intracellular Zn^{2+} increases can critically contribute to SD appears to have been completely unrecognized prior to these studies. There are a number of reasons that may have contributed to the lack of previous studies of Zn^{2+} in this context. Most previous studies of Zn^{2+} effects on CNS neurons have involved application of relatively high levels of exogenous Zn^{2+} to study degenerative mechanisms. Relatively few laboratories have evaluated the contributions of endogenous Zn^{2+} to pathophysiological processes, and none have made single neuron measurements of Zn^{2+} levels in neurons in intact slice preparations that are essential for studies of SD mechanisms. Chapters 2 and 5 show that there are conditions where Zn^{2+} accumulation is absolutely required for SD, and that during ouabain or OGD exposure, chelation of Zn^{2+} is sufficient to completely prevent the event, even during very protracted stimulation protocols. These new data suggest that part of the beneficial effects of Zn^{2+} chelation in injury models may be due to prevention of SD-like events (see below), and also imply that approaches to determine Zn^{2+} influx pathways could provide promising new targets for neuronal injury.

A paradox of Ca^{2+} channels and Ca^{2+} entry in SD

Studies in Chapters 2 and 5 provide evidence that Zn^{2+} can be required for initiating SD, and these results appear to resolve a significant paradox in the SD literature. As described in the preceding chapters, previous reports of the effects of Ca^{2+} removal on SD were mixed. Ca^{2+} removal has had some effect on SD elicited by high K^+ in both retina and acute brain slices (Nedergaard et al., 1995; Peters et al., 2003), but no effect on blocking SD by hypoxia, ouabain, or OGD has been reported (Balestrino and Somjen, 1986; Herreras et al., 1994; Basarsky et al., 1998; Balestrino et al., 1999; Bahar et al., 2000). Furthermore, in some cases, Ca^{2+}-free media appeared to accelerate the hypoxic SD response (Balestrino and Somjen, 1986; Somjen, 2001). When these data were considered together, influential reviews tended to make the generalized conclusion that Ca^{2+} was not an essential contributor to the initiation or propagation of SD (Somjen, 2001). This view has made it difficult to reconcile a report showing that some non-selective Ca^{2+} channel blockers can block or delay hypoxia-induced SD, and completely prevent the propagation of K^+-induced SD (Jing et al., 1993). It seemed paradoxical that Ca^{2+} channel blockers could prevent SD, but Ca^{2+} removal did not have the same effect. Because of this concern, this apparent contradiction had been dismissed as being due to non-specific effects of the channel blockers used in that study, and argued that they could be blocking SD by effects on other, perhaps novel, channels that are essential for SD (Somjen, 2001).

With this background, it was very interesting that the studies in Chapter 2 (Figures 2.1 and 2.4) showed a very clear demonstration of this same paradox. Thus, L-type Ca^{2+} channel blockers were very successful in preventing SD, but Ca^{2+} removal was not effective. In this case, the blockers used are not known to have significant non-specific effects on other channels or transporters. This demonstration of a mismatch between Ca^{2+} channel blockers and Ca^{2+} removal, in the same preparation, motivated the search for other cations that could be responsible for Ca^{2+} channel effects.

Zn^{2+} influx via L-type channels

Results from Chapter 2 demonstrate that Zn^{2+} influx through L-type Ca^{2+} channels may help explain the paradox highlighted above. Three biophysical properties of L-type channels support their involvement in ouabain-induced Zn^{2+} accumulation. First, L-type channels require a relatively large depolarization to activate (Hille, 2001) which is likely the state that neuronal membranes are in following inhibition of Na^+/K^+ ATPase activity. One can predict that with this homeostatic mechanism blocked, a slow progressive depolarization will occur. Second, L-type channels lack rapid inactivation and this feature allows for large cation flux once the channel opens (Hille, 2001). Third, Zn^{2+} permeates L-type channels. Zn^{2+} flux via L-type channels was first shown in studies where cultured cortical neurons were exposed to 300μM Zn^{2+} (Weiss et al., 1993). In these experiments, the Zn^{2+} sensitive dye TSQ revealed Zn^{2+} accumulations which were prevented by the Ca^{2+} channel blockers La^{3+} or diltiazem and significant neuroprotection was afforded by nimodipine (Weiss et al., 1993). Subsequent whole-cell patch clamp

studies identified the IV relationship of Zn^{2+} mediated L-type flux, and showed that Zn^{2+} currents through L-type channels were unaffected by the presence or absence of Ca^{2+} (Kerchner et al., 2000). This work shows that Zn^{2+} influx can be significant through L-type channels and raised the possibility that Zn^{2+} could explain the Ca^{2+} channel paradox in Chapter 2.

The single-neuron intracellular Zn^{2+} measurements described in Chapter 2 appear to be the first from neurons in slice. The high affinity indicator FluoZin-3 is selective for Zn^{2+}, and consistent with this, fluorescence changes prior to SD were abolished by the Zn^{2+} chelator TPEN, but not by Ca^{2+} removal. FluoZin-3 is a single-wavelength indicator, and therefore, unlike measurements with the ratiometric Ca^{2+} indicators, it is not possible to reliably calibrate these signals to estimate neuronal Zn^{2+} concentrations. Chapter 2 shows a significant FluoZin-3 increase prior to the onset of SD, that was completely abolished by L-type Ca^{2+} channel blockers, suggesting translocation from the extracellular space. To address this question further, extracellular Zn^{2+} measurements were also made, using FluoZin-3 included in the superfusate (**Appendix figure A.1**). This approach has been used previously to monitor synaptic release of Zn^{2+} in the CA1 region (Qian and Noebels, 2006), and showed a clear decrease in extracellular FluoZin-3 fluorescence prior to SD. This decrease corresponded temporally very well with the intracellular Zn^{2+} increases in CA1 neurons. Furthermore, intracellular Zn^{2+} increases and extracellular Zn^{2+} decreases were prevented by L-type channel block, further strengthening the conclusion that Zn^{2+} was translocating from the extracellular space into CA1 neurons, through L-type channels.

Detection of Zn^{2+}

Chapter 2 included some discussion of the ability to distinguish Zn^{2+} from Ca^{2+} signals using the indicators FluoZin-3 and Fura-6F, respectively. This issue is important, because it was noted over two decades ago that some indicators that are very widely used for Ca^{2+} measurements can report Zn^{2+} increases as well. For example, Fura-2 was reported to have a K_D value for Zn^{2+} of ~2nM, which is approximately 100 times lower than that of Ca^{2+} at 224nM (Grynkiewicz et al., 1985). Subsequent studies using Fura-2 as a Zn^{2+} indicator found that the molecule could report changes in Zn^{2+} using isolated ventricular myocytes in response to electrical stimulation (Atar et al., 1995) and cultured forebrain neurons in response to glutamate (Cheng and Reynolds, 1998). These studies suggested that the R_{max} for the indicator is different depending on whether Zn^{2+} or Ca^{2+} is bound to the molecule, where the R_{max} for Ca^{2+} is twice as large as that for Zn^{2+} (Atar et al., 1995; Cheng and Reynolds, 1998). This suggests that Fura-2 is more sensitive to Zn^{2+} in the absence of Ca^{2+} and hinted that at least part of the signal reported by Fura-2 in prior excitotoxicity studies may be due to Zn^{2+} (Cheng and Reynolds, 1998). Subsequent work demonstrated that this problem could be avoided if low affinity Ca^{2+} indicators were used, rather than the high affinity indicator Fura-2. For example, Ca^{2+} and Zn^{2+} signals could be reliably distinguished in cultured neurons co-loaded with the low-affinity Ca^{2+} indicator Fura-2FF and FluoZin-3 (Devinney et al., 2005). Similar observations were made in the present work, where FluoZin-3/Fura-6F co-loading permitted identification of Zn^{2+} and Ca^{2+} responses, without demonstrable cross-contamination of signals.

This issue is noteworthy in light of recent debate, as some studies have sought to re-examine the role that Ca^{2+} and Zn^{2+} may play in neurotoxicity and propose that previous suggestions of Ca^{2+} being a key contributor to cell death may be over-stated and the role for Zn^{2+} may be underappreciated (Martin et al., 2006; Stork and Li, 2006). The authors of these papers point to the lack of specificity in Ca^{2+} indicators as described above to report Ca^{2+} (Stork and Li, 2006) as cause for concern in interpreting prior ion-toxicity studies. While these may be valid claims, it appears that these concerns have already been addressed in previous work discussed above (Devinney et al., 2005; Reynolds et al., 2006; Dineley, 2007; Stork and Li, 2007). Based on these discussions, it seems very reasonable to claim that prior to SD, there is no demonstrable cytosolic Ca^{2+} increase, but significant increases in neuronal Zn^{2+} levels appear to contribute critically to SD initiation.

Sources of Zn^{2+}

Given the significant role that Zn^{2+} appears to play in this model of neuronal degeneration, it was important to determine whether the source for the Zn^{2+} was intracellular or extracellular, particularly with keeping the idea of therapeutics in mind. Identification of the source(s) of Zn^{2+} could dramatically change the strategy of drug delivery if in fact it can be proven that Zn^{2+} has a critical role in human pathology.

Initial studies used the Zn^{2+}-specific chelator TPEN to show that binding all available free Zn^{2+} prevented SD. However, as TPEN is membrane permeable, these results shed little light into the specific sources of Zn^{2+}. As described in Chapter 1, there are

relatively large amounts of Zn^{2+} within cells that are predominantly bound to proteins. It was considered that liberation from these intracellular stores could be a major source of Zn^{2+} responsible for initiating SD with ouabain or OGD. However, a variety of data from the previous Chapters indicate that this is not the case, at least for Zn^{2+} accumulation in CA1 neurons. In Chapter 2, it was shown that plasma membrane channel blockers and a membrane-impermeable Zn^{2+} chelator (BAPTA) were able to prevent Zn^{2+} accumulation and prevent SD, implying that influx from the extracellular space was responsible for triggering SD.

The chelator studies in Chapter 2 also shed light on the proximity of Zn^{2+} release, in relation to plasma membrane L-type Ca^{2+} channels. The strategy that was used was derived from studies of Ca^{2+} microdomains which takes advantage of the differences in on/off binding kinetics of EGTA and BAPTA (Borst and Sakmann, 1996; Naraghi and Neher, 1997; Muller et al., 2007). The on-rate kinetics for these two chelators differ by nearly 100-fold, with BAPTA able to chelate ions much faster than EGTA (4.0×10^8 $M^{-1}sec^{-1}$ for BAPTA vs. 2.5×10^6 $M^{-1}sec^{-1}$ for EGTA (Naraghi and Neher, 1997)). While it is well established that these are very good Ca^{2+} chelators, it is also known that they chelate Zn^{2+} with even higher affinity ($K_{D,Zn}$= 8 nM vs. $K_{D,Ca}$=160 nM for BAPTA; $K_{D,Zn}$=8 pM vs. $K_{D,Ca}$=0.4nM for EGTA). Using this information it was found that the slower chelator, EGTA, had little effect on intracellular Zn^{2+} influxes or the incidence of SD. However, the faster chelator, BAPTA, was able to significantly reduce the Zn^{2+} influx and blocked SD over 50% of the time. These results suggest the novel idea of a "Zn^{2+} microdomain" in the proximity of influx channels. Similar to the previous

intracellular Ca^{2+} microdomain studies, BAPTA appears able to bind a portion of Zn^{2+} that is very near the membrane before it can enter the cell, whereas, the slower on-rate of EGTA does not permit capture of Zn^{2+}, before it enters channels that are very close to the release site (Figure 2.4). This is an intriguing possibility, especially in the setting of high adenosine receptor activation where vesicular release is expected to be low. If there is an extracellular pool of chelatable Zn^{2+} which becomes available only in the immediate vicinity of influx channels, then any therapeutic strategy that involves the removal of Zn^{2+} would have to take this into account, and slow on-rate chelators, such as the commonly used CaEDTA, would not be expected to be effective. In contrast, Zn^{2+} selective chelators that have very rapid on-rates, and which are permeable to the blood-brain barrier would seem to be much more promising therapeutic agents.

While the evidence above suggests that Zn^{2+} becomes available from sources very close to the L-type influx channels, the actual source of Zn^{2+} is not yet known. Synaptically packaged Zn^{2+} can be released and be taken up by post-synaptic cells (Assaf and Chung, 1984; Howell et al., 1984; Frederickson et al., 1989) and is one candidate. The presence of the adenosine A1 receptor agonist CPA markedly reduces synaptic transmission evoked by single presynaptic stimuli (see **Appendix figure A.2**), but this does not rule out the possibility that strong depolarization of nerve terminals prior to SD could still release significant Zn^{2+}. Synaptic release may not be incompatible with the microdomain suggestion, since previous studies of Zn^{2+} release at mossy fiber synapses have suggested that the slow chelators may not be fast enough to chelate synaptically released Zn^{2+} before it enters CA3 neurons (Vogt et al., 2000). One future approach to test the

hypothesis that synaptic release of Zn^{2+} contributes to SD would be to use mice in which the transporter that allows Zn^{2+} packaging in synaptic vesicles (ZnT3) has been knocked out (Palmiter et al., 1996). If SD is prevented in these mice, this would be evidence that synaptic vesicles are the source of the Zn^{2+}. However, the lack of effects during Ca^{2+}-removal suggests that, in such a case, Ca^{2+}-independent release would be involved.

A very different alternative source which has been suggested is a chelatable pool of extracellular Zn^{2+} that is associated with the plasma membrane, rather than sequestered in synaptic vesicles (Kay, 2003). It has been hypothesized that there is a Zn^{2+} "veneer" that is loosely associated with plasma membrane-bound molecules that can be liberated upon membrane depolarization. It seems conceivable that Zn^{2+} influx prior to SD may result from liberation from the external surface of the plasma membrane, and enter neurons through L-type channels that are immediately adjacent to the release site. The current data cannot distinguish between the possibilities of synaptic release or liberation of membrane associated Zn^{2+}, but the question remains of significant interest for the development of effective therapeutic interventions.

Mechanisms coupling Zn^{2+} increases to SD

While these experiments demonstrate an important contribution of Zn^{2+} accumulation to SD, the mechanism(s) by which Zn^{2+} triggers SD are not yet known with certainty. However, since previous work has implicated metabolic dysfunction in SD initiation

(Bahar et al., 2000; Gerich et al., 2006), the observation of Zn^{2+}-dependent mitochondrial depolarization in Chapter 2 allows some suggestions to be made below.

Mitochondrial depolarization

Mitochondrial dysfunction has been suggested to underlie SD in hippocampal slices and intact cortical recordings. Slow mitochondrial depolarizations that occur prior to SD have been described during hypoxia (Bahar et al., 2000) and Gerich et al., have argued that mitochondrial dysfunction preceding SD is a likely underlying cause of SD during hypoxia (Gerich et al., 2006). However, it was observed that the hastening of hypoxia-induced SD by respiratory chain inhibitors does not seem to depend on reduced ATP levels (Gerich et al., 2006).

Chapter 2 provided the first evidence that accumulation of endogenous Zn^{2+} can lead to significant mitochondrial membrane depolarization. Figure 2.2 shows that there is a slow mitochondrial depolarization, that persists for approximately 5 minutes prior to the onset of SD and appears very similar to that described previously during hypoxia (Bahar et al., 2000). In pathophysiological conditions, loss of mitochondrial inner membrane potential is generally accepted to be due to accumulation of significant amounts of Ca^{2+}, as this cation is readily transported down its concentration gradient through the uniporter (Nicholls and Budd, 2000). Since L-type channel blockers completely abolished mitochondrial depolarization, Ca^{2+} influx initially seemed a strong candidate for this response. However, similar to the situation described above, Ca^{2+} removal did not mimic

the effects of L-type blockers, raising the possibility that Zn^{2+} was also responsible for this mitochondrial effect.

Like Ca^{2+}, Zn^{2+} is transported by the mitochondrial uniporter (Malaiyandi et al., 2005) and is well-established to produce mitochondrial depolarization (Sensi et al., 1999; Sensi et al., 2003; Dineley et al., 2005). Since mitochondrial ATP production relies on the driving force for protons across the mitochondrial inner membrane, it is possible that severe depolarization by Zn^{2+} accumulation could be sufficient to compromise ATP production and trigger SD. However, the degree of depolarization is not very severe, and in fact, the effects of Zn^{2+} chelation suggest that mitochondrial depolarization alone is not sufficient to trigger SD. In the presence of TPEN, SD was not observed, yet there was still a delayed slow mitochondrial depolarization that was due to Ca^{2+} accumulation (Figure 2.6). Even if this event was permitted to progressively increase to quite high levels, SD was not observed, implying that mitochondrial depolarization alone is insufficient to trigger SD and argues against the conclusion of Gerich and colleagues based on a simple correlation between mitochondrial depolarization and SD (Gerich et al., 2006). The observation that Zn^{2+} was an essential requirement for SD suggests that other deleterious effects of Zn^{2+} on mitochondria (or other targets) are much more likely candidates for SD initiation.

In addition to simple depolarization due to Zn^{2+} influx, several studies have indicated that Zn^{2+} inhibits energy production as well. A sensitive location for Zn^{2+} inhibition of the electron transport chain is cytochrome complex bc_1, which is located in Complex III (**Figure 6.2**) (Skulachev et al., 1967; Nicholls and Malviya, 1968; Kleiner, 1974; Lorusso et al., 1991; Link and von Jagow, 1995). A decrease in electron transport chain activity could lead to an accumulation of TCA cycle products, and severe ATP depletion. Alternatively, Zn^{2+} impairment of energy production could be direct inhibition of enzymes in the TCA cycle (Dineley et al., 2003). Chapter 3 provides some evidence of this where it is shown that addition of the Zn^{2+} chelator alone slightly changes the redox state of the mitochondria. If this is true, it would imply that the presence of Zn^{2+} at basal levels results in a small inhibition of NAD(P)H production and the presence of larger amounts of Zn^{2+} that occur prior to SD result in a relatively larger effect on TCA cycle. All of these mechanisms would be expected to lead to significant Zn^{2+}-dependent decreases in energy production.

Mitochondrial ROS production by Zn^{2+}

One attractive hypothesis for Zn^{2+} dependent mitochondrial degeneration is the Zn^{2+}-dependent production of reactive oxygen species (ROS). In an important series of studies, the Weiss group showed that Zn^{2+} entry into mitochondria produced ROS approximately 100 times more potently than did Ca^{2+}, implicating this cation as a major contributor to ROS production, under circumstances where mitochondrial Zn^{2+} accumulation is significant (Sensi et al., 2000; Jiang et al., 2001; Sensi et al., 2003). Additionally, the presence of TPEN dramatically decreased the amount of ROS generation under these same conditions (Sensi et al., 2003). ROS are well established to produce substantial inhibition of a variety of effectors that could lead to metabolic failure and SD, as suggested by experiments where photoactivation of Rose Bengal induced SD in retina, which was altered by the presence of the potent antioxidant trolox (Netto et al., 1999). In the experiments here then, it is suggested that mitochondrial depolarization serves as a convenient marker for mitochondrial Zn^{2+} accumulation, but that mitochondrial Zn^{2+}-dependent ROS production is a possible candidate for triggering SD.

Other Targets for Zn^{2+} in SD

Despite the interest in mitochondrial mechanisms, it is also noted that Zn^{2+} has a range of other potential targets that could also provide a link to SD initiation in these studies. For example, a recent report by Allen and colleagues described a preferential role for glycolysis in the initiation of anoxic depolarization (Allen et al., 2005). Anoxic

depolarization is the single cell response which corresponds to arrival of SD. In this paper, several locations along the energy production pathway were systematically blocked, and it was found that when glycolysis was allowed to persist in the absence of mitochondrial function, anoxic depolarization could be prevented. Therefore, Zn^{2+} inhibition of key glycolytic enzymes (Ikeda et al., 1980; Krotkiewska and Banas, 1992) could provide another avenue for the induction of SD by Zn^{2+} accumulation.

6.3 Ca^{2+} in Spreading Depression

Ca^{2+}-dependent propagation in recoverable models of SD

As discussed above, much previous work has emphasized the idea that intracellular Ca^{2+} accumulation is a consequence of SD, rather than a critical contributor to the propagating event itself. However, it is noteworthy that most of the literature cited for Ca^{2+}-independence of SD has involved models involving metabolic compromise, such as hypoxia-SD, or models that mimic consequences of metabolic compromise, such as ouabain (Balestrino and Somjen, 1986; Basarsky et al., 1998; Balestrino et al., 1999; Bahar et al., 2000). Perhaps this reflects the emphasis of the field on finding approaches to block SD associated with ischemic injury. However, despite this emphasis on Ca^{2+}-independence of SD, it has been shown very clearly by some authors that some forms of SD can be blocked by Ca^{2+} removal. What has not been highlighted in some reviews on the general topic of SD is that Ca^{2+} removal is effective when tested against SD that is known to be recoverable (i.e. high K^+, mechanical or electrical stimulation). For example, in 1974, Martins-Ferreira and colleagues described a situation in retina where

Ca^{2+} removal blocked the propagation of SD induced by mechanical stimulation (Martins-Ferreira et al., 1974). Similar findings were reported over 20 years later in retina and juvenile neocortical slices following SD elicited by high K^+ (Nedergaard et al., 1995; Peters et al., 2003).

Results of Chapters 2 and 5 are consistent with these prior observations, since at least for ouabain- or OGD-induced SD, removal of Ca^{2+} had no effect on the characteristics of SD. However, the results from Chapter 5 also reveal that Ca^{2+} plays a prominent role in the propagation of high K^+-induced SD in these same preparations. Therefore, one of the conclusions from the results of this work is that now the SD literature can be re-evaluated with respect to cation dependence.

Ca^{2+} and mitochondria

One of the perplexing pieces of data from this project was the observation that there was still clearly a mitochondrial depolarization occurring due to Ca^{2+} despite the fact that neuronal cytosolic Ca^{2+} levels did not appear to change prior to SD (Chapter 2). Support for a Ca^{2+} effect on mitochondria was presented in Chapter 3 where NAD(P)H increases prior to SD were described for the first time and were shown to be dependent on Ca^{2+} influx through L-type channels. The hypothesis that a privileged pathway between L-type channels and mitochondria that allows Ca^{2+} to effect mitochondrial function was tested using a method described previously in cultured neurons (Carriedo et al., 2000). In that previous work, brief exposures of the mitochondrial proton ionophore FCCP were

used to release Ca^{2+} sequestered in mitochondria by collapsing the mitochondrial membrane potential. Results from Chapter 3 indicate that a bolus of FCCP produced a partial depolarization of the mitochondrial membrane, resulting in the release of Ca^{2+} from the organelle into the cytoplasm (as reported by Fura-2). When the same experiment was performed following blockade of L-type channels, no increase in cytoplasmic Ca^{2+} was observed. This provides evidence that L-type channels may be coupled to neuronal mitochondria, and it is possible that mitochondrial uptake of Ca^{2+} at these channels could occur faster than Fura-2 can report significant Ca^{2+} accumulation in the cytoplasm.

The use of Ca^{2+} imaging techniques was attempted to seek additional evidence that Ca^{2+} was entering mitochondria. The mitochondrial Ca^{2+} indicator Rhod-2 was tested, but the signals appeared to be due primarily to cytosolic, rather than mitochondrial sources (see **Appendix figure A.3**).

With evidence that Ca^{2+} enters mitochondria during the onset of ouabain exposures, the conclusion was reached that Ca^{2+} was responsible for the increases in NAD(P)H autofluorescence during this time period. As discussed in Chapters 1 and 3, it is well established that Ca^{2+} at low levels can activate key TCA cycle enzymes. Specifically, Ca^{2+} can activate pyruvate dehydrogenase, 2-oxoglutarate dehydrogenase, and isocitrate dehydrogenase (Denton and McCormack, 1990; McCormack et al., 1990) resulting in NADH production. The comparison of NAD(P)H and flavoprotein autofluorescence supported the conclusion that signals were of mitochondrial origin. Flavin adenine

dinucleotide (FAD) is the oxidized form of another electron carrier, $FADH_2$, generated by TCA cycle activity and oxidized in the electron transport chain. Unlike NADH, $FADH_2$ is not fluorescent, but FAD displays green fluorescence after excitation in the blue range. Consequently, FAD fluorescence signals should be opposite in sign to NAD(P)H changes if these signals reflect mitochondrial metabolism (Brennan et al., 2006). The inverse relationship in these signals (Figure 3.1) suggest an effect on mitochondrial metabolism, possibly by increasing activation of TCA cycle enzymes by Ca^{2+}.

These results raise the intriguing possibility that Ca^{2+} may actually have a protective effect in some models of SD. Ca^{2+}-dependent activation of TCA enzymes may transiently increase energy production prior to SD, and occurs at the same time as Zn^{2+} flux into mitochondria may be having deleterious effects on energy production (see above). It is possible that beneficial effects of Ca^{2+} accumulation are sufficient to prevent depolarization under some circumstances, for example with mild or brief insults. However, with sustained pump inhibition or loss of metabolic substrates, it appears that any possible beneficial effects are overcome by the severely detrimental effects of persistent Zn^{2+} accumulation (Yin and Weiss, 1995; Sensi et al., 1999; Dineley et al., 2003; Sensi et al., 2003).

6.4 Damage following SD

Ca^{2+} increases following SD

Numerous studies have described a role for Ca^{2+} in injury models involving neurons and it has been well established that high cytosolic Ca^{2+} levels initiate cell death (Choi, 1985; Lee et al., 1999; Lipton, 1999). Previous work has shown that the massive depolarization that occurs during SD is not alone responsible for cell death, rather it appears that it is the combination of the high Ca^{2+} loads and mitochondrial compromise that results in the "terminal" nature of SD during OGD (Tanaka et al., 1997; Yamamoto et al., 1997; Somjen, 2001). If Ca^{2+} is removed prior to oxygen withdrawal, neurons appear to recover function following a period of hypoxia that otherwise would have caused irreversible damage. Further, it appears that Ca^{2+} alone cannot kill cells because cellular function may be regained if oxygen is restored soon after the onset of OGD-induced SD, even after large amounts of Ca^{2+} have entered the cell (Balestrino and Somjen, 1986; Roberts and Sick, 1988; Tanaka et al., 1997; Yamamoto et al., 1997).

The results in Chapters 2 and 5 are consistent with a critical role of Ca^{2+} in rapid degeneration following ouabain- and OGD-induced SD. In both of these models, Ca^{2+} was observed to rapidly increase to micromolar levels. Rapid loss of indicator fluorescence was noted within 10 minutes under these conditions, which is a sign of rapid compromise of the plasma membrane, permitting leakage of the charged indicator molecule (Randall and Thayer, 1992). However, since the Ca^{2+} indicator is used in the dual-wavelength excitation mode, estimates of Ca^{2+} concentration are not significantly

influenced by changes in indicator concentration, and sustained micromolar increases in intracellular Ca^{2+} levels are reported. While these studies do not demonstrate that Ca^{2+} is responsible for neuronal demise, these findings provide the first single-neuron Ca^{2+} measurements following SD using ouabain or OGD as stimuli, and certainly support previous conclusions concerning the critical role of Ca^{2+} in neurodegeneration (Lee et al., 1999; Lipton, 1999).

A very different profile of intracellular Ca^{2+} signals was observed with high K^+-induced SD. Ca^{2+} levels initially increased to micromolar levels in dendrites and somata, as would be predicted from previous studies of extracellular cation levels (see Kraig and Nicholson, 1978; Nicholson et al., 1978). However, in contrast to the ouabain and OGD models, Ca^{2+} levels recovered relatively rapidly throughout neurons, with no detectable indicator loss, or other signs of neuronal injury. The very different Ca^{2+} responses seen with the two different types of stimuli seem very likely to account for the ultimate fate of neurons following SD.

Results in Chapters 2 and 5 suggest that the basis for the very different Ca^{2+} signaling in these models may be related to differences in the metabolic capacity of neurons when they become involved in the SD response. It has been suggested previously that the availability of energy substrates are critical for the re-establishment of ion homeostasis following SD (Somjen, 2001), and work here shows that sustained mitochondrial depolarization always occurs before SD that leads to non-recoverable damage (ouabain and OGD), whereas it appears that high K^+-induced SD involves neurons with very little

delay and no appreciable disruption of mitochondrial function prior to arrival of SD at a particular site. These results suggest that the metabolic demands of Ca^{2+} sequestration and extrusion may be readily met if neurons have not previously endured a slow and sustained metabolic challenge (as in high K^+-induced SD). In contrast, if ATP supply is already partially compromised (as indicated by mitochondrial depolarization prior to SD in ouabain or OGD, Figure 2.2 and **Appendix figure A.4**) then neurons may not have the capacity to normalize the very large Ca^{2+} loads produced by the SD event.

Zn^{2+} increases following SD

From the studies utilizing extracellular FluoZin-3, it was found that large increases in detectable Zn^{2+} occurred in the extracellular space, closely following the wave of spreading depression. It is likely that this large Zn^{2+} signal is a product of the coordinated depolarization that occurs with SD, since similar profiles of the FluoZin-3 fluorescence occurred in all three types of SD (ouabain, OGD and high K^+). This is the first demonstration of wave-like extracellular Zn^{2+} increases, and the observation raises a number of questions about the sources and consequences of these events. Among the possible sources, profound depolarization of nerve terminals and release of Zn^{2+} from synaptic vesicles appear a good candidate. Such a mechanism could be tested in the future with slices prepared from ZnT3 knockout animals, which lack synaptic Zn^{2+} (Palmiter et al., 1996). If extracellular Zn^{2+} waves were still detected in these animals, it would seem appropriate to test the possibility that the very large cation disruptions of SD could result in liberation of Zn^{2+} from intracellular binding sites (Lee et al., 2000b).

Removal of the major Zn^{2+} binding protein MT3 could be useful to test this hypothesis (Lee et al., 2003). If these major Zn^{2+} sources were not involved, then liberation from extracellular binding sites, as has been proposed by Kay (2003), would be a third possibility.

Regardless of the source, it is noteworthy that large intracellular Zn^{2+} increases are also observed following SD. The absolute magnitude of these increases is difficult to estimate with a single wavelength indicator such as FluoZin-3. Another drawback of single-wavelength indicators is that it is not possible to distinguish between loss of indicator from neurons, and decreases in fluorescence that are actually due to decreases in levels of intracellular Zn^{2+}. This is problematic following the onset of SD, since it is established that there is pronounced loss of Fura-6F fluorescence, at the same time that FluoZin-3 levels are decreasing. In the case of the ratiometric Ca^{2+} measurements, it is clear that Ca^{2+} levels remain high, despite indicator loss. It seems reasonable to suggest that the same may also be true of Zn^{2+}, but this remains difficult to test without the availability of ratiometric indicators with specificity for Zn^{2+}. However, it is possible that the Zn^{2+} increases following SD could further add to the metabolic burden on neurons, and that in the case of ouabain and OGD, this could be a significant co-contributor with Ca^{2+} to neuronal compromise following SD.

Blocking SD does not prevent eventual neuronal damage

The idea that blocking SD will prevent neuronal damage has recently been explored with the use of sigma receptor agonists (Anderson et al., 2005). In that report, the authors emphasize the goal of blocking SD without altering normal cellular activity, but it is noteworthy that only quite brief exposures to ouabain or OGD were tested (10 minutes). It is therefore interesting that results in Chapter 4 demonstrate that protracted ouabain exposures can cause Ca^{2+} deregulation, even if SD is prevented. **Appendix figure A.5** demonstrates that severe neuronal damage is apparent from the appearance of dendrite beading and loss of structure following 30 minutes ouabain exposure in nimodipine (where SD is blocked). **Appendix figure A.6** shows that this eventual Ca^{2+} overload is not specific to the ouabain model, as it also occurs following persistent exposure to OGD despite the lack of SD.

The studies in chapter 4 are an important adjunct to the studies of SD mechanisms, since all of the experiments were conducted under conditions that prevented SD, and permitted more detailed evaluation of mechanisms that may be more important for the ischemic core. In these studies, when ouabain-induced SD was blocked by nimodipine, there was a slow Ca^{2+} propagation along dendrites prior to somatic involvement. Very similar events were observed with persistent activation of NMDA channels (Figure 4.3). This study provides the first description that persistent NMDA exposure, in the presence of nimodipine, results in a progressive Ca^{2+} overload that originates in the apical dendrites of CA1 neurons in mature preparations. These results are similar to previous studies

which found that dendritic origins of Ca^{2+} overload following exposure to another glutamate receptor agonist, kainate (Shuttleworth and Connor, 2001). Ongoing studies in the laboratory using persistent NMDA exposure (Vander Jagt et al., submitted) suggest that Na^{+} accumulation, and subsequent localized metabolic dysfunction, is responsible for progression of events along dendrites and the subsequent Ca^{2+} overload responsible for ultimate neuronal demise (Vander Jagt et al., submitted). Results in chapter 4 also provide the first evidence that if intracellular Na^{+} is raised to sufficiently high levels (using ouabain), then reverse-operation NCX activity could contribute to Ca^{2+} deregulation in apical dendrites (Figure 4.5).

It is not yet clear how the progressive Ca^{2+} deregulation in neuronal dendrites (in the absence of SD; as described here with NMDA and ouabain) contributes to ischemic injuries *in vivo*. However, one possibility is that persistent glutamate exposure within the initial ischemic core leads to necrosis in that region. Ca^{2+} deregulation would be expected to initiate in fine apical dendrites where high glutamate receptor density and large surface area/volume ratio contributes to localized deregulation. Responses then progress to somata, killing the neurons relatively rapidly. SD would not contribute to this initial injury, as neurons within the ischemic core would already be partially depolarized, removing the ability of the SD event to initiate. In contrast, neurons around the core are sufficiently competent to restore resting membrane potential and these penumbral regions are susceptible to invasion of SD responses. If metabolic substrate are partially compromised, then repetitive PIDs could progressively deplete the ability of neurons to restore ionic gradients, ultimately contributing to enlargement of the injury zone. It is not

yet known whether the pattern of Ca^{2+} deregulation following PIDs *in vivo* is exactly as described here with the rather severe stimuli used to generate SD in slices. Thus, although Chapter 5 describes very rapid involvement of Ca^{2+} deregulation in all neuronal compartments during OGD exposures (Figure 5.2), it also seems possible that in penumbral regions, PIDs could lead to Ca^{2+} deregulation first in smaller dendritic compartments, before involving the entire neuron. These and other possibilities remain to be determined, presumably utilizing 2-photon imaging methods *in vivo*.

6.5 Bench to Bedside – Clinical Implications for this Research

As mentioned earlier in this Chapter, as well as in Chapter 5, the identification of two types ionic mechanisms for SD could be an exciting revelation in the field. The results presented here suggest novel tools to distinguish between these two types of SD in future research. Specifically, it is intriguing to consider that these two types of SD may in fact be relevant in two very different disease models. Previously, SD has been associated with migraine aura, as well as the spread of injury following ischemia or traumatic brain injury. The present work provides novel support for the idea that recoverable forms of SD may be the prominent form in migraine, whereas the non-recoverable types of SD represent a model of ischemic or traumatic death.

Migraine aura

The link between SD and migraine aura has been established for nearly 50 years (Milner, 1958). Lashley (1941) provided an extensive description of his own visual aura that

involved an event that almost always started from the center of his field of vision and spread peripherally at a predicted rate of 3 mm/min. The duration of this type of an event varied, but the symptoms often subsided between 5 minutes to about half an hour (Lashley, 1941). In a recent review, neurologist Michael Cutrer has also noted that the recovery of his own visual scotomas often occurs in the same sequence in which vision was affected (Cutrer and Huerter, 2007), suggesting that the recovery of function in the visual areas of the cortex also occurs as a spreading event.

The International Headache Society has defined migraine aura as a "recurrent disorder manifesting in attacks of reversible focal neurological symptoms that usually develop gradually over 5-20 minutes and last for less than 60 minutes" (Ramadan and Olesen, 2006). A key word in this definition as it pertains to SD may be „reversible". The data presented in Chapter 5 suggest that different stimuli can produce SD with extremely different sequelae. While this is not a new observation, few have suggested that there may be differences in the mechanisms of these different events (Tegtmeier, 1993) or that these differences are associated with different pathologies (Obeidat and Andrew, 1998). The present data suggests that there are indeed differences in the mechanisms leading to the different outcomes, and strongly supports the idea of breaking the field of SD into two models: recoverable SD and non-recoverable SD.

If one were to re-examine the data with this classification in mind, simple conclusions can be made regarding the mechanisms of initiation and propagation of recoverable SD. The results in Chapter 5 are consistent with prior findings that Ca^{2+} removal can prevent

the propagation of recoverable SD (Martins-Ferreira et al., 1974; Nedergaard et al., 1995; Peters et al., 2003). Consistent with this role of Ca^{2+} in recoverable SD, recent work using blockers of P/Q channels inhibited SD (Kunkler and Kraig, 2004). This work extended previous findings where genetic alteration of P/Q-type Ca^{2+} channels increased the threshold for SD evoked by KCl application to intact brain (Ayata et al., 2000). Results from both of these studies suggest a presynaptic site of action as impairing this channel can significantly depress neurotransmitter release (Ayata et al., 2000). This suggests the possibility that the mechanism of propagation in recoverable SD has a strong contribution from synaptic neurotransmission.

These results also have strikingly strong correlations to studies of inheritable migraines. Over half of patients who have inherited familial hemiplegic migraine (FHM) appear to have a missense mutation in the *CACNA1A* gene, the gene that codes for the pore forming α1A subunit of the P/Q-type channel (Ophoff et al., 1996). This mutation alters the single channel properties so that there is an increase in Ca^{2+} influx by shifting the activation curve of these channels to more hyperpolarized voltages, thus increasing their open probability (Tottene et al., 2002). The potential relevance of this defect to SD may be that FHM patients could have increased Ca^{2+} influx through P/Q-type channels leading to localized increases in transmitter release, possibly enhancing the susceptibility to SD. This may be an important link that can be used for therapeutic approaches for migraine in the future.

In contrast to the recoverable form of SD above, which occurs in otherwise normal brain tissue, SD which occurs in tissue undergoing metabolic stress, as in ischemia or traumatic brain injury (TBI), has been shown to exacerbate neuronal injury both in situ and in brain slices (Nedergaard and Astrup, 1986; Nedergaard and Hansen, 1993; Gido et al., 1994; Busch et al., 1996; Hossmann, 1996; Obeidat and Andrew, 1998; Church and Andrew, 2005). The results provided here suggest that Zn^{2+} is critically important in injurious forms of SD, but not in recoverable forms of SD. This could be a useful strategy to separate these different types of SD in future research.

One important aspect of the ischemic environment that is often overlooked during *in vitro* experiments is the observation that adenosine is released during *in vivo* ischemia (Rudolphi et al., 1992). This project has taken advantage of this observation and reveals that activation of A1 receptors may play a critical role in attenuating cell injury. Activation of adenosine A1 receptors is thought to be a protective mechanism by the cells in response to a variety of neurotoxic stimuli (Dunwiddie and Masino, 2001). This neuroprotection is likely through the inhibition of transmitter release by blocking pre-synaptic Ca^{2+} channels (predominantly N- and P/Q-type) involved in this process. While the prevailing thought is that the block of glutamate release is the predominant reason for this protection, it is likely that A1 receptor activation is also limiting synaptic Zn^{2+} release as well. If Zn^{2+} contributes to cell death to the extent previously suggested (Koh et al., 1996; Calderone et al., 2004) then adenosine release and subsequent activation of its

receptors may actually be trying to block this toxic mechanism. While the studies in Chapters 2 and 4 indicate that A1 receptor activation alone is not enough to block cell damage induced by SD, these receptors appear to have a clear role under ischemic conditions.

The discovery of SD-like events occurring in these disease models is exciting, particularly given the probability that peri-infarct depolarizations, contribute to the expansion of neuronal injury (Hartings et al., 2003; Strong and Dardis, 2005; Strong et al., 2007). With the likelihood that Zn^{2+} may be a key player in this type of SD, a bridge may have been found to link the fields of PID-induced neuronal death and that of Zn^{2+} neurotoxicity. It is tempting to speculate that the neuroprotection afforded by Zn^{2+} chelators during *in vivo* stroke models was due to the blockade of SD-like events involved on the spread of injury (Koh et al., 1996; Hartings et al., 2003; Calderone et al., 2004; Strong et al., 2007). If this were found to be true, the landscape of treating stroke would be dramatically changed.

6.6 Critique of Work

Acute slice preparations

The phenomenon of spreading depression depends critically on the close packing of neurons, which presumably allows the regenerative phenomenon to progress smoothly through a brain region. This event can therefore not be recapitulated in dissociated culture preparations, and is therefore studied either *in vivo*, or in brain slice preparations.

The ability to manipulate experimental conditions (i.e. temperature, flow rate, etc.) using acute slices is uncomplicated and is generally easier than in *in vivo* preparations. All work here was done using acutely prepared brain slices, which have the advantage of including relatively mature neurons with most of their synaptic connections intact, but it is fully acknowledged that obvious differences exist between acute slice preparations and intact brain which may be particularly important in SD studies, including oxygen availability and arterial perfusion. Specifically, it is impossible to mimic ischemic injury architecture (i.e. core vs. penumbra) in slice preparations. While there are definite limitations for the extrapolation of our results to *in vivo* disease models, this study has identified key cellular mechanisms that may be able to be expanded upon in whole animal experiments. Future experiments in which arterial occlusion models of stroke resulting in peri-infarct depolarizations can build upon the insights gained from the studies here, especially if the role of Zn^{2+} in these events is investigated and reveals a potential therapeutic strategy for ischemic brain injury.

Assessing Cell Death

One of the conclusions of the study is that SD can lead to neuronal injury if Zn^{2+} accumulation is involved (ouabain, or OGD), but does not cause long-term damage to neuronal function if SD invades brain regions with uncompromised metabolic function (high K^{+}). One of the drawbacks of the acute slice preparations used here is that it is difficult to perform long-term studies of neuronal death pathways, and thus conclusions concerning neuronal death are indirect. The measure used here was based on retention of

the fluorescent Ca^{2+} indicator Fura-6F, which is normally very well retained in single neurons because of its charge. It has previously been shown that the maintenance of sustained very high Ca^{2+} levels result in rapid neuronal death, and that this can be relatively easily monitored by leakage of the 835 MW indicator from the neuron (Randall and Thayer, 1992). This can be clearly documented as indicator loss when measured at the isobestic point of the indicator (360nm), but can also been observed as a dramatic loss of fluorescence following excitation at 350nm, despite the maintenance of a high 350/380nm fluorescence ratio (Shuttleworth and Connor, 2001). It was recently shown in our laboratory that this indicator loss is indeed Ca^{2+} dependent (Vander Jagt et al., submitted). For these reasons, in Chapters 2, 4, and 5, cell death was assessed by the rate of 350nm fluorescence, under conditions where Fura-6F ratio was sustained at saturating levels. Although it is acknowledged that examining the loss of an indicator does not provide direct evidence for cell death, when plasma membrane permeability of a 835 MW indicator was taken together with the fact that there was never any suggestion of recovery of cytosolic Ca^{2+} levels, this was considered to imply a rapid and necrotic cell death process.

It may be of interest in the future to study further the mechanisms of SD- induced cell death, and also whether "non-injurious" SD such as evoked by high K^+ stimulation may actually lead to some detrimental effects over much longer timer periods. For these studies, it is noted that quantification of cell death is considerably more straightforward in cultured preparations (either dissociated or slice culture), since neurons damaged by the dissection or slicing procedure are generally removed by the time the experiment is

begun. For this reason, it would seem that slice cultures would be useful preparations in which to pursue these questions.

Recording Temperature

The normal brain temperature of an unanaesthetized mouse is ~37^{o}C, and all experiments in this study were performed at lower recording temperatures. For technical reasons, this is almost always done for slice physiology studies, particularly when single neuron recordings are required. The reasons for this include the viability of the slices, which are difficult to maintain for long recording periods above 36^{o}C. In addition, the success rate for seal formation, required for recording and filling single neurons, is very much higher at room temperature, than at physiological temperatures. To achieve reasonable yields for this study, single neuron recording and loading was at 30^{o}C and then for most experiments slices were warmed after removal of the filling electrode, to temperatures somewhat closer to physiological (32-35^{o}C).

Excitability changes based on temperature has been, at least in part, a hypothesis for the protective effects of hypothermia following brain injury. Careful attention was therefore paid to the influence of even quite small temperature changes, and the mechanisms involved. The results from Chapter 2 suggest that a likely mechanism for the differences in responses is the differences in the release of adenosine and subsequent activation of adenosine A1 receptors at (Masino and Dunwiddie, 1999). Given these considerations, experimental temperatures were carefully monitored and adenosine tone of the slice was

clamped at high or low levels in a majority of the experiments. These results may be of particular interest in the field of SD, where experimental protocols involve temperatures between 30°C and 37°C. The relative roles that adenosine receptor activation may be playing at these different temperatures may account for some of the confusion in the literature, as routes of Zn^{2+} entry contributing to SD are modified by A1 receptor activation

6.7 Perspectives

It is becoming increasingly clear that SD-like events are involved in the expansion of injury following ischemic injury. At the same time, there is growing evidence that Zn^{2+} plays a critical role in neuronal injury. Results from this study are the first to suggest that accumulation of endogenous Zn^{2+} may play a critical role in SD leading to neuronal injury. This is an exciting finding which reveals the potential interplay between Zn^{2+} and Ca^{2+} in mediating ischemic injury and may provide important insights into potential therapies to reduce ischemic neuronal injury.

Appendix A: Supplemental Data

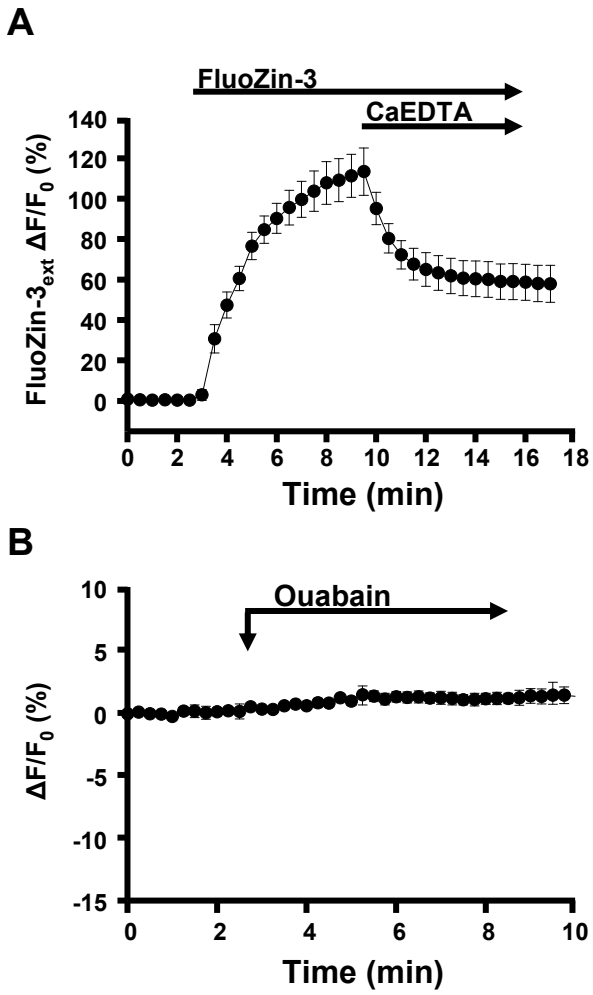

Figure A.1: Recording conditions for extracellular FluoZin-3 fluorescence studies. **A:** Fluorescence intensity changes in response to extracellular application of FluoZin-3 (2μM) in the superfusing ACSF. Measurements (Ex 495 nm, Em 535/50 nm) were made from the slice surface, and showed a large fluorescence increase that was reduced by approximately 50% by the slow Zn^{2+} chelator CaEDTA (1mM). Data are mean ± SEM from 5 preparations. **B:** Control studies from preparations not loaded with FluoZin-3, to test for possible artifacts due to tissue autofluorescence changes (n=5) following ouabain (30μM) application. Autofluorescence was excited with the same wavelength and filter set as used for FluoZin-3 studies (Ex 495 nm, Em 535/50 nm). When exposed to ouabain, no decrease in autofluorescence was observed, implying that autofluorescence changes do not contribute to the extracellular FluoZin-3 dynamics reported in Figure 2.5.

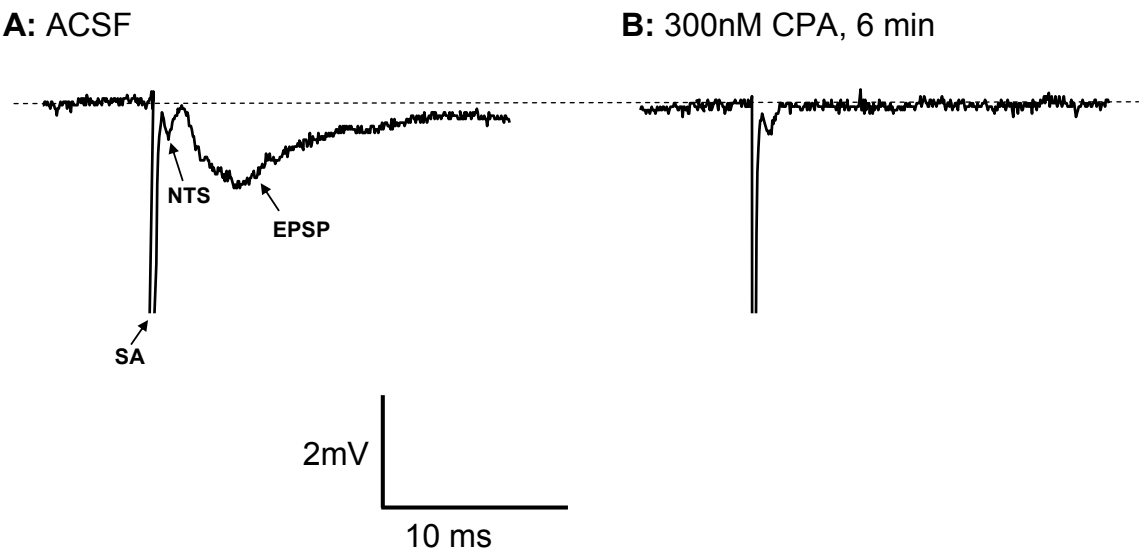

Figure A.2: Effect of CPA on fEPSP. **A:** Example of field excitatory postsynaptic potential (fEPSP) in ACSF at 35°C measured by placing a stimulating electrode and applying a single shock to the Schaffer collaterals and recording electrode in the *s. radiatum* of the CA1 region. SA: stimulus artifact from the single shock; NTS: nerve terminal spike. **B:** Recording from the same preparation as in A after the A1 receptor agonist N^6-cyclopentyladenosine (CPA) was applied for 6 minutes. The loss of the postsynaptic response suggests that this concentration of CPA effectively limits neurotransmission.

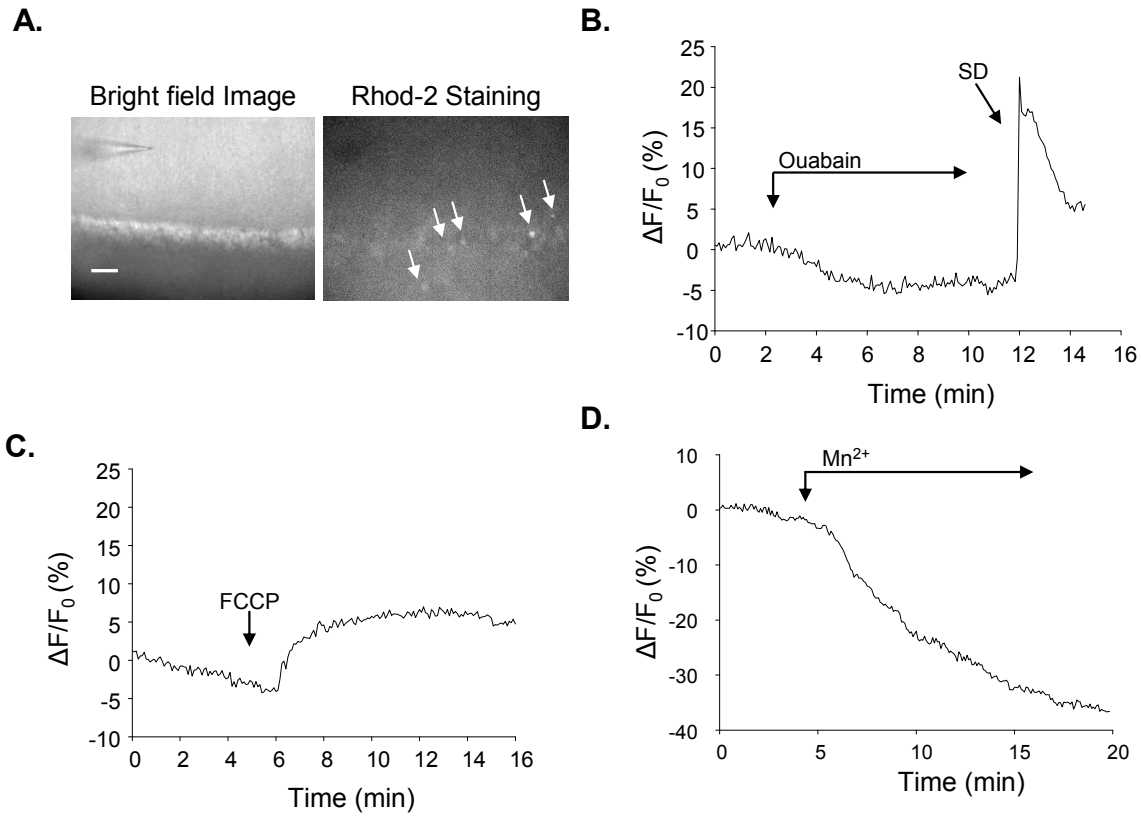

Figure A.3: Rhod-2 loading did not permit selective monitoring of mitochondrial Ca^{2+} levels. **A:** Representative images showing a bright field image of the hippocampal slice on the left and the Rhod-2 staining in the same slice. Several areas of fluorescence (arrows) can be seen after incubating the slice in 15µM Rhod-2 for thirty minutes followed by a 2 hour washout, as described by Mironov and Richter, 2001. Scale bar: 100µm. **B:** 30µM ouabain produced a decrease in Rhod-2 fluorescence prior to SD. This was inconsistent with mitochondrial accumulation, described in Chapter 3. **C:** To test the possibility that Rhod-2 was reporting changes in cytosolic Ca^{2+} rather than mitochondrial Ca^{2+}, an FCCP bolus was applied (similar to Figure 3.4). The application of FCCP should produce a fluorescence decrease if the indicator is reporting mitochondrial Ca^{2+} because the FCCP will cause Ca^{2+} to leave mitochondria. However, the signal increased. Combined with the drop in fluorescence in B., this strongly implies that Rhod-2 was reporting cytoplasmic Ca^{2+}. **D:** Mn^{2+} quenches cytosolic Rhod-2 fluorescence, and was used to test the source of the Rhod-2 signals. Mn^{2+} caused a large decrease in fluorescence, supporting a cytosolic, rather than mitochondrial source.

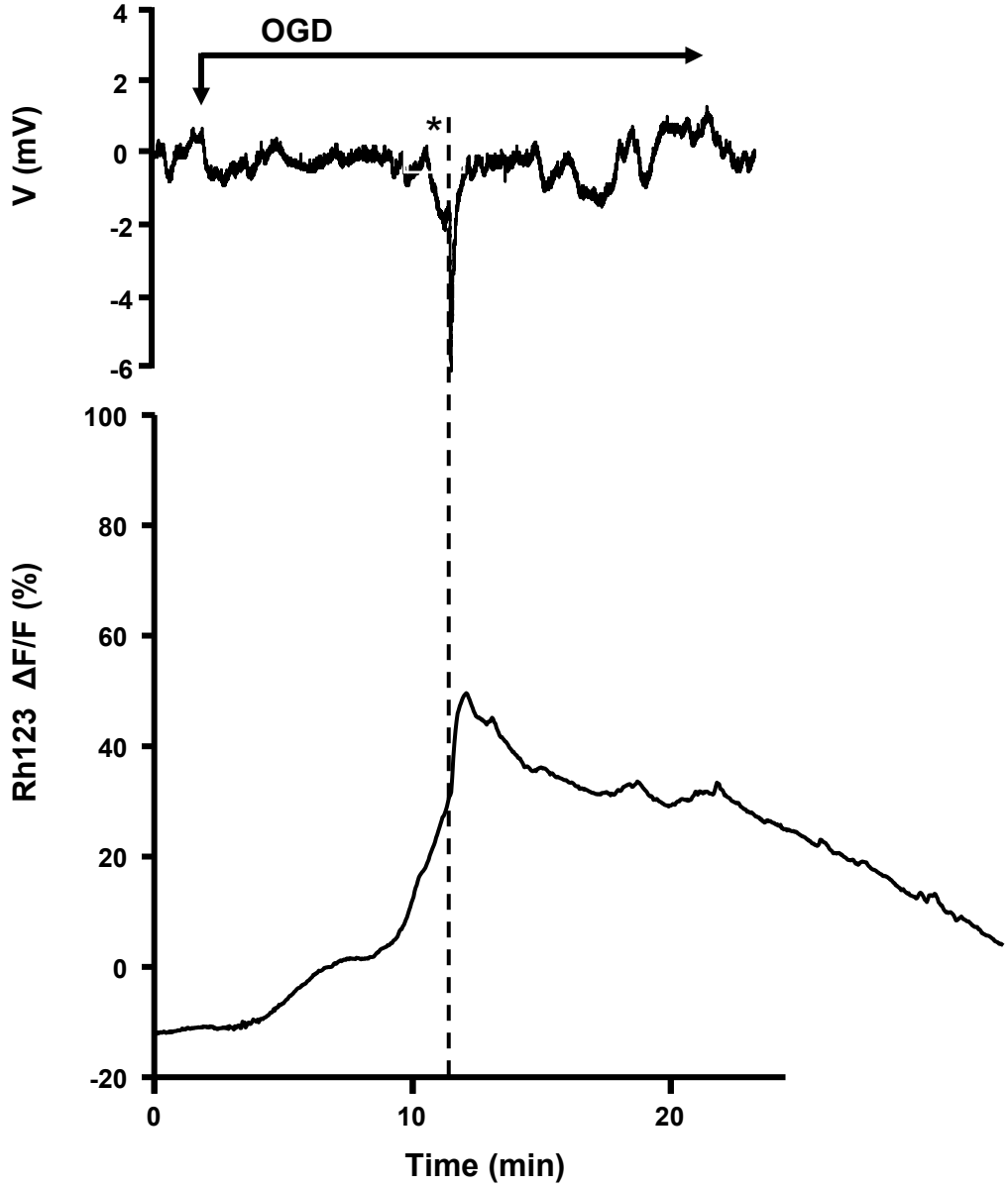

Figure A.4: Mitochondrial depolarization induced by OGD prior to SD. Representative records showing electrically measured SD (top trace, asterisk), with Rh123 fluorescence signals monitored simultaneously from the same slice (bottom trace) exposed to OGD (32°C). Rh123 is in the quenched mode under these loading conditions, and a two phases of Rh123 fluorescence increase were observed prior to the sharp fluorescence increase which accompanied SD.

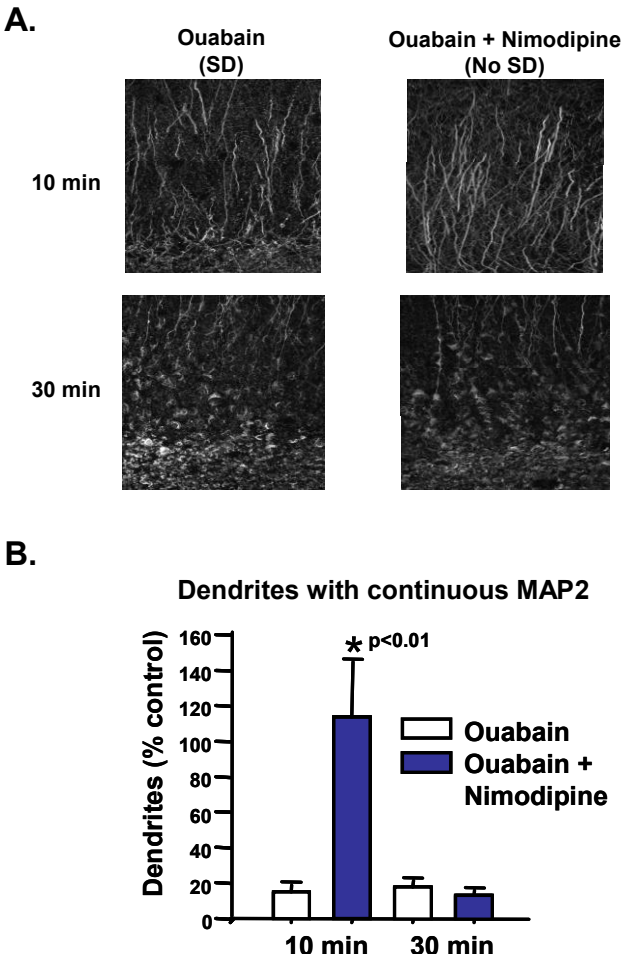

Figure A.5: Blocking SD does not prevent dendritic damage. **A:** Representative images showing MAP2 (microtubule-associated protein 2) immuoreactivity in CA1 stratum radiatum. When slices were fixed 10 min following ouabain exposure (top panels), significant disruption of MAP2 labeling was observed when SD occurred (without nimodipine), but dendritic structure appeared near-normal if SD was prevented (nimodipine). In contrast, if ouabain exposure was extended for 30 min (bottom panels), large rounded dendritic swellings were observed, regardless of whether or not SD occurred (i.e. with or without nimodipine). This suggests that excessive dendritic Ca^{2+} elevations may ultimately result in similar injury, whether SD occurs or is blocked. Scale bar: 10μm. **B:** Mean data from a group of experiments as illustrated in A (n=4-5). Uninjured dendrite segments were assessed by continuity of MAP2 labeling and were compared with labeling in a group of control slices (not exposed to ouabain). These experiments were performed in collaboration with Dr. Meg Hoskison.

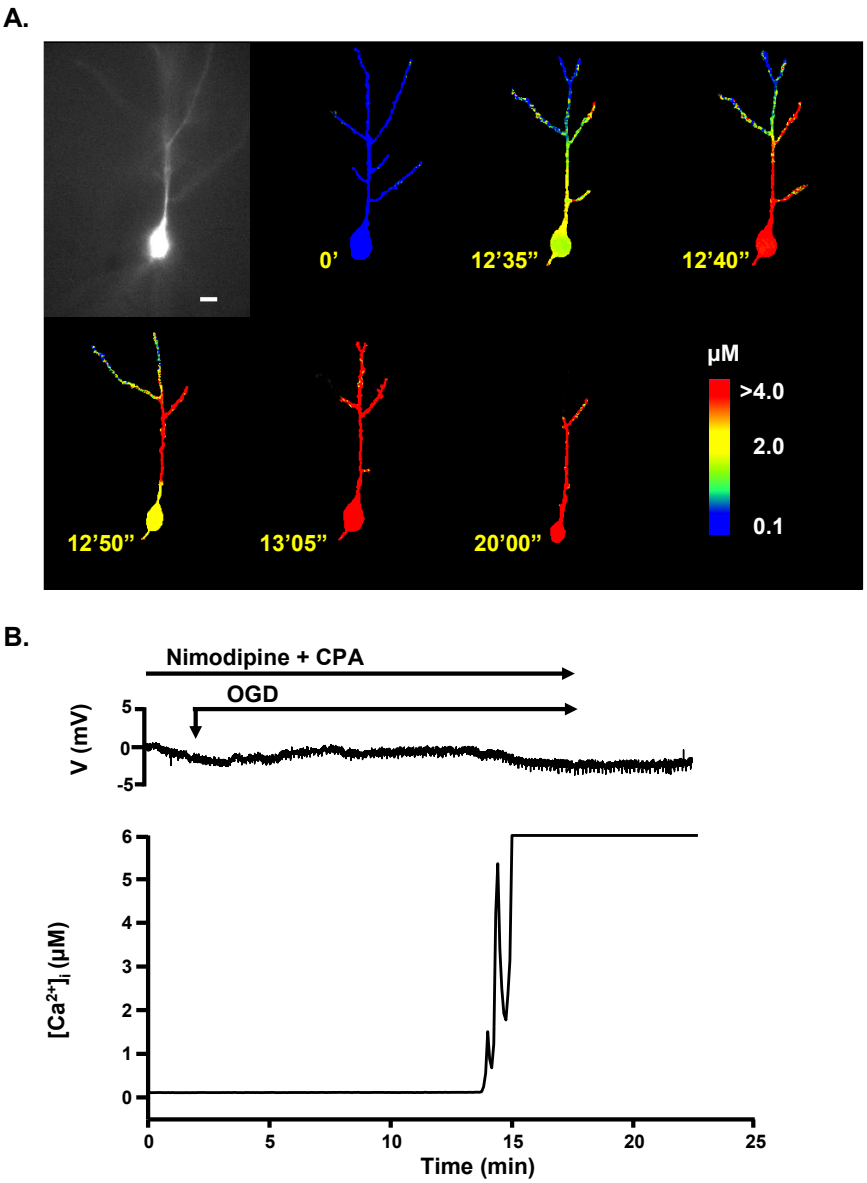

Figure A.6: Nimodipine can block OGD-induced SD. A: Single CA1 neuron loaded with Ca^{2+} indicator Fura-2 via sharp microelectrode exposed to OGD following pre-exposure to nimodipine (10μM) and CPA (300nM). The first panel shows raw 380nm fluorescence and subsequent panels are pseudocolor images that represent intracellular $[Ca^{2+}]$. Despite the fact that SD was blocked, intracellular Ca^{2+} homeostasis is eventually compromised (~12.5 minutes following OGD application), but with different Ca^{2+} kinetics than SD (Figure 5.2). It appears that the cell attempts to recover the high Ca^{2+} load, but is unable to and $[Ca^{2+}]$ stays high until recording is stopped. Scale bar: 10μm. Times are relative to OGD application (mm"ss") **B:** Simultaneous extracellular voltage recording and $[Ca^{2+}]$ from the same preparation as in A showing no sign of SD despite loss of Ca^{2+} homeostasis. The $[Ca^{2+}]$ was cut off at 6μM to reflect the saturating concentration for Fura-2. SD was blocked in 8/12 slices exposed to nimodipine and CPA and was significantly delayed in the remaining slices.

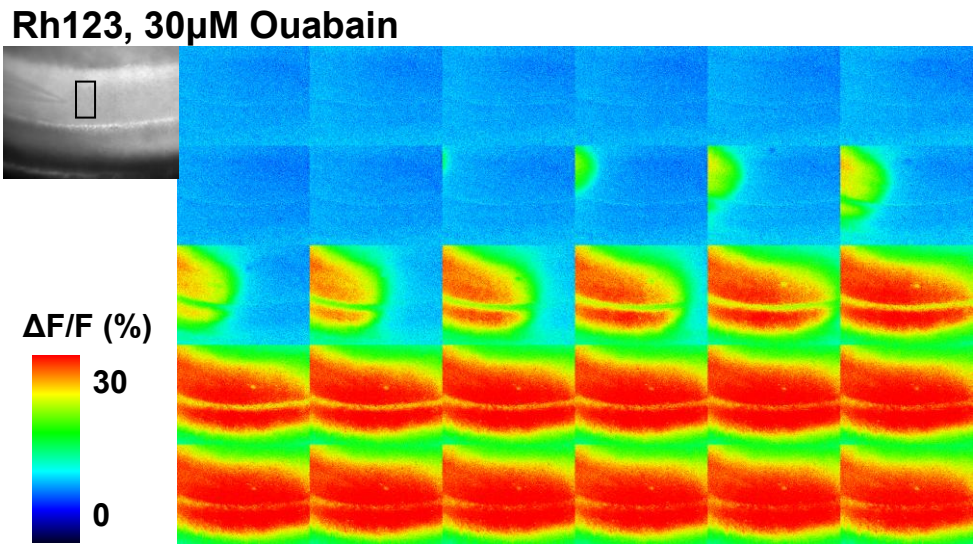

Figure A.7: SD induces a wave of mitochondrial depolarization. Example of the propagation of mitochondrial depolarization as recorded by Rh123 during exposure to 30µM ouabain at 35°C. Rh123 was loaded in the quenched mode (see methods in Chapter 2) and increases in fluorescence were interpreted as depolarization of the inner mitochondrial membrane. The first box shows a bright field image showing the placement of the recording electrode and a region of interest from which data was collected. The subsequent images show the relative change in fluorescence and are sequential showing that a wave of mitochondrial depolarization increase propagates across the slice concurrent with SD.

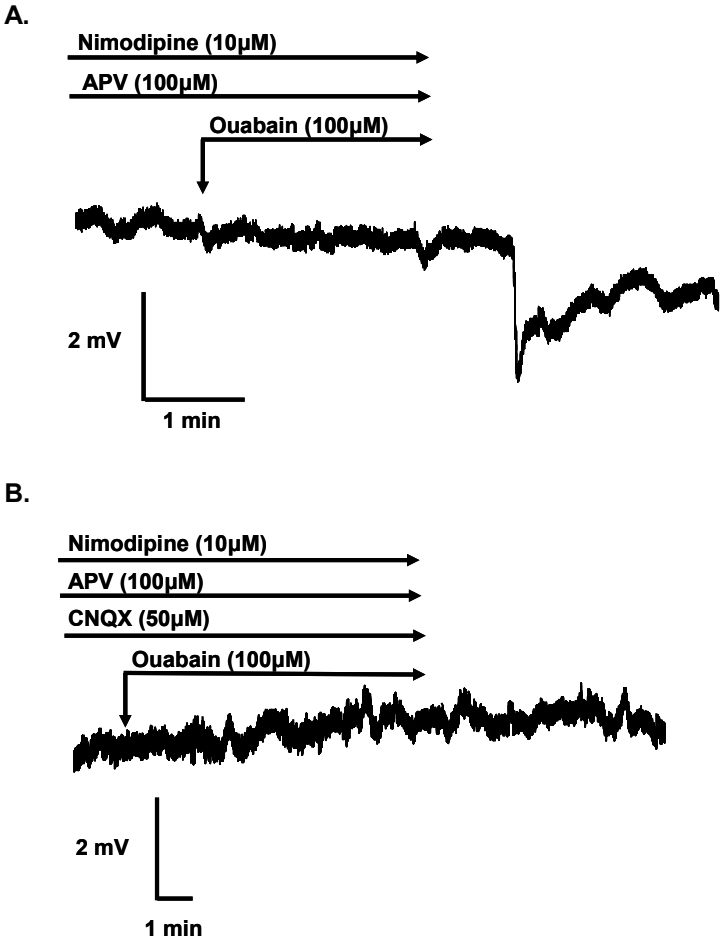

Figure A.8: Multiple entry routes contribute to SD following 100μM ouabain application. A: Example trace of extracellular DC recording showing that pre-exposure to nimodipine and NMDA receptor antagonist APV are not sufficient to block SD when slice is exposed to 100μM ouabain at 35°C. **B:** However, additional block of AMPA receptors by CNQX is able to prevent SD, suggesting that additional influx pathways contribute following stronger stimulus to trigger SD.

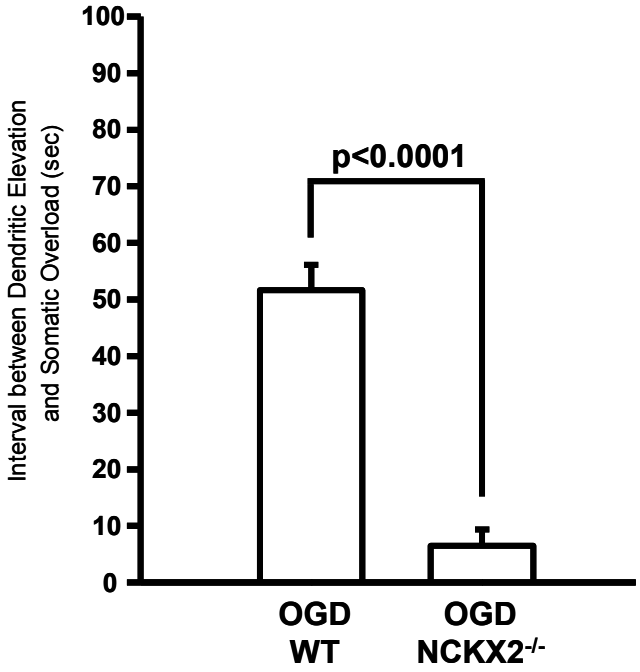

Figure A.9. Effect of NCKX2$^{-/-}$ on Ca^{2+} overload. Single CA1 pyramidal neurons were filled with Fura-6F and subjected to OGD. Slices were pre-exposed to KB-R7943 and nimodipine for 20 minutes prior to OGD application. Extracellular DC potential was monitored for evidence of spreading depression (SD). Upon arrival of SD, the apical dendrites of the neurons went high with Ca^{2+}, but the time it took for the entire cell to be have high amounts of Ca^{2+} varied between the wild type (WT) mice and mice with the K^+-dependent Na^+/Ca^{2+} exchanger 2 (NCKX2) knocked out. This data provides evidence that NCKX2 may contribute to maintaining Ca^{2+} homeostasis when operating in the forward mode. These experiments were performed in collaboration with Dr. Lech Kiedrowski from the University of Chicago.

Abbreviations Used

ACSF	artificial cerebral spinal fluid
AMPA	α-amino-3-hydroxy-5-methylisoxazole-4-propionic acid
ATP	adenosine triphosphate
BAPTA	1,2-bis(o-aminophenoxy)ethane-N,N,N',N'-tetraacetic acid
CPA	N^6-cyclopentyladenosine
DPCPX	8-cyclopentyl-1,3-dipropylxanthine
EDTA	ethylenediaminetetraacetic acid
EGTA	ethylene glycol-bis(2-aminoethylether)-N,N,N',N'-tetraacetic acid
FCCP	carbonylcyanide-p-trifluoromethoxyphenylhydrazone
FHM	familial hemiplegic migraine
HSD	spreading depression-like hypoxic depolarization
NCX	sodium calcium exchanger
NCKX	potassium-dependent sodium calcium exchanger
NMDA	N-methyl-D-aspartic acid
OGD	oxygen and glucose deprivation
PID	peri-infarct depolarization
SEM	standard error of the mean
SD	spreading depression
sp	stratum pyramidale
sr	stratum radiatum
TCA	tricarboxylic acid
TPEN	N,N,N‘‘,N‘‘-tetrakis-(2-pyridylmethyl)-ethylenediamine

References

Adler EM, Augustine GJ, Duffy SN, Charlton MP (1991) Alien intracellular calcium chelators attenuate neurotransmitter release at the squid giant synapse. J Neurosci 11:1496-1507.

Aitken PG, Tombaugh GC, Turner DA, Somjen GG (1998) Similar propagation of SD and hypoxic SD-like depolarization in rat hippocampus recorded optically and electrically. J Neurophysiol 80:1514-1521.

Aitken PG, Fayuk D, Somjen GG, Turner DA (1999) Use of intrinsic optical signals to monitor physiological changes in brain tissue slices. Methods 18:91-103.

Aizenman E, Stout AK, Hartnett KA, Dineley KE, McLaughlin B, Reynolds IJ (2000) Induction of neuronal apoptosis by thiol oxidation: putative role of intracellular zinc release. J Neurochem 75:1878-1888.

Akaike N, Ishibashi H, Hara H, Oyama Y, Ueha T (1993) Effect of KB-2796, a new diphenylpiperazine Ca2+ antagonist, on voltage-dependent Ca2+ currents and oxidative metabolism in dissociated mammalian CNS neurons. Brain Res 619:263-270.

Allen NJ, Karadottir R, Attwell D (2005) A preferential role for glycolysis in preventing the anoxic depolarization of rat hippocampal area CA1 pyramidal cells. J Neurosci 25:848-859.

Anderson TR, Andrew RD (2002) Spreading depression: imaging and blockade in the rat neocortical brain slice. J Neurophysiol 88:2713-2725.

Anderson TR, Jarvis CR, Biedermann AJ, Molnar C, Andrew RD (2005) Blocking the anoxic depolarization protects without functional compromise following simulated stroke in cortical brain slices. J Neurophysiol 93:963-979.

Andreeva N, Khodorov B, Stelmashook E, Cragoe E, Jr., Victorov I (1991) Inhibition of Na+/Ca2+ exchange enhances delayed neuronal death elicited by glutamate in cerebellar granule cell cultures. Brain Res 548:322-325.

Andrew RD, Jarvis CR, Obeidat AS (1999) Potential sources of intrinsic optical signals imaged in live brain slices. Methods 18:185-196, 179.

Annunziato L, Pignataro G, Di Renzo GF (2004) Pharmacology of brain Na+/Ca2+ exchanger: from molecular biology to therapeutic perspectives. Pharmacol Rev 56:633-654.

Arundine M, Tymianski M (2003) Molecular mechanisms of calcium-dependent neurodegeneration in excitotoxicity. Cell Calcium 34:325-337.

Aschner M, Cherian MG, Klaassen CD, Palmiter RD, Erickson JC, Bush AI (1997) Metallothioneins in brain--the role in physiology and pathology. Toxicol Appl Pharmacol 142:229-242.

Assaf SY, Chung SH (1984) Release of endogenous Zn2+ from brain tissue during activity. Nature 308:734-736.

Atar D, Backx PH, Appel MM, Gao WD, Marban E (1995) Excitation-transcription coupling mediated by zinc influx through voltage-dependent calcium channels. J Biol Chem 270:2473-2477.

Ayata C, Shimizu-Sasamata M, Lo EH, Noebels JL, Moskowitz MA (2000) Impaired neurotransmitter release and elevated threshold for cortical spreading depression in mice with mutations in the alpha1A subunit of P/Q type calcium channels. Neuroscience 95:639-645.

Back T, Kohno K, Hossmann KA (1994) Cortical negative DC deflections following middle cerebral artery occlusion and KCl-induced spreading depression: effect on blood flow, tissue oxygenation, and electroencephalogram. J Cereb Blood Flow Metab 14:12-19.

Back T, Ginsberg MD, Dietrich WD, Watson BD (1996) Induction of spreading depression in the ischemic hemisphere following experimental middle cerebral artery occlusion: effect on infarct morphology. J Cereb Blood Flow Metab 16:202-213.

Bahar S, Fayuk D, Somjen GG, Aitken PG, Turner DA (2000) Mitochondrial and intrinsic optical signals imaged during hypoxia and spreading depression in rat hippocampal slices. J Neurophysiol 84:311-324.

Balestrino M, Somjen GG (1986) Chlorpromazine protects brain tissue in hypoxia by delaying spreading depression-mediated calcium influx. Brain Res 385:219-226.

Balestrino M, Young J, Aitken P (1999) Block of (Na+,K+)ATPase with ouabain induces spreading depression-like depolarization in hippocampal slices. Brain Res 838:37-44.

Bano D, Young KW, Guerin CJ, Lefeuvre R, Rothwell NJ, Naldini L, Rizzuto R, Carafoli E, Nicotera P (2005) Cleavage of the plasma membrane Na+/Ca2+ exchanger in excitotoxicity. Cell 120:275-285.

Basarsky TA, Duffy SN, Andrew RD, MacVicar BA (1998) Imaging spreading depression and associated intracellular calcium waves in brain slices. J Neurosci 18:7189-7199.

Blaustein MP, Lederer WJ (1999) Sodium/calcium exchange: its physiological implications. Physiol Rev 79:763-854.

Bolay H, Reuter U, Dunn AK, Huang Z, Boas DA, Moskowitz MA (2002) Intrinsic brain activity triggers trigeminal meningeal afferents in a migraine model. Nat Med 8:136-142.

Bonanni L, Chachar M, Jover-Mengual T, Li H, Jones A, Yokota H, Ofengeim D, Flannery RJ, Miyawaki T, Cho CH, Polster BM, Pypaert M, Hardwick JM, Sensi SL, Zukin RS, Jonas EA (2006) Zinc-dependent multi-conductance channel activity in mitochondria isolated from ischemic brain. J Neurosci 26:6851-6862.

Borst JG, Sakmann B (1996) Calcium influx and transmitter release in a fast CNS synapse. Nature 383:431-434.

Boscia F, Gala R, Pignataro G, de Bartolomeis A, Cicale M, Ambesi-Impiombato A, Di Renzo G, Annunziato L (2006) Permanent focal brain ischemia induces isoform-dependent changes in the pattern of Na+/Ca2+ exchanger gene expression in the ischemic core, periinfarct area, and intact brain regions. J Cereb Blood Flow Metab 26:502-517.

Bossy-Wetzel E, Talantova MV, Lee WD, Scholzke MN, Harrop A, Mathews E, Gotz T, Han J, Ellisman MH, Perkins GA, Lipton SA (2004) Crosstalk between nitric oxide and zinc pathways to neuronal cell death involving mitochondrial dysfunction and p38-activated K+ channels. Neuron 41:351-365.

Bowyer S (1999) Cortical spreading depression (CSD) and migraine. Cephalalgia 19:542.

Bramanti P, Grugno R, Vitetta A, Di Bella P, Muscara N, Nappi G (2005) Migraine with and without aura: electrophysiological and functional neuroimaging evidence. Funct Neurol 20:29-32.

Brandes R, Bers DM (1999) Analysis of the mechanisms of mitochondrial NADH regulation in cardiac trabeculae. Biophys J 77:1666-1682.

Branston NM, Strong AJ, Symon L (1977) Extracellular potassium activity, evoked potential and tissue blood flow. Relationships during progressive ischaemia in baboon cerebral cortex. J Neurol Sci 32:305-321.

Breder J, Sabelhaus CF, Opitz T, Reymann KG, Schroder UH (2000) Inhibition of different pathways influencing Na(+) homeostasis protects organotypic hippocampal slice cultures from hypoxic/hypoglycemic injury. Neuropharmacology 39:1779-1787.

Brennan AM, Connor JA, Shuttleworth CW (2006) NAD(P)H fluorescence transients after synaptic activity in brain slices: predominant role of mitochondrial function. J Cereb Blood Flow Metab.

Brennan AM, Connor JA, Shuttleworth CW (2007) Modulation of the amplitude of NAD(P)H fluorescence transients after synaptic stimulation. J Neurosci Res 85:3233-3243.

Brown AM, Kristal BS, Effron MS, Shestopalov AI, Ullucci PA, Sheu KF, Blass JP, Cooper AJ (2000) Zn2+ inhibits alpha-ketoglutarate-stimulated mitochondrial respiration and the isolated alpha-ketoglutarate dehydrogenase complex. J Biol Chem 275:13441-13447.

Bures J, Buresova O, Krivanek J (1984) The meaning and significance of Leao's spreading depression. An Acad Bras Cienc 56:385-400.

Buresova O, Bures J (1969) The effect of prolonged cortical spreading depression on learning and memory in rats. J Neurobiol 1:135-146.

Busch E, Hoehn-Berlage M, Eis M, Gyngell ML, Hossmann KA (1995) Simultaneous recording of EEG, DC potential and diffusion-weighted NMR imaging during potassium induced cortical spreading depression in rats. NMR Biomed 8:59-64.

Busch E, Gyngell ML, Eis M, Hoehn-Berlage M, Hossmann KA (1996) Potassium-induced cortical spreading depressions during focal cerebral ischemia in rats: contribution to lesion growth assessed by diffusion-weighted NMR and biochemical imaging. J Cereb Blood Flow Metab 16:1090-1099.

Buzzi MG, Moskowitz MA (2005) The pathophysiology of migraine: year 2005. J Headache Pain 6:105-111.

Calderone A, Jover T, Mashiko T, Noh KM, Tanaka H, Bennett MV, Zukin RS (2004) Late calcium EDTA rescues hippocampal CA1 neurons from global ischemia-induced death. J Neurosci 24:9903-9913.

Canals S, Makarova I, Lopez-Aguado L, Largo C, Ibarz JM, Herreras O (2005) Longitudinal depolarization gradients along the somatodendritic axis of CA1 pyramidal cells: a novel feature of spreading depression. J Neurophysiol 94:943-951.

Cao Y, Welch KM, Aurora S, Vikingstad EM (1999) Functional MRI-BOLD of visually triggered headache in patients with migraine. Arch Neurol 56:548-554.

Carriedo SG, Sensi SL, Yin HZ, Weiss JH (2000) AMPA exposures induce mitochondrial Ca(2+) overload and ROS generation in spinal motor neurons in vitro. J Neurosci 20:240-250.

Chappell RL, Zakevicius J, Ripps H (2003) Zinc modulation of hemichannel currents in Xenopus oocytes. Biol Bull 205:209-211.

Charriaut-Marlangue C, Margaill I, Represa A, Popovici T, Plotkine M, Ben-Ari Y (1996) Apoptosis and necrosis after reversible focal ischemia: an in situ DNA fragmentation analysis. J Cereb Blood Flow Metab 16:186-194.

Cheng C, Reynolds IJ (1998) Calcium-sensitive fluorescent dyes can report increases in intracellular free zinc concentration in cultured forebrain neurons. J Neurochem 71:2401-2410.

Choi DW (1985) Glutamate neurotoxicity in cortical cell culture is calcium dependent. Neurosci Lett 58:293-297.

Choi DW, Koh JY (1998) Zinc and brain injury. Annu Rev Neurosci 21:347-375.

Choi DW, Yokoyama M, Koh J (1988) Zinc neurotoxicity in cortical cell culture. Neuroscience 24:67-79.

Christine CW, Choi DW (1990) Effect of zinc on NMDA receptor-mediated channel currents in cortical neurons. J Neurosci 10:108-116.

Church AJ, Andrew RD (2005) Spreading depression expands traumatic injury in neocortical brain slices. J Neurotrauma 22:277-290.

Cole TB, Robbins CA, Wenzel HJ, Schwartzkroin PA, Palmiter RD (2000) Seizures and neuronal damage in mice lacking vesicular zinc. Epilepsy Res 39:153-169.

Connor JA, Cormier RJ (2000) Cumulative effects of glutamate microstimulation on Ca(2+) responses of CA1 hippocampal pyramidal neurons in slice. J Neurophysiol 83:90-98.

Connor JA, Wadman WJ, Hockberger PE, Wong RK (1988) Sustained dendritic gradients of Ca2+ induced by excitatory amino acids in CA1 hippocampal neurons. Science 240:649-653.

Crompton M, Heid I (1978) The cycling of calcium, sodium, and protons across the inner membrane of cardiac mitochondria. Eur J Biochem 91:599-608.

Crompton M, Hediger M, Carafoli E (1978) The effect of inorganic phosphate on calcium influx into rat heart mitochondria. Biochem Biophys Res Commun 80:540-546.

Cruz NF, Adachi K, Dienel GA (1999) Rapid efflux of lactate from cerebral cortex during K+ -induced spreading cortical depression. J Cereb Blood Flow Metab 19:380-392.

Cutrer FM, Huerter K (2007) Migraine aura. Neurologist 13:118-125.

Czyz A, Kiedrowski L (2002) In depolarized and glucose-deprived neurons, Na+ influx reverses plasmalemmal K+-dependent and K+-independent Na+/Ca2+ exchangers and contributes to NMDA excitotoxicity. J Neurochem 83:1321-1328.

Czyz A, Baranauskas G, Kiedrowski L (2002) Instrumental role of Na+ in NMDA excitotoxicity in glucose-deprived and depolarized cerebellar granule cells. J Neurochem 81:379-389.

Dalkara T, Zervas NT, Moskowitz MA (2006) From spreading depression to the trigeminovascular system. Neurol Sci 27 Suppl 2:S86-90.

Davies JA, Annels SJ, Dickie BG, Ellis Y, Knott NJ (1995) A comparison between the stimulated and paroxysmal release of endogenous amino acids from rat cerebellar, striatal and hippocampal slices: a manifestation of spreading depression? J Neurol Sci 131:8-14.

Denton RM, McCormack JG (1990) Ca2+ as a second messenger within mitochondria of the heart and other tissues. Annu Rev Physiol 52:451-466.

Deshpande LS, Limbrick DD, Jr., Sombati S, DeLorenzo RJ (2007) Activation of a novel injury-induced calcium-permeable channel that plays a key role in causing extended neuronal depolarization and initiating neuronal death in excitotoxic neuronal injury. J Pharmacol Exp Ther 322:443-452.

Devinney MJ, 2nd, Reynolds IJ, Dineley KE (2005) Simultaneous detection of intracellular free calcium and zinc using fura-2FF and FluoZin-3. Cell Calcium 37:225-232.

Dineley KE (2007) On the use of fluorescent probes to distinguish Ca2+ from Zn2+ in models of excitotoxicity. Cell Calcium 42:341-342; author reply 343-344.

Dineley KE, Votyakova TV, Reynolds IJ (2003) Zinc inhibition of cellular energy production: implications for mitochondria and neurodegeneration. J Neurochem 85:563-570.

Dineley KE, Richards LL, Votyakova TV, Reynolds IJ (2005) Zinc causes loss of membrane potential and elevates reactive oxygen species in rat brain mitochondria. Mitochondrion 5:55-65.

Dirnagl U, Iadecola C, Moskowitz MA (1999) Pathobiology of ischaemic stroke: an integrated view. Trends Neurosci 22:391-397.

do Carmo RJ, Leao AA (1972) On the relation of glutamic acid and some allied compounds to cortical spreading depression. Brain Res 39:515-518.

Dong H, Dunn J, Lytton J (2002) Stoichiometry of the Cardiac Na+/Ca2+ exchanger NCX1.1 measured in transfected HEK cells. Biophys J 82:1943-1952.

Duchen MR (1992) Ca(2+)-dependent changes in the mitochondrial energetics in single dissociated mouse sensory neurons. Biochem J 283 (Pt 1):41-50.

Duchen MR, Smith PA, Ashcroft FM (1993) Substrate-dependent changes in mitochondrial function, intracellular free calcium concentration and membrane channels in pancreatic beta-cells. Biochem J 294 (Pt 1):35-42.

Duchen MR, Surin A, Jacobson J (2003) Imaging mitochondrial function in intact cells. Methods Enzymol 361:353-389.

Dunwiddie TV, Masino SA (2001) The role and regulation of adenosine in the central nervous system. Annu Rev Neurosci 24:31-55.

Fabricius M, Jensen LH, Lauritzen M (1993) Microdialysis of interstitial amino acids during spreading depression and anoxic depolarization in rat neocortex. Brain Res 612:61-69.

Flippen C, Welch KM (1997) Imaging the brain of migraine sufferers. Curr Opin Neurol 10:226-230.

Frederickson CJ (1989) Neurobiology of zinc and zinc-containing neurons. Int Rev Neurobiol 31:145-238.

Frederickson CJ, Hernandez MD, McGinty JF (1989) Translocation of zinc may contribute to seizure-induced death of neurons. Brain Res 480:317-321.

Freund WD, Reddig S (1994) AMPA/Zn(2+)-induced neurotoxicity in rat primary cortical cultures: involvement of L-type calcium channels. Brain Res 654:257-264.

Fujioka Y, Komeda M, Matsuoka S (2000) Stoichiometry of Na+-Ca2+ exchange in inside-out patches excised from guinea-pig ventricular myocytes. J Physiol 523 Pt 2:339-351.

Furlan M, Marchal G, Viader F, Derlon JM, Baron JC (1996) Spontaneous neurological recovery after stroke and the fate of the ischemic penumbra. Ann Neurol 40:216-226.

Gaskin F, Kress Y, Brosnan C, Bornstein M (1978) Abnormal tubulin aggregates induced by zinc sulfate in organotypic cultures of nerve tissue. Neuroscience 3:1117-1128.

Gazaryan IG, Krasnikov BF, Ashby GA, Thorneley RN, Kristal BS, Brown AM (2002) Zinc is a potent inhibitor of thiol oxidoreductase activity and stimulates reactive oxygen species production by lipoamide dehydrogenase. J Biol Chem 277:10064-10072.

Gerich FJ, Hepp S, Probst I, Muller M (2006) Mitochondrial inhibition prior to oxygen-withdrawal facilitates the occurrence of hypoxia-induced spreading depression in rat hippocampal slices. J Neurophysiol 96:492-504.

Gido G, Kristian T, Siesjo BK (1994) Induced spreading depressions in energy-compromised neocortical tissue: calcium transients and histopathological correlates. Neurobiol Dis 1:31-41.

Gill R, Andine P, Hillered L, Persson L, Hagberg H (1992) The effect of MK-801 on cortical spreading depression in the penumbral zone following focal ischaemia in the rat. J Cereb Blood Flow Metab 12:371-379.

Gottron FJ, Ying HS, Choi DW (1997) Caspase inhibition selectively reduces the apoptotic component of oxygen-glucose deprivation-induced cortical neuronal cell death. Mol Cell Neurosci 9:159-169.

Grafstein B (1956) Mechanism of spreading cortical depression. J Neurophysiol 19:154-171.

Grynkiewicz G, Poenie M, Tsien RY (1985) A new generation of Ca2+ indicators with greatly improved fluorescence properties. J Biol Chem 260:3440-3450.

Gursoy-Ozdemir Y, Qiu J, Matsuoka N, Bolay H, Bermpohl D, Jin H, Wang X, Rosenberg GA, Lo EH, Moskowitz MA (2004) Cortical spreading depression activates and upregulates MMP-9. J Clin Invest 113:1447-1455.

Hadjikhani N, Sanchez Del Rio M, Wu O, Schwartz D, Bakker D, Fischl B, Kwong KK, Cutrer FM, Rosen BR, Tootell RB, Sorensen AG, Moskowitz MA (2001) Mechanisms of migraine aura revealed by functional MRI in human visual cortex. Proc Natl Acad Sci U S A 98:4687-4692.

Haglund MM, Schwartzkroin PA (1990) Role of Na-K pump potassium regulation and IPSPs in seizures and spreading depression in immature rabbit hippocampal slices. J Neurophysiol 63:225-239.

Hajnoczky G, Robb-Gaspers LD, Seitz MB, Thomas AP (1995) Decoding of cytosolic calcium oscillations in the mitochondria. Cell 82:415-424.

Hansen AJ (1985) Effect of anoxia on ion distribution in the brain. Physiol Rev 65:101-148.

Hansford RG (1985) Relation between mitochondrial calcium transport and control of energy metabolism. Rev Physiol Biochem Pharmacol 102:1-72.

Hartings JA, Rolli ML, Lu XC, Tortella FC (2003) Delayed secondary phase of peri-infarct depolarizations after focal cerebral ischemia: relation to infarct growth and neuroprotection. J Neurosci 23:11602-11610.

Hartley DM, Choi DW (1989) Delayed rescue of N-methyl-D-aspartate receptor-mediated neuronal injury in cortical culture. J Pharmacol Exp Ther 250:752-758.

Hasegawa Y, Latour LL, Formato JE, Sotak CH, Fisher M (1995) Spreading waves of a reduced diffusion coefficient of water in normal and ischemic rat brain. J Cereb Blood Flow Metab 15:179-187.

Hashimoto M, Takeda Y, Sato T, Kawahara H, Nagano O, Hirakawa M (2000) Dynamic changes of NADH fluorescence images and NADH content during spreading depression in the cerebral cortex of gerbils. Brain Res 872:294-300.

Hell JW, Westenbroek RE, Warner C, Ahlijanian MK, Prystay W, Gilbert MM, Snutch TP, Catterall WA (1993) Identification and differential subcellular localization of the neuronal class C and class D L-type calcium channel alpha 1 subunits. J Cell Biol 123:949-962.

Heron A, Pollard H, Dessi F, Moreau J, Lasbennes F, Ben-Ari Y, Charriaut-Marlangue C (1993) Regional variability in DNA fragmentation after global ischemia evidenced by combined histological and gel electrophoresis observations in the rat brain. J Neurochem 61:1973-1976.

Herreras O, Somjen GG (1993) Analysis of potential shifts associated with recurrent spreading depression and prolonged unstable spreading depression induced by microdialysis of elevated K+ in hippocampus of anesthetized rats. Brain Res 610:283-294.

Herreras O, Largo C, Ibarz JM, Somjen GG, Martin del Rio R (1994) Role of neuronal synchronizing mechanisms in the propagation of spreading depression in the in vivo hippocampus. J Neurosci 14:7087-7098.

Hille B (2001) Ion Channels of Excitable Membranes, 3rd Edition. Sunderland, MA: Sinauer Associates, Inc.

Hochstrate P, Schlue WR (2001) The ouabain-induced [Ca2+]i increase in leech Retzius neurones is mediated by voltage-dependent Ca2+ channels. Brain Res 892:248-254.

Hossmann KA (1996) Periinfarct depolarizations. Cerebrovasc Brain Metab Rev 8:195-208.

Howell GA, Welch MG, Frederickson CJ (1984) Stimulation-induced uptake and release of zinc in hippocampal slices. Nature 308:736-738.

Hoyt KR, Arden SR, Aizenman E, Reynolds IJ (1998) Reverse Na+/Ca2+ exchange contributes to glutamate-induced intracellular Ca2+ concentration increases in cultured rat forebrain neurons. Mol Pharmacol 53:742-749.

Iadecola C, Kraig RP (1991) Focal elevations in neocortical interstitial K+ produced by stimulation of the fastigial nucleus in rat. Brain Res 563:273-277.

Iijima T, Mies G, Hossmann KA (1992) Repeated negative DC deflections in rat cortex following middle cerebral artery occlusion are abolished by MK-801: effect on volume of ischemic injury. J Cereb Blood Flow Metab 12:727-733.

Ikeda T, Kimura K, Morioka S, Tamaki N (1980) Inhibitory effects of Zn2+ on muscle glycolysis and their reversal by histidine. J Nutr Sci Vitaminol (Tokyo) 26:357-366.

Imaizumi T, Kocsis JD, Waxman SG (1997) Anoxic injury in the rat spinal cord: pharmacological evidence for multiple steps in Ca(2+)-dependent injury of the dorsal columns. J Neurotrauma 14:299-311.

Iwamoto T, Shigekawa M (1998) Differential inhibition of Na+/Ca2+ exchanger isoforms by divalent cations and isothiourea derivative. Am J Physiol 275:C423-430.

Iwamoto T, Kita S (2004) Development and application of Na+/Ca2+ exchange inhibitors. Mol Cell Biochem 259:157-161.

Iwamoto T, Watano T, Shigekawa M (1996) A novel isothiourea derivative selectively inhibits the reverse mode of Na+/Ca2+ exchange in cells expressing NCX1. J Biol Chem 271:22391-22397.

Iwamoto T, Inoue Y, Ito K, Sakaue T, Kita S, Katsuragi T (2004) The exchanger inhibitory peptide region-dependent inhibition of Na+/Ca2+ exchange by SN-6 [2-[4-(4-nitrobenzyloxy)benzyl]thiazolidine-4-carboxylic acid ethyl ester], a novel benzyloxyphenyl derivative. Mol Pharmacol 66:45-55.

Jarvis CR, Anderson TR, Andrew RD (2001) Anoxic depolarization mediates acute damage independent of glutamate in neocortical brain slices. Cereb Cortex 11:249-259.

Jiang D, Sullivan PG, Sensi SL, Steward O, Weiss JH (2001) Zn(2+) induces permeability transition pore opening and release of pro-apoptotic peptides from neuronal mitochondria. J Biol Chem 276:47524-47529.

Jing J, Aitken PG, Somjen GG (1993) Role of calcium channels in spreading depression in rat hippocampal slices. Brain Res 604:251-259.

Jobsis FF (1977) Noninvasive, infrared monitoring of cerebral and myocardial oxygen sufficiency and circulatory parameters. Science 198:1264-1267.

Kager H, Wadman WJ, Somjen GG (2000) Simulated seizures and spreading depression in a neuron model incorporating interstitial space and ion concentrations. J Neurophysiol 84:495-512.

Kaube H, Goadsby PJ (1994) Anti-migraine compounds fail to modulate the propagation of cortical spreading depression in the cat. Eur Neurol 34:30-35.

Kavalali ET, Zhuo M, Bito H, Tsien RW (1997) Dendritic Ca2+ channels characterized by recordings from isolated hippocampal dendritic segments. Neuron 18:651-663.

Kay AR (2003) Evidence for chelatable zinc in the extracellular space of the hippocampus, but little evidence for synaptic release of Zn. J Neurosci 23:6847-6855.

Keilin D, Mann T (1940) Carbonic anhydrase. Purification and nature of the enzyme. Biochem J 34:1163-1176.

Kempski O, Otsuka H, Seiwert T, Heimann A (2000) Spreading depression induces permanent cell swelling under penumbra conditions. Acta Neurochir Suppl 76:251-255.

Kerchner GA, Canzoniero LM, Yu SP, Ling C, Choi DW (2000) Zn2+ current is mediated by voltage-gated Ca2+ channels and enhanced by extracellular acidity in mouse cortical neurones. J Physiol 528 Pt 1:39-52.

Kiedrowski L (1999) N-methyl-D-aspartate excitotoxicity: relationships among plasma membrane potential, Na(+)/Ca(2+) exchange, mitochondrial Ca(2+) overload, and cytoplasmic concentrations of Ca(2+), H(+), and K(+). Mol Pharmacol 56:619-632.

Kiedrowski L (2004) High activity of K+-dependent plasmalemmal Na+/Ca2+ exchangers in hippocampal CA1 neurons. Neuroreport 15:2113-2116.

Kiedrowski L, Brooker G, Costa E, Wroblewski JT (1994) Glutamate impairs neuronal calcium extrusion while reducing sodium gradient. Neuron 12:295-300.

Kiedrowski L, Czyz A, Li XF, Lytton J (2002) Preferential expression of plasmalemmal K-dependent Na+/Ca2+ exchangers in neurons versus astrocytes. Neuroreport 13:1529-1532.

Kiedrowski L, Czyz A, Baranauskas G, Li XF, Lytton J (2004) Differential contribution of plasmalemmal Na/Ca exchange isoforms to sodium-dependent calcium influx and NMDA excitotoxicity in depolarized neurons. J Neurochem 90:117-128.

Kim EY, Koh JY, Kim YH, Sohn S, Joe E, Gwag BJ (1999) Zn2+ entry produces oxidative neuronal necrosis in cortical cell cultures. Eur J Neurosci 11:327-334.

Kim YH, Koh JY (2002) The role of NADPH oxidase and neuronal nitric oxide synthase in zinc-induced poly(ADP-ribose) polymerase activation and cell death in cortical culture. Exp Neurol 177:407-418.

Kimelberg HK, Goderie SK, Higman S, Pang S, Waniewski RA (1990) Swelling-induced release of glutamate, aspartate, and taurine from astrocyte cultures. J Neurosci 10:1583-1591.

Kip SN, Gray NW, Burette A, Canbay A, Weinberg RJ, Strehler EE (2006) Changes in the expression of plasma membrane calcium extrusion systems during the maturation of hippocampal neurons. Hippocampus 16:20-34.

Kleiner D (1974) The effect of Zn2+ ions on mitochondrial electron transport. Arch Biochem Biophys 165:121-125.

Koh JY, Choi DW (1994) Zinc toxicity on cultured cortical neurons: involvement of N-methyl-D-aspartate receptors. Neuroscience 60:1049-1057.

Koh JY, Goldberg MP, Hartley DM, Choi DW (1990) Non-NMDA receptor-mediated neurotoxicity in cortical culture. J Neurosci 10:693-705.

Koh JY, Suh SW, Gwag BJ, He YY, Hsu CY, Choi DW (1996) The role of zinc in selective neuronal death after transient global cerebral ischemia. Science 272:1013-1016.

Kow LM, van Harreveld A (1972) Ion and water movements in isolated chicken retinas during spreading depression. Neurobiology 2:61-69.

Kraev A, Quednau BD, Leach S, Li XF, Dong H, Winkfein R, Perizzolo M, Cai X, Yang R, Philipson KD, Lytton J (2001) Molecular cloning of a third member of the potassium-dependent sodium-calcium exchanger gene family, NCKX3. J Biol Chem 276:23161-23172.

Kraig RP, Nicholson C (1978) Extracellular ionic variations during spreading depression. Neuroscience 3:1045-1059.

Kraig RP, Dong LM, Thisted R, Jaeger CB (1991) Spreading depression increases immunohistochemical staining of glial fibrillary acidic protein. J Neurosci 11:2187-2198.

Kreisman NR, Lamanna JC, Rosenthal M, Sick TJ (1981) Oxidative metabolic responses with recurrent seizures in rat cerebral cortex: role of systemic factors. Brain Res 218:175-188.

Krotkiewska B, Banas T (1992) Interaction of Zn2+ and Cu2+ ions with glyceraldehyde-3-phosphate dehydrogenase from bovine heart and rabbit muscle. Int J Biochem 24:1501-1505.

Kunkler PE, Kraig RP (2004) P/Q Ca2+ channel blockade stops spreading depression and related pyramidal neuronal Ca2+ rise in hippocampal organ culture. Hippocampus 14:356-367.

LaManna JC, Rosenthal M (1975) Effect of ouabain and phenobarbital on oxidative metabolic activity associated with spreading cortical depression in cats. Brain Res 88:145-149.

Lambert GA, Michalicek J, Storer RJ, Zagami AS (1999) Effect of cortical spreading depression on activity of trigeminovascular sensory neurons. Cephalalgia 19:631-638.

Lashley K (1941) Patterns of cerebral integration indicated by the scotomas of migraine. Arch Neurol Psychiatry 46:259-264.

Leao A (1944) Spreading Depression of activity in the cerebral cortex. J Neurophysiol 7:359-390.

Leao A (1947) Further observations on the spreading depression of activity in the cerebral cortex. J Neurophysiol 10:409-414.

Leao AAP, Morrison RS (1945) Propagation of spreading cortical depression. Journal of Neurophysiology 8:33-45.

Lee JM, Zipfel GJ, Choi DW (1999) The changing landscape of ischaemic brain injury mechanisms. Nature 399:A7-14.

Lee JM, Grabb MC, Zipfel GJ, Choi DW (2000a) Brain tissue responses to ischemia. J Clin Invest 106:723-731.

Lee JY, Cole TB, Palmiter RD, Koh JY (2000b) Accumulation of zinc in degenerating hippocampal neurons of ZnT3-null mice after seizures: evidence against synaptic vesicle origin. J Neurosci 20:RC79.

Lee JY, Kim JH, Palmiter RD, Koh JY (2003) Zinc released from metallothionein-iii may contribute to hippocampal CA1 and thalamic neuronal death following acute brain injury. Exp Neurol 184:337-347.

Legendre P, Westbrook GL (1990) The inhibition of single N-methyl-D-aspartate-activated channels by zinc ions on cultured rat neurones. J Physiol 429:429-449.

Li S, Jiang Q, Stys PK (2000) Important role of reverse Na(+)-Ca(2+) exchange in spinal cord white matter injury at physiological temperature. J Neurophysiol 84:1116-1119.

Li XF, Kraev AS, Lytton J (2002) Molecular cloning of a fourth member of the potassium-dependent sodium-calcium exchanger gene family, NCKX4. J Biol Chem 277:48410-48417.

Li XF, Kiedrowski L, Tremblay F, Fernandez FR, Perizzolo M, Winkfein RJ, Turner RW, Bains JS, Rancourt DE, Lytton J (2006) Importance of K+-dependent Na+/Ca2+-exchanger 2, NCKX2, in Motor Learning and Memory. J Biol Chem 281:6273-6282.

Link TA, von Jagow G (1995) Zinc ions inhibit the QP center of bovine heart mitochondrial bc1 complex by blocking a protonatable group. J Biol Chem 270:25001-25006.

Linnik MD, Zobrist RH, Hatfield MD (1993) Evidence supporting a role for programmed cell death in focal cerebral ischemia in rats. Stroke 24:2002-2008; discussion 2008-2009.

Linnik MD, Zahos P, Geschwind MD, Federoff HJ (1995) Expression of bcl-2 from a defective herpes simplex virus-1 vector limits neuronal death in focal cerebral ischemia. Stroke 26:1670-1674; discussion 1675.

Lipton P (1999) Ischemic cell death in brain neurons. Physiol Rev 79:1431-1568.

Lobner D, Canzoniero LM, Manzerra P, Gottron F, Ying H, Knudson M, Tian M, Dugan LL, Kerchner GA, Sheline CT, Korsmeyer SJ, Choi DW (2000) Zinc-induced neuronal death in cortical neurons. Cell Mol Biol (Noisy-le-grand) 46:797-806.

Lorincz A, Rozsa B, Katona G, Vizi ES, Tamas G (2007) Differential distribution of NCX1 contributes to spine-dendrite compartmentalization in CA1 pyramidal cells. Proc Natl Acad Sci U S A 104:1033-1038.

Lorusso M, Cocco T, Sardanelli AM, Minuto M, Bonomi F, Papa S (1991) Interaction of Zn2+ with the bovine-heart mitochondrial bc1 complex. Eur J Biochem 197:555-561.

Lothman E, Lamanna J, Cordingley G, Rosenthal M, Somjen G (1975) Responses of electrical potential, potassium levels, and oxidative metabolic activity of the cerebral neocortex of cats. Brain Res 88:15-36.

MacManus JP, Buchan AM, Hill IE, Rasquinha I, Preston E (1993) Global ischemia can cause DNA fragmentation indicative of apoptosis in rat brain. Neurosci Lett 164:89-92.

Magee JC, Johnston D (1995) Characterization of single voltage-gated Na+ and Ca2+ channels in apical dendrites of rat CA1 pyramidal neurons. J Physiol 487 (Pt 1):67-90.

Malaiyandi LM, Vergun O, Dineley KE, Reynolds IJ (2005) Direct visualization of mitochondrial zinc accumulation reveals uniporter-dependent and -independent transport mechanisms. J Neurochem 93:1242-1250.

Marler JR, Goldstein LB (2003) Medicine. Stroke--tPA and the clinic. Science 301:1677.

Martin JL, Stork CJ, Li YV (2006) Determining zinc with commonly used calcium and zinc fluorescent indicators, a question on calcium signals. Cell Calcium 40:393-402.

Martinez-Sanchez M, Striggow F, Schroder UH, Kahlert S, Reymann KG, Reiser G (2004) Na(+) and Ca(2+) homeostasis pathways, cell death and protection after oxygen-glucose-deprivation in organotypic hippocampal slice cultures. Neuroscience 128:729-740.

Martinou JC, Dubois-Dauphin M, Staple JK, Rodriguez I, Frankowski H, Missotten M, Albertini P, Talabot D, Catsicas S, Pietra C, et al. (1994) Overexpression of BCL-2 in transgenic mice protects neurons from naturally occurring cell death and experimental ischemia. Neuron 13:1017-1030.

Martins-Ferreira H, Nedergaard M, Nicholson C (2000) Perspectives on spreading depression. Brain Res Brain Res Rev 32:215-234.

Martins-Ferreira H, De Oliveira Castro G, Struchiner CJ, Rodrigues PS (1974) Circling spreading depression in isolated chick retina. J Neurophysiol 37:773-784.

Masino SA, Dunwiddie TV (1999) Temperature-dependent modulation of excitatory transmission in hippocampal slices is mediated by extracellular adenosine. J Neurosci 19:1932-1939.

Matsuda T, Arakawa N, Takuma K, Kishida Y, Kawasaki Y, Sakaue M, Takahashi K, Takahashi T, Suzuki T, Ota T, Hamano-Takahashi A, Onishi M, Tanaka Y, Kameo K, Baba A (2001) SEA0400, a novel and selective inhibitor of the Na+-Ca2+ exchanger, attenuates reperfusion injury in the in vitro and in vivo cerebral ischemic models. J Pharmacol Exp Ther 298:249-256.

Mayer ML, Westbrook GL (1987) Permeation and block of N-methyl-D-aspartic acid receptor channels by divalent cations in mouse cultured central neurones. J Physiol 394:501-527.

Mayevsky A, Chance B (1974) Repetitive patterns of metabolic changes during cortical spreading depression of the awake rat. Brain Res 65:529-533.

Mayevsky A, Chance B (1975) Metabolic responses of the awake cerebral cortex to anoxia hypoxia spreading depression and epileptiform activity. Brain Res 98:149-165.

Mayevsky A, Weiss HR (1991) Cerebral blood flow and oxygen consumption in cortical spreading depression. J Cereb Blood Flow Metab 11:829-836.

Mayevsky A, Doron A, Manor T, Meilin S, Zarchin N, Ouaknine GE (1996) Cortical spreading depression recorded from the human brain using a multiparametric monitoring system. Brain Res 740:268-274.

McCormack JG, Denton RM (1993) The role of intramitochondrial Ca2+ in the regulation of oxidative phosphorylation in mammalian tissues. Biochem Soc Trans 21 (Pt 3):793-799.

McCormack JG, Halestrap AP, Denton RM (1990) Role of calcium ions in regulation of mammalian intramitochondrial metabolism. Physiol Rev 70:391-425.

Mies G, Iijima T, Hossmann KA (1993) Correlation between peri-infarct DC shifts and ischaemic neuronal damage in rat. Neuroreport 4:709-711.

Mies G, Kohno K, Hossmann KA (1994) Prevention of periinfarct direct current shifts with glutamate antagonist NBQX following occlusion of the middle cerebral artery in the rat. J Cereb Blood Flow Metab 14:802-807.

Milner PM (1958) Note on a possible correspondence between the scotomas of migraine and spreading depression of Leao. Electroencephalogr Clin Neurophysiol 10:705.

Minelli A, Castaldo P, Gobbi P, Salucci S, Magi S, Amoroso S (2006) Cellular and subcellular localization of Na(+)-Ca(2+) exchanger protein isoforms, NCX1, NCX2, and NCX3 in cerebral cortex and hippocampus of adult rat. Cell Calcium.

Mironov SL, Richter DW (2001) Oscillations and hypoxic changes of mitochondrial variables in neurons of the brainstem respiratory centre of mice. J Physiol 533:227-236.

Muller A, Kukley M, Uebachs M, Beck H, Dietrich D (2007) Nanodomains of single Ca2+ channels contribute to action potential repolarization in cortical neurons. J Neurosci 27:483-495.

Naraghi M, Neher E (1997) Linearized buffered Ca2+ diffusion in microdomains and its implications for calculation of [Ca2+] at the mouth of a calcium channel. J Neurosci 17:6961-6973.

Nedergaard M, Astrup J (1986) Infarct rim: effect of hyperglycemia on direct current potential and [14C]2-deoxyglucose phosphorylation. J Cereb Blood Flow Metab 6:607-615.

Nedergaard M, Hansen AJ (1988) Spreading depression is not associated with neuronal injury in the normal brain. Brain Res 449:395-398.

Nedergaard M, Hansen AJ (1993) Characterization of cortical depolarizations evoked in focal cerebral ischemia. J Cereb Blood Flow Metab 13:568-574.

Nedergaard M, Cooper AJ, Goldman SA (1995) Gap junctions are required for the propagation of spreading depression. J Neurobiol 28:433-444.

Netto M, Do Carmo RJ, Martins-Ferreira H (1999) Retinal spreading depression induced by photoactivation: involvement of free radicals and potassium. Brain Res 827:221-224.

Nicholls DG (1978) The regulation of extramitochondrial free calcium ion concentration by rat liver mitochondria. Biochem J 176:463-474.

Nicholls DG (1985) A role for the mitochondrion in the protection of cells against calcium overload? Prog Brain Res 63:97-106.

Nicholls DG, Budd SL (2000) Mitochondria and neuronal survival. Physiol Rev 80:315-360.

Nicholls DG, Chalmers S (2004) The integration of mitochondrial calcium transport and storage. J Bioenerg Biomembr 36:277-281.

Nicholls P, Malviya AN (1968) Inhibition of nonphosphorylating electron transfer by zinc. The problem of delineating interaction sites. Biochemistry 7:305-310.

Nicholson C, Kraig RP, ten Bruggencate G, Stockle H, Steinberg R (1978) Potassium, calcium, chloride and sodium changes in extracellular space during spreading depression in cerebellum [proceedings]. Arzneimittelforschung 28:874-875.

Noh KM, Koh JY (2000) Induction and activation by zinc of NADPH oxidase in cultured cortical neurons and astrocytes. J Neurosci 20:RC111.

Noh KM, Kim YH, Koh JY (1999) Mediation by membrane protein kinase C of zinc-induced oxidative neuronal injury in mouse cortical cultures. J Neurochem 72:1609-1616.

O'Halloran TV (1993) Transition metals in control of gene expression. Science 261:715-725.

Obeidat AS, Andrew RD (1998) Spreading depression determines acute cellular damage in the hippocampal slice during oxygen/glucose deprivation. Eur J Neurosci 10:3451-3461.

Obeidat AS, Jarvis CR, Andrew RD (2000) Glutamate does not mediate acute neuronal damage after spreading depression induced by O2/glucose deprivation in the hippocampal slice. J Cereb Blood Flow Metab 20:412-422.

Obrenovitch TP, Zilkha E (1995) High extracellular potassium, and not extracellular glutamate, is required for the propagation of spreading depression. J Neurophysiol 73:2107-2114.

Obrenovitch TP, Zilkha E, Urenjak J (1996) Evidence against high extracellular glutamate promoting the elicitation of spreading depression by potassium. J Cereb Blood Flow Metab 16:923-931.

Ochs S, Hunt K, Booker H (1961) Spreading depression using chronically implanted electrodes. Am J Physiol 200:1211-1214.

Ohta K, Graf R, Rosner G, Heiss WD (2001) Calcium ion transients in peri-infarct depolarizations may deteriorate ion homeostasis and expand infarction in focal cerebral ischemia in cats. Stroke 32:535-543.

Okamoto M, Matsumoto M, Ohtsuki T, Taguchi A, Mikoshiba K, Yanagihara T, Kamada T (1993) Internucleosomal DNA cleavage involved in ischemia-induced neuronal death. Biochem Biophys Res Commun 196:1356-1362.

Olney JW (1978) Neurotoxicity of excitatory amino acids. In: Kainic acid as a tool in neurobiology (E.G. McGreer JWOaPLME, ed), pp 95-121. New York: Raven.

Ophoff RA, Terwindt GM, Vergouwe MN, van Eijk R, Oefner PJ, Hoffman SM, Lamerdin JE, Mohrenweiser HW, Bulman DE, Ferrari M, Haan J, Lindhout D, van Ommen GJ, Hofker MH, Ferrari MD, Frants RR (1996) Familial hemiplegic migraine and episodic ataxia type-2 are caused by mutations in the Ca2+ channel gene CACNL1A4. Cell 87:543-552.

Osuga S, Hakim AM, Osuga H, Hogan MJ (1997) In vivo uptake of [3H]nimodipine into brain during cortical spreading depression. J Cereb Blood Flow Metab 17:586-590.

Ouardouz M, Zamponi GW, Barr W, Kiedrowski L, Stys PK (2005) Protection of ischemic rat spinal cord white matter: Dual action of KB-R7943 on Na+/Ca2+ exchange and L-type Ca2+ channels. Neuropharmacology 48:566-575.

Palmiter RD, Cole TB, Quaife CJ, Findley SD (1996) ZnT-3, a putative transporter of zinc into synaptic vesicles. Proc Natl Acad Sci U S A 93:14934-14939.

Papa M, Canitano A, Boscia F, Castaldo P, Sellitti S, Porzig H, Taglialatela M, Annunziato L (2003) Differential expression of the Na+-Ca2+ exchanger transcripts and proteins in rat brain regions. J Comp Neurol 461:31-48.

Paulson OB, Newman EA (1987) Does the release of potassium from astrocyte endfeet regulate cerebral blood flow? Science 237:896-898.

Perez-Pinzon MA, Tao L, Nicholson C (1995) Extracellular potassium, volume fraction, and tortuosity in rat hippocampal CA1, CA3, and cortical slices during ischemia. J Neurophysiol 74:565-573.

Peters O, Schipke CG, Hashimoto Y, Kettenmann H (2003) Different mechanisms promote astrocyte Ca2+ waves and spreading depression in the mouse neocortex. J Neurosci 23:9888-9896.

Peters S, Koh J, Choi DW (1987) Zinc selectively blocks the action of N-methyl-D-aspartate on cortical neurons. Science 236:589-593.

Petrozzino JJ, Connor JA (1994) Dendritic Ca2+ accumulations and metabotropic glutamate receptor activation associated with an N-methyl-D-aspartate receptor-independent long-term potentiation in hippocampal CA1 neurons. Hippocampus 4:546-558.

Pignataro G, Tortiglione A, Scorziello A, Giaccio L, Secondo A, Severino B, Santagada V, Caliendo G, Amoroso S, Di Renzo G, Annunziato L (2004a) Evidence for a protective role played by the Na+/Ca2+ exchanger in cerebral ischemia induced by middle cerebral artery occlusion in male rats. Neuropharmacology 46:439-448.

Pignataro G, Gala R, Cuomo O, Tortiglione A, Giaccio L, Castaldo P, Sirabella R, Matrone C, Canitano A, Amoroso S, Di Renzo G, Annunziato L (2004b) Two sodium/calcium exchanger gene products, NCX1 and NCX3, play a major role in the development of permanent focal cerebral ischemia. Stroke 35:2566-2570.

Pitter JG, Maechler P, Wollheim CB, Spat A (2002) Mitochondria respond to Ca2+ already in the submicromolar range: correlation with redox state. Cell Calcium 31:97-104.

Pralong WF, Hunyady L, Varnai P, Wollheim CB, Spat A (1992) Pyridine nucleotide redox state parallels production of aldosterone in potassium-stimulated adrenal glomerulosa cells. Proc Natl Acad Sci U S A 89:132-136.

Qian J, Noebels JL (2005) Visualization of transmitter release with zinc fluorescence detection at the mouse hippocampal mossy fibre synapse. J Physiol 566:747-758.

Qian J, Noebels JL (2006) Exocytosis of vesicular zinc reveals persistent depression of neurotransmitter release during metabotropic glutamate receptor long-term depression at the hippocampal CA3-CA1 synapse. J Neurosci 26:6089-6095.

Rader RK, Lanthorn TH (1989) Experimental ischemia induces a persistent depolarization blocked by decreased calcium and NMDA antagonists. Neurosci Lett 99:125-130.

Raffin CN, Harrison M, Sick TJ, Rosenthal M (1991) EEG suppression and anoxic depolarization: influences on cerebral oxygenation during ischemia. J Cereb Blood Flow Metab 11:407-415.

Rajdev S, Reynolds IJ (1994) Glutamate-induced intracellular calcium changes and neurotoxicity in cortical neurons in vitro: effect of chemical ischemia. Neuroscience 62:667-679.

Ramadan NM, Olesen J (2006) Classification of headache disorders. Semin Neurol 26:157-162.

Ramos JG (1975) Ionic movements in the isolated chicken retina during spreading depression. Acta Physiol Lat Am 25:112-119.

Randall RD, Thayer SA (1992) Glutamate-induced calcium transient triggers delayed calcium overload and neurotoxicity in rat hippocampal neurons. J Neurosci 12:1882-1895.

Reinert KC, Dunbar RL, Gao W, Chen G, Ebner TJ (2004) Flavoprotein autofluorescence imaging of neuronal activation in the cerebellar cortex in vivo. J Neurophysiol 92:199-211.

Rex A, Pfeifer L, Fink F, Fink H (1999) Cortical NADH during pharmacological manipulations of the respiratory chain and spreading depression in vivo. J Neurosci Res 57:359-370.

Reynolds I, Dineley KE, Vergun O (2006) Zinc has not been ignored. Journal of Neuroscience (eLetter).

Richter F, Ebersberger A, Schaible HG (2002) Blockade of voltage-gated calcium channels in rat inhibits repetitive cortical spreading depression. Neurosci Lett 334:123-126.

Roberts EL, Jr., Sick TJ (1988) Calcium-sensitive recovery of extracellular potassium and synaptic transmission in rat hippocampal slices exposed to brief anoxia. Brain Res 456:113-119.

Robertson C (2000) Editorial Comment on: Factors influencing the frequency of fluorescence transients as markers of peri-infarct depolarizations in focal cerebral ischemia. Stroke 31:221-222.

Rohacs T, Tory K, Dobos A, Spat A (1997) Intracellular calcium release is more efficient than calcium influx in stimulating mitochondrial NAD(P)H formation in adrenal glomerulosa cells. Biochem J 328 (Pt 2):525-528.

Rosamond W, Flegal K, Friday G, Furie K, Go A, Greenlund K, Haase N, Ho M, Howard V, Kissela B, Kittner S, Lloyd-Jones D, McDermott M, Meigs J, Moy C, Nichol G, O'Donnell CJ, Roger V, Rumsfeld J, Sorlie P, Steinberger J, Thom T, Wasserthiel-Smoller S, Hong Y (2007) Heart disease and stroke statistics--2007 update: a report from the American Heart Association Statistics Committee and Stroke Statistics Subcommittee. Circulation 115:e69-171.

Rosenthal M, Somjen G (1973) Spreading depression, sustained potential shifts, and metabolic activity of cerebral cortex of cats. J Neurophysiol 36:739-749.

Rossi CS, Lehninger AL (1964) Stoichiometry Of Respiratory Stimulation, Accumulation Of Ca++ And Phosphate, And Oxidative Phosphorylation In Rat Liver Mitochondria. J Biol Chem 239:3971-3980.

Rudolphi KA, Schubert P, Parkinson FE, Fredholm BB (1992) Neuroprotective role of adenosine in cerebral ischaemia. Trends Pharmacol Sci 13:439-445.

Scheuss V, Yasuda R, Sobczyk A, Svoboda K (2006) Nonlinear [Ca2+] signaling in dendrites and spines caused by activity-dependent depression of Ca2+ extrusion. J Neurosci 26:8183-8194.

Schneck MJ, Biller J (2005) New treatments in acute ischemic stroke. Curr Treat Options Neurol 7:499-511.

Schroder UH, Breder J, Sabelhaus CF, Reymann KG (1999) The novel Na+/Ca2+ exchange inhibitor KB-R7943 protects CA1 neurons in rat hippocampal slices against hypoxic/hypoglycemic injury. Neuropharmacology 38:319-321.

Sekizawa S, Bonham AC (2006) Group I metabotropic glutamate receptors on second-order baroreceptor neurons are tonically activated and induce a Na+-Ca2+ exchange current. J Neurophysiol 95:882-892.

Sensi SL, Jeng JM (2004) Rethinking the excitotoxic ionic milieu: the emerging role of Zn(2+) in ischemic neuronal injury. Curr Mol Med 4:87-111.

Sensi SL, Yin HZ, Weiss JH (2000) AMPA/kainate receptor-triggered Zn2+ entry into cortical neurons induces mitochondrial Zn2+ uptake and persistent mitochondrial dysfunction. Eur J Neurosci 12:3813-3818.

Sensi SL, Yin HZ, Carriedo SG, Rao SS, Weiss JH (1999) Preferential Zn2+ influx through Ca2+-permeable AMPA/kainate channels triggers prolonged mitochondrial superoxide production. Proc Natl Acad Sci U S A 96:2414-2419.

Sensi SL, Canzoniero LM, Yu SP, Ying HS, Koh JY, Kerchner GA, Choi DW (1997) Measurement of intracellular free zinc in living cortical neurons: routes of entry. J Neurosci 17:9554-9564.

Sensi SL, Ton-That D, Sullivan PG, Jonas EA, Gee KR, Kaczmarek LK, Weiss JH (2003) Modulation of mitochondrial function by endogenous Zn2+ pools. Proc Natl Acad Sci U S A 100:6157-6162.

Sheline CT, Behrens MM, Choi DW (2000) Zinc-induced cortical neuronal death: contribution of energy failure attributable to loss of NAD(+) and inhibition of glycolysis. J Neurosci 20:3139-3146.

Sheline CT, Ying HS, Ling CS, Canzoniero LM, Choi DW (2002) Depolarization-induced 65zinc influx into cultured cortical neurons. Neurobiol Dis 10:41-53.

Shinohara M, Dollinger B, Brown G, Rapoport S, Sokoloff L (1979) Cerebral glucose utilization: local changes during and after recovery from spreading cortical depression. Science 203:188-190.

Shuttleworth CW, Connor JA (2001) Strain-dependent differences in calcium signaling predict excitotoxicity in murine hippocampal neurons. J Neurosci 21:4225-4236.

Shuttleworth CW, Brennan AM, Connor JA (2003) NAD(P)H fluorescence imaging of postsynaptic neuronal activation in murine hippocampal slices. J Neurosci 23:3196-3208.

Sick TJ, Perez-Pinzon MA (1999) Optical methods for probing mitochondrial function in brain slices. Methods 18:104-108.

Siesjo BK, Bengtsson F (1989) Calcium fluxes, calcium antagonists, and calcium-related pathology in brain ischemia, hypoglycemia, and spreading depression: a unifying hypothesis. J Cereb Blood Flow Metab 9:127-140.

Skulachev VP, Chistyakov VV, Jasaitis AA, Smirnova EG (1967) Inhibition of the respiratory chain by zinc ions. Biochem Biophys Res Commun 26:1-6.

Sloviter RS (1985) A selective loss of hippocampal mossy fiber Timm stain accompanies granule cell seizure activity induced by perforant path stimulation. Brain Res 330:150-153.

Smith JM, Bradley DP, James MF, Huang CL (2006) Physiological studies of cortical spreading depression. Biol Rev Camb Philos Soc 81:457-481.

Smith MI, Read SJ, Chan WN, Thompson M, Hunter AJ, Upton N, Parsons AA (2000) Repetitive cortical spreading depression in a gyrencephalic feline brain: inhibition by the novel benzoylamino-benzopyran SB-220453. Cephalalgia 20:546-553.

Smith PD, Liesegang GW, Berger RL, Czerlinski G, Podolsky RJ (1984) A stopped-flow investigation of calcium ion binding by ethylene glycol bis(beta-aminoethyl ether)-N,N'-tetraacetic acid. Anal Biochem 143:188-195.

Snider BJ, Gottron FJ, Choi DW (1999) Apoptosis and necrosis in cerebrovascular disease. Ann N Y Acad Sci 893:243-253.

Sobolevsky AI, Khodorov BI (1999) Blockade of NMDA channels in acutely isolated rat hippocampal neurons by the Na+/Ca2+ exchange inhibitor KB-R7943. Neuropharmacology 38:1235-1242.

Somjen GG (2001) Mechanisms of spreading depression and hypoxic spreading depression-like depolarization. Physiol Rev 81:1065-1096.

Somjen GG (2005) Aristides Leao's discovery of cortical spreading depression. J Neurophysiol 94:2-4.

Sonn J, Mayevsky A (2000) Effects of brain oxygenation on metabolic, hemodynamic, ionic and electrical responses to spreading depression in the rat. Brain Res 882:212-216.

Stork CJ, Li YV (2006) Intracellular zinc elevation measured with a "calcium-specific" indicator during ischemia and reperfusion in rat hippocampus: a question on calcium overload. J Neurosci 26:10430-10437.

Stork CJ, Li YV (2007) Don't we want to know whether zinc accumulation contributes to the calcium transient measured with these 'calcium' fluorophores? Cell Calcium 42:343-344.

Strong AJ (2005) Dr. Bernice Grafstein's paper on the mechanism of spreading depression. J Neurophysiol 94:5-7.

Strong AJ, Dardis R (2005) Depolarisation phenomena in traumatic and ischaemic brain injury. Adv Tech Stand Neurosurg 30:3-49.

Strong AJ, Venables GS, Gibson G (1983) The cortical ischaemic penumbra associated with occlusion of the middle cerebral artery in the cat: 1. Topography of changes in blood flow, potassium ion activity, and EEG. J Cereb Blood Flow Metab 3:86-96.

Strong AJ, Hartings JA, Dreier JP (2007) Cortical spreading depression: an adverse but treatable factor in intensive care? Curr Opin Crit Care 13:126-133.

Strong AJ, Fabricius M, Boutelle MG, Hibbins SJ, Hopwood SE, Jones R, Parkin MC, Lauritzen M (2002) Spreading and synchronous depressions of cortical activity in acutely injured human brain. Stroke 33:2738-2743.

Strong AJ, Smith SE, Whittington DJ, Meldrum BS, Parsons AA, Krupinski J, Hunter AJ, Patel S, Robertson C (2000) Factors influencing the frequency of fluorescence transients as markers of peri-infarct depolarizations in focal cerebral ischemia. Stroke 31:214-222.

Stys PK, Waxman SG, Ransom BR (1992) Ionic mechanisms of anoxic injury in mammalian CNS white matter: role of Na+ channels and Na(+)-Ca2+ exchanger. J Neurosci 12:430-439.

Sugaya E, Takato M, Noda Y (1975) Neuronal and glial activity during spreading depression in cerebral cortex of cat. J Neurophysiol 38:822-841.

Szatkowski M, Barbour B, Attwell D (1990) Non-vesicular release of glutamate from glial cells by reversed electrogenic glutamate uptake. Nature 348:443-446.

Szerb JC (1991) Glutamate release and spreading depression in the fascia dentata in response to microdialysis with high K+: role of glia. Brain Res 542:259-265.

Takagi H, Takashima M, Liou SY (1998) [Effect of KB-2796, a novel calcium channel blocker, on spreading depression in rat hippocampal slices]. Nippon Yakurigaku Zasshi 111:309-316.

Takano T, Tian GF, Peng W, Lou N, Lovatt D, Hansen AJ, Kasischke KA, Nedergaard M (2007) Cortical spreading depression causes and coincides with tissue hypoxia. Nat Neurosci 10:754-762.

Takeuchi Y, Morii H, Tamura M, Hayaishi O, Watanabe Y (1991) A possible mechanism of mitochondrial dysfunction during cerebral ischemia: inhibition of mitochondrial respiration activity by arachidonic acid. Arch Biochem Biophys 289:33-38.

Tanaka E, Yamamoto S, Kudo Y, Mihara S, Higashi H (1997) Mechanisms underlying the rapid depolarization produced by deprivation of oxygen and glucose in rat hippocampal CA1 neurons in vitro. J Neurophysiol 78:891-902.

Tanaka E, Yamamoto S, Inokuchi H, Isagai T, Higashi H (1999) Membrane dysfunction induced by in vitro ischemia in rat hippocampal CA1 pyramidal neurons. J Neurophysiol 81:1872-1880.

Tegtmeier F (1993) Differences Between Spreading Depression and Ischemia. In: Migraine: Basic Mechansims and Treatment (Lehmenkuhler A, ed), pp 511-532: Urban and Schwarzenberg.

Thompson CL, Drewery DL, Atkins HD, Stephenson FA, Chazot PL (2002) Immunohistochemical localization of N-methyl-D-aspartate receptor subunits in the adult murine hippocampal formation: evidence for a unique role of the NR2D subunit. Brain Res Mol Brain Res 102:55-61.

Thompson RB, Whetsell WO, Jr., Maliwal BP, Fierke CA, Frederickson CJ (2000) Fluorescence microscopy of stimulated Zn(II) release from organotypic cultures of mammalian hippocampus using a carbonic anhydrase-based biosensor system. J Neurosci Methods 96:35-45.

Tottene A, Fellin T, Pagnutti S, Luvisetto S, Striessnig J, Fletcher C, Pietrobon D (2002) Familial hemiplegic migraine mutations increase Ca(2+) influx through single human CaV2.1 channels and decrease maximal CaV2.1 current density in neurons. Proc Natl Acad Sci U S A 99:13284-13289.

Tymianski M, Charlton MP, Carlen PL, Tator CH (1993) Source specificity of early calcium neurotoxicity in cultured embryonic spinal neurons. J Neurosci 13:2085-2104.

Umegaki M, Sanada Y, Waerzeggers Y, Rosner G, Yoshimine T, Heiss WD, Graf R (2005) Peri-infarct depolarizations reveal penumbra-like conditions in striatum. J Neurosci 25:1387-1394.

Vaillend C, Mason SE, Cuttle MF, Alger BE (2002) Mechanisms of neuronal hyperexcitability caused by partial inhibition of Na+-K+-ATPases in the rat CA1 hippocampal region. J Neurophysiol 88:2963-2978.

Vallee BL, Coleman JE, Auld DS (1991) Zinc fingers, zinc clusters, and zinc twists in DNA-binding protein domains. Proc Natl Acad Sci U S A 88:999-1003.

Van Harreveld A (1978) Two mechanisms for spreading depression in the chicken retina. J Neurobiol 9:419-431.

Van Harreveld A, Khattab FI (1967) Changes in cortical extracellular space during spreading depression investigated with the electron microscope. J Neurophysiol 30:911-929.

Van Harreveld A, Fifkova E (1970) Glutamate release from the retina during spreading depression. J Neurobiol 2:13-29.

VanHarreveld A (1959) Compounds in brain extracts causing spreading depression of cerebral cortical activity and contraction of crustacean muscle. J Neurochem 3:300-315.

Vogt K, Mellor J, Tong G, Nicoll R (2000) The actions of synaptically released zinc at hippocampal mossy fiber synapses. Neuron 26:187-196.

Voronina S, Sukhomlin T, Johnson PR, Erdemli G, Petersen OH, Tepikin A (2002) Correlation of NADH and Ca2+ signals in mouse pancreatic acinar cells. J Physiol 539:41-52.

Vyskocil F, Kritz N, Bures J (1972) Potassium-selective microelectrodes used for measuring the extracellular brain potassium during spreading depression and anoxic depolarization in rats. Brain Res 39:255-259.

Weiss JH, Sensi SL (2000) Ca2+-Zn2+ permeable AMPA or kainate receptors: possible key factors in selective neurodegeneration. Trends Neurosci 23:365-371.

Weiss JH, Sensi SL, Koh JY (2000) Zn(2+): a novel ionic mediator of neural injury in brain disease. Trends Pharmacol Sci 21:395-401.

Weiss JH, Hartley DM, Koh JY, Choi DW (1993) AMPA receptor activation potentiates zinc neurotoxicity. Neuron 10:43-49.

Welch KM (1993) Drug therapy of migraine. N Engl J Med 329:1476-1483.

Wenzel HJ, Cole TB, Born DE, Schwartzkroin PA, Palmiter RD (1997) Ultrastructural localization of zinc transporter-3 (ZnT-3) to synaptic vesicle membranes within mossy fiber boutons in the hippocampus of mouse and monkey. Proc Natl Acad Sci U S A 94:12676-12681.

White RJ, Reynolds IJ (1995) Mitochondria and Na+/Ca2+ exchange buffer glutamate-induced calcium loads in cultured cortical neurons. J Neurosci 15:1318-1328.

Xu C, Wu M, Morozova E, Alreja M (2006) Muscarine activates the sodium-calcium exchanger via M receptors in basal forebrain neurons. Eur J Neurosci 24:2309-2313.

Yamamoto S, Tanaka E, Shoji Y, Kudo Y, Inokuchi H, Higashi H (1997) Factors that reverse the persistent depolarization produced by deprivation of oxygen and glucose in rat hippocampal CA1 neurons in vitro. J Neurophysiol 78:903-911.

Yin HZ, Weiss JH (1995) Zn(2+) permeates Ca(2+) permeable AMPA/kainate channels and triggers selective neural injury. Neuroreport 6:2553-2556.

Yokoyama M, Koh J, Choi DW (1986) Brief exposure to zinc is toxic to cortical neurons. Neurosci Lett 71:351-355.

Young JN, Somjen GG (1992) Suppression of presynaptic calcium currents by hypoxia in hippocampal tissue slices. Brain Res 573:70-76.

Zachar J, Zacharova D (1963) [Mechanism Of The Origin Of Spreading Cortical Depression.]. Lek Pr 3:3-110.